



Unione Europea



Ministero dell'Istruzione,  
dell'Università e della Ricerca



Università degli Studi di Salerno

DIPARTIMENTO DI INGEGNERIA INDUSTRIALE

*Dottorato di Ricerca in Ingegneria Meccanica*  
**XIV Ciclo N.S. (2012-2015)**

***“Additive Manufacturing of metal alloy for  
aerospace by means of Powder Laser Cladding:  
station tuning and clad characterization”***

**Ing. Ilaria Fierro**

**Tutor:**

**Prof. Vincenzo Sergi**

**Coordinatore:**

**Prof. Vincenzo Sergi**







## TABLE OF CONTENTS

<b>Preface on the Additive Manufacturing</b> .....	<b>- 1 -</b>
<b>Abstract</b> .....	<b>- 7 -</b>
<b>Chapter I</b>	
<b>Introduction to Laser Cladding</b> .....	<b>- 9 -</b>
1.1 Process fundamentals .....	- 9 -
1.2 Why Laser Cladding?.....	- 10 -
1.3 Applications .....	- 13 -
1.3.1 Coating .....	- 14 -
1.3.2 Parts Repair and Refurbishment.....	- 17 -
1.3.3 Rapid Prototyping and Tooling .....	- 19 -
1.4 The state of the art.....	- 21 -
<b>Chapter II</b>	
<b>Laser Cladding process</b> .....	<b>- 27 -</b>
2.1 Laser Cladding Technique .....	- 27 -
2.1.1 Two-step process: pre-placed laser cladding .....	- 28 -
2.1.2 One-step process .....	- 30 -
2.1.2.1 Laser cladding by powder injection .....	- 31 -
2.1.2.2 Laser Cladding by wire feeding .....	- 32 -
2.1.2.3 Laser Cladding by Paste .....	- 34 -
2.2 A scheme of the process.....	- 34 -
2.2.1 Physical process .....	- 35 -
2.2.1.1 Laser-powder interactions .....	- 37 -
2.2.1.2 Heat transfer, fusion, fluid flow, and solidification. ....	- 40 -
2.2.2 Particles powder .....	- 43 -
2.2.3 Carrier gas .....	- 44 -

2.2.4 Process results .....	- 46 -
2.2.4.1 Porosity .....	- 46 -
2.2.4.2 Powder catchment efficiency .....	- 47 -
2.2.4.3 Surface finish.....	- 47 -
2.2.4.4 Surface hardness.....	- 48 -
2.2.4.5 Tensile and yield strengths .....	- 49 -
2.2.4.6 Residual stresses .....	- 49 -
2.2.4.7 Clad Dimensional Characteristics.....	- 50 -
2.3 Physical models.....	- 53 -

## **Chapter III**

<b>Laser Cladding Equipment .....</b>	<b>- 55 -</b>
3.1 Laser source .....	- 56 -
3.1.1 Construction of a laser .....	- 57 -
3.1.2 Lasers their types and characteristics .....	- 58 -
3.1.3 Characteristics of laser beam .....	- 63 -
3.1.4 High power disk lasers .....	- 68 -
3.2 Powder feeder .....	- 71 -
3.3 Laser deposition line .....	- 73 -
3.3.1 Off-axis powder injection.....	- 77 -
3.3.2 Continuous coaxial powder injection .....	- 78 -
3.3.3 Discontinuous coaxial powder injection .....	- 80 -

## **Chapter IV**

<b>Laser cladding station and process tuning.....</b>	<b>- 81 -</b>
4.1 Laser deposition line .....	- 81 -
4.1.1 Laser source .....	- 82 -
4.1.2 Laser Cladding head.....	- 82 -

4.1.3 Manipulate system .....	- 85 -
4.1.4 Powder delivery and monitoring system .....	- 85 -
4.2 Process tuning .....	- 89 -
4.2.1 Powder mass flow setting.....	- 89 -
4.2.2 Laser spot diameter setting.....	- 91 -
4.3 Trials execution.....	- 94 -

## Chapter V

<b>Experimental test .....</b>	<b>- 95 -</b>
5.1 Single clad deposition on AA2024 plates .....	- 96 -
5.1.1 Test sample and powder features .....	- 96 -
5.1.2 Experimental procedure .....	- 99 -
5.1.2.1 Laser deposition line .....	- 99 -
5.1.2.2 Design of Experiments .....	- 99 -
5.1.3 Results and discussion.....	- 102 -
5.1.3.1 Defects and geometric analysis .....	- 102 -
5.1.3.2 Microstructure and micro-hardness .....	- 105 -
5.1.4 Adjustment of the process conditions .....	- 108 -
5.1.4.1 Experimental conditions .....	- 108 -
5.1.4.2 Results and discussion .....	- 109 -
5.2 Laser cladding into a pre-machined V-groove of AA2024 aluminium alloy .....	- 112 -
5.2.1 Preliminary test .....	- 114 -
5.2.2 Analysis strategy layer by layer: process parameters. -	116 -
5.2.3 Buckling, deformation and dilution analyzes.....	- 119 -
5.2.4 Results and discussion.....	- 121 -
5.2.4.1 Defects analysis.....	- 122 -
5.2.4.2 Metallurgical analysis.....	- 124 -

5.2.4.3	SEM examination .....	- 128 -
5.2.4.4	Vickers micro-hardness.....	- 131 -
5.2.4.5	Tensile tests .....	- 138 -
5.2.4.6	Fatigue tests.....	- 139 -
5.3	Laser cladding into a pre-machined V-groove of A357 aluminium alloy .....	- 141 -
5.3.1	Test sample and powder features .....	- 141 -
5.3.2	Experimental procedure .....	- 144 -
5.3.3	Results and discussion.....	- 146 -
5.3.3.1	Buckling and deformation analysis .....	- 147 -
5.3.3.2	Defects analysis and X-ray inspections .....	- 148 -
5.3.3.3	The effect of artificial aging: metallurgical and mechanical analysis.....	- 151 -
5.3.3.4	Tensile tests .....	- 170 -
5.4	The cost of Laser Cladding process .....	- 171 -
	<b>Conclusions</b> .....	<b>- 175 -</b>
	<b>References</b> .....	<b>- 177 -</b>



## Preface on the Additive Manufacturing

The reduction of lead time and cost is very important for the development of new industrial products for the manufacturing industry. Time to market and increased competition are two of the important issues for the 21<sup>st</sup> century businesses to achieve success. 21<sup>st</sup> century manufacturers have to not only produce high quality, low cost and much more functional products, but also respond their customer demands more responsively and quickly speeding up the tooling lead times to put on a product to the market quickly because today's market wants rapid product availability. Global competition requires manufacturers to fabricate their products in reduced cycle times besides high quality with low costs [1].

The Additive manufacturing (AM) technologies have been recognized as a unique technologic method to achieve this aim [2].

According to their first standard, ASTM F2792-10, AM is defined as:

*“The process of joining materials to make objects from 3D model data, usually layer upon layer, as opposed to subtractive manufacturing technologies.”*

Over the past 20 years, additive manufacturing (AM) has evolved from 3D printers used for rapid prototyping to sophisticated rapid manufacturing that can create parts directly without the use of tooling. AM technologies are the direct descendents of the work in 3D printing and could revolutionize many sectors of manufacturing by reducing component lead time, cost, material waste, energy usage, and carbon footprint. Furthermore, AM has the potential to enable novel product designs that could not be fabricated using conventional subtractive processes and extend the life of in-service parts through innovative repair methodologies.

Although a majority of the current global activity in AM is using polymer-based systems, there has been a good deal of activity and interest in metallic part fabrication. Metallic part fabrication has been of interest due to the possibility for

direct fabrication of net or near-net shape components without the need for tooling or machining. There has been particular interest in aerospace and biomedical industries owing to the possibility for high performance parts with reduced overall cost for manufacturing.

For the aerospace industry this could lead to a reduction of required raw materials used to fabricate an in-service component, which is known as the “buy-to-fly” ratio. AM could also lead to new innovations for lightweight structures that could see application in unmanned aerial vehicles. For the medical industry, AM is already leading to a revolution in customized medicine where dental implants, orthopedics, and hearing aids are manufactured to fit an individual’s unique physiology [3].

These processes are known also as Solid Freeform Fabrication (SFF) to indicate a method of manufacturing solid mechanical parts without part-specific tooling or human intervention.

In the following scheme a classification of the most important AM technologies is shown.

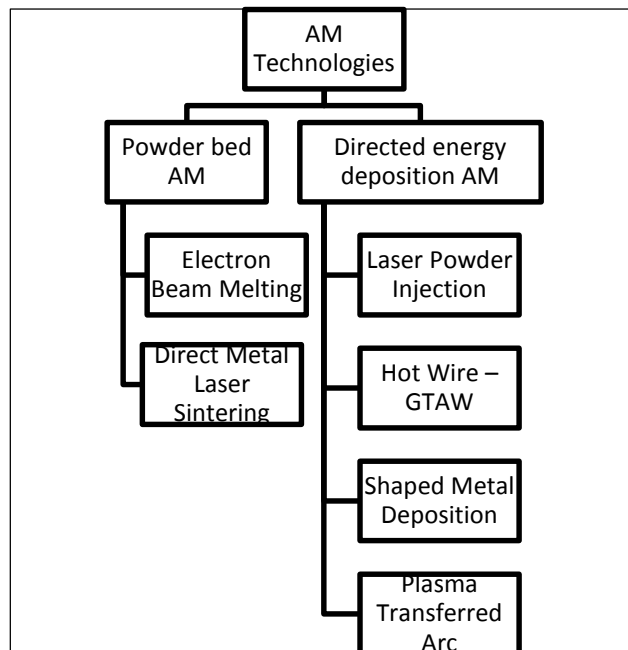


Fig. 1. AM technologies: Powder bed AM and Directed energy deposition AM.

## **Powder Bed AM**

In powder bed AM systems, the build envelope is an enclosed chamber that can be operated in vacuum or filled with an inert gas to prevent oxidation of reactive metal powders like titanium and aluminum. In the center of the chamber, a reservoir of metal powder is smoothed using a leveling system. The chamber is then pre-heated to a pre-determined temperature depending on the process, around 100°C for laser based and 700°C for electron beam. The laser or electron beam is then scanned over the surface of the metal powder in the pattern of the part, building up a single layer, usually between 20 and 200  $\mu\text{m}$  thick. The build reservoir is then lowered a single layer thickness, a leveling system provides fresh powder on top of the part, and the process is repeated until the final build is finished. It has more advantageous for construction of 3D structures with over-hanging parts – since the powder bed acts as a supporting structure.

### *Electron Beam Melting*

The technology uses a heated powder bed of metal in a vacuum that is then melted and formed layer by layer using an electron beam energy source similar to that of an electron microscope. This EBM technology is one of the most widely used AM technologies. Avio, an Italian aerospace company, has been working with ARCAM to develop capability to manufacture  $\gamma$ -TiAl intermetallic components for applications like turbine blades or other high-temperature areas of engines. This is an important advance because TiAl is a useful high-temperature material. However, due to its intermetallic structure, it is brittle and difficult to machine. These intermetallic components are excellent examples of how near-net shape processing using AM is enabling new engineering advances. A primary advantage of using the EBM technology is that the build chamber is kept relatively hot, typically between 700 and 1000°C. This leads to lower induced stresses in the parts because of smaller amounts of cooling during the build cycle. It has been shown that Ti-6Al-4V processed using the EBM process can have comparable ultimate tensile strength and elongation properties as wrought material. Another advantage of the EBM process is that it has a faster build rate compared to laser-based powder bed systems. However, the surface roughness for EBM parts is higher and post machining is necessary for many applications.

#### *Direct Metal Laser Sintering*

The DMLS process works by melting fine powders of metal in a powder bed, layer by layer. A laser supplies the necessary energy and the system operates in a protective atmosphere of nitrogen or argon. The materials currently available include Al-Si-10Mg, a CoCr superalloy, tool steel, stainless steel, Ti-6Al-4V Grade 5, Ti 6Al-4V Grade 23, and CP-Ti. Nickel alloys 625 and 718 are currently under development. EOS continually works with designated centers of excellence to develop new powders for the process.

The surface finish produced is superior to the EBM process with a surface finish of around 8.75 Ra. However, the build rate is slower than using EBM. Since the powder bed is held at a relatively low temperature, stresses can be induced in parts so innovative supports are required to prevent distortion of certain types of builds. Anisotropy can also develop in the build section due to heating and/or cooling cycles. Post-fabrication heat treatments can be required to normalize the properties in the x-y and z build directions depending on application requirements.

Upon the completion of a single layer, the powder bed is lowered by the height of the deposited layer, a new bed of powder is deposited with a roller, and the process is repeated. This repetitious process results in excess metal powder which can help in supporting the part during the build and can also result in powder remaining in the part if it consists of passages/channels in the design.

#### **Directed energy deposition AM**

The additive manufacturing processes in which material is fused as it is deposited, by the means of focused thermal energy.

#### *Laser Powder Injection (Laser cladding):*

Another approach to metals AM uses powder injection to provide the material to be deposited. Instead of a bed of powder that is reacted with an energy beam, powder is injected through a nozzle that is then melted to deposit material. The powder may be injected through an inert carrier gas or by gravity feed. With either powder injection methods, a separate supply of shielding gas is used to protect the molten weld pool from oxidation. The part is typically attached to a table that is rotated in the x and y directions. The table is fixed and the laser head is raised or repositioned for each layer to be deposited.

The laser powder injection approach is valuable because it can be used to add material to existing high-value parts for repair and the powder material

injected can be varied to fabricate compositionally graded parts. The powder injection approach is not constrained to a confined volume as the powder bed systems are. Therefore, these systems can be used to deposit features on large parts such as forgings. In general, this technology is not able to deposit the same volume of material as the powder bed techniques but it is more useful for repair and cladding.

It is based on a powder injection system that is coupled with a fiber laser on a robotic arm. It is well-suited for repair of existing tooling, adding features to large parts, or for the manufacture of new parts. To the combined material/energy delivery method, it can be readily utilized for creating functional graded/composed parts with varying material/alloy concentrations. Finally, preform mixing can be accomplished with it – such as coaxial powder delivery and lateral wire feeding.

### **Other techniques**

In addition to the powder injection techniques, there are a range of other approaches that use other types of energy inputs or materials. The energy inputs are electron beam welders, arc welding equipment, or ultrasonic energy.

#### *Plasma Transferred Arc Selective Free Form Fabrication*

Plasma Transferred Arc – Selective Free Form Fabrication (PTA-SFFF) uses wire and powder filler materials to deposit metals. A PTA torch and positioning stage are manipulated by a robot or multi-axis controller and the path is preprogrammed. Powder is introduced both through the shielding gas and the orifice gas, and the plasma arc welding system provides the energy for melting.

#### *Shaped Metal Deposition (SMD)*

The current SMD setup uses a computer controlled synergic gas tungsten arc welding (GTAW) power source that is integrated with a robot.

#### *Hot Wire – GTAW*

Along with plasma arc welding (PAW) and cold wire GTAW (SMD), HW-GTAW is used to produce free form fabrication parts in a range of alloys from steels, to stainless steels, nickel alloys, and titanium alloys. By using HW-GTAW in contrast to the other arc-based free form fabrication approaches the

deposition rate can be increased by roughly an order of magnitude. This improved deposition rate opens up many opportunities including in aerospace and oil and gas manufacturing.

## Abstract

This thesis investigates the application of continuous coaxial laser cladding by powder injection as repair and cover process. The investigation aimed to check the possibility of repairing a V-groove geometry on a substrate of AA2024 and A357 aluminum alloy.

Chapter one is an introduction to the laser cladding. This presents a general overview of the laser cladding methods and some applications for the processes.

In the second chapter, the laser cladding process is analysed in terms of process parameters and responses. First of all a basic description of the process is presented with a classification of the technology: laser cladding technology could be carried out in one step and two steps. The feeding deposited material could be powders, wire or paste.

Chapter three provides a comprehensive comparison of available lasers, powder feeders, and nozzles to demonstrate their potential and suitability for use in laser cladding technology. It is very important to know the field of application of the different configurations, which depend on the particular condition and use.

In chapter four details of the laser cladding station and of the experimental setup used in this research are presented. The last section of this chapter describes the process tuning.

In chapter five, the experimental tests and the final analyzes for each experimentation are discussed.

The first one is a test of single deposition on a AA2024 aluminum alloy plate carried out in order to understand the alloy characteristics for this process and to analyze the most important responses of the laser cladding process. The effect of the most significant parameters is analysed in terms of main effect and interaction plots by Minitab statistic software.

The second one is about a filling milled grooves through laser cladding for repair applications. In particular a pre-machined V-grooves on AA 2024 aluminum plates has been repaired by the laser cladding process with AA 2024 aluminum powders alloy.

In order to analyse the process for another aluminum alloy, the same groove has been milled and filled on A357 aluminum alloy plates. This alloy exhibits a relatively high flowability, which is preferred for Additive Manufacturing processes. It is a precipitation-hardenable A357 alloy, so an analysis pre and post heat treatment is carried out.

In conclusion a model to analyse the laser cladding cost is shown.



# Chapter I

## Introduction to Laser Cladding

The rapid growth of laser technology and the reduced cost of laser systems, have increased the interest for this technology in a variety of industries in the past few decades. Aerospace, automotive, navy, defense, and many other sectors are already used laser technology for welding, cutting, and hardening. In recent years laser cladding has received significant attention for material processing such as metallic coating, high-value components repair, prototyping, becoming one of the most significant additive manufacturing technology. Its rapid growth is due to a change of the production processing philosophy that favors the repair of the components instead of replacing.

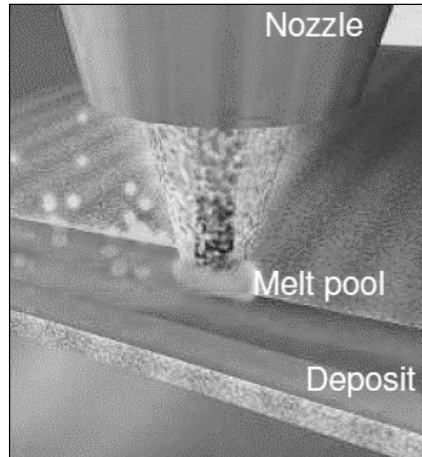
### 1.1 Process fundamentals

Laser cladding is an interdisciplinary technology utilizing laser technology, computer-aided design and manufacturing, robotics, sensors and control, and powder metallurgy [4] .

The aim of the laser cladding is to fuse one or more layers of a desired metal onto a solid substrate using a continuous wave or pulsed laser power source. The deposited material can be transferred to the substrate by several methods: powder injection, pre-placed powder on the substrate, or by wire feeding [5]. Among the different alternatives to perform this process, powder injection has been proved to be the most flexible, robust and effective way to supply the precursor material for the laser cladding process [6].

In this process, the laser beam melts the powder particles and a thin layer of the moving substrate to deposit a layer of the powder particles on the substrate as shown in the figure 1.

A great variety of materials can be deposited on a substrate using laser cladding by powder injection to form a layer with thicknesses ranging from 0.05 to 2 mm and widths as narrow as 0.4 mm.



*Fig. 1.1: Laser cladding process*

In addition to metallic coating applications, the laser cladding process offers a revolutionary layered manufacturing and prototyping technique. Integration of the laser cladding technology with a three-dimensional CAD solid model, which is sliced into many layers, provides the ability to fabricate complex components without intermediate steps.

The development of the laser cladding technology depends on enhancement of the technologies involved. Understanding the interconnections between the involved technologies and the process quality is a major step for the development of laser cladding. However, numerous interactions between the technologies involved in laser cladding not only increase the complexity of the process but also increase the number of process parameters [4].

## **1.2 Why Laser Cladding?**

Nowadays, one of the major aeronautic industry interests is to reduce cost during the different manufacturing stages of a component, starting from the conceptual design and prototyping, manufacturing and finally repair and maintenance works. More flexible and efficient manufacturing processes are necessary for reducing production time and improving performance and service life of different components.

Unlike conventional methods, laser cladding can be considered precise and, because of this, with a small heat-affected zone (HAZ). The quality of the deposit is also high which means that laser clads can be made with low porosity

and few imperfections. However, high cooling rates increase the sensibility of the clad and HAZ to cracking, and precautions such as preheating might be necessary. This process offers many advantages over conventional coating processes such as arc welding and plasma spraying. The laser cladding technique can produce a much better coating, with minimal dilution, minimal distortion, and better surface quality.

The general aim is to produce a clad with appropriate service properties, a strong bond to the substrate, with the highest coverage rate, the minimum use of alloy addition and minimum distortion.

The material deposited also has good grain structure, and has properties similar to, or even better than the intrinsic materials. Both pre-placed and powder injection laser cladding offer these features; however, laser cladding by powder injection has fewer material limitations than pre-placed in which it does not require secondary placing powder laminating operations and it can be used to repair parts as well as to fabricate them.

Due to its additive nature, laser cladding can be applied in a variety of ways to parts, tools and advanced manufacturing to overcome the limitations of existing metal fabrication technologies. This results in a number of benefits as follows:

1. Reduction of production time: The length of time required to build a prototype is a problem for new product development. In many cases, both prototype and production tooling are needed; therefore, the length of time to produce a prototype and the necessary tooling can be several months. The laser cladding process can reduce this time by fabricating tools and main prototypes directly from the CAD solid model .
2. Enhancement of thermal control: The laser cladding process offers a well-controlled heat-treated zone due to the nature of the laser beam. A high-power laser beam is well confined and tense and, as a result, the rapid heating and cooling that occur in the process have little effect of heat on the base material. Therefore, the original properties of the base material are affected to a limited extent only. In addition, this thermal zone can be monitored and optimized during the process, which can significantly improve the quality of the tools produced. Laser cladding also offers a controllable energy over the surface of the desired tool to

control the rate of solidification, which is the main parameter in the formation of microstructure and mechanical properties.

3. Parts repair: Current tool repair technology relies on destructive, high-temperature welding processes. In addition, machining errors or last-minute engineering changes can affect on-time delivery of tooling, and potentially impact the introduction date of a new product. Laser cladding can be applied as a safe technology to repair tooling, especially on critical contacting surfaces. Laser cladding increases tool life and in many cases can save a high-value tool that would otherwise need to be replaced.
4. Production of a functionally graded part: In conventional metallic fabrication, it is difficult to produce a part from different materials layers. Laser cladding offers a method to produce functionally graded parts by injecting different materials during the fabrication of the parts. It is also possible to produce desired alloys by injection of different powders through various nozzles around the process zone.
5. Production of smart structure: In conventional metallic fabrication methods, embedding objects into the tools is impossible due to the nature of manufacturing. Laser cladding, with its additive nature, offers the ability to create “smart structure” by embedding objects such as sensors and magnets during fabrication. Encapsulating these objects reduces the potential for damage or failure from temperature and environmental conditions.
6. Reduction of material: the laser metal deposition technique can reduce the quantity of material employed in the manufacturing or repairing of a component: when the part is manufactured by machining, the starting point is a large forged pre-form, being necessary to remove a sizable quantity of material until the final geometry is reached [7].

Despite its obvious benefits, laser cladding is not yet widely utilized. While laser cladding clearly offers a number of advantages over conventional fabrication technologies, the process can also have some drawbacks. Due to disturbances in the process, the clad quality may vary significantly. Variations of the quality may even be observed between processing cycles performed using the same operating conditions. This poor reproducibility arises from the high sensitivity of laser cladding to small changes in the operating parameters such as laser power, beam velocity and powder feed rate, as well as to process

disturbances such as variations in absorptivity. Finding an optimal set of parameters experimentally and using them in an open-loop laser cladding process may not result in a good quality clad due to random or periodic disturbances in the system.

Therefore, development of an intelligent closed-loop control system is essential for overcoming the effects of disturbances in the process.

However the principal disadvantages of laser cladding to industrial application is related to cost and unfamiliarity with the process. The capital cost of the equipment is much higher than for many conventional techniques. Applications are required to be of sufficient volume, or add sufficient value to the part, to be economically feasible.

A simplified comparison of the various techniques of surface coating is given in Table 1 where SMA, shielded metal arc; MIG, metal inert gas; SA, submerged arc; TIG, tungsten inert gas and HVOF, high velocity oxy-fuel are compared.

*Tab. 1-1: Comparison of the various techniques of surface coating*

	Laser cladding	SMA	MIG	SA	TIG	Plasma spraying	Flame	HVOF	Plasma arc
<b>Thickness [mm]</b>	0.2-2.0	1.6-10	1-6	2-10	0.5-3.0	0.1-0.2	0.8-2	0.3-1.5	1-5
<b>Deposition rate [kg h<sup>-1</sup>]</b>	0.2-7	0.5-2.5	2.3-11	5-25	0.5-3.5	0.5-7	0.4-2.7	1-5	2.5-6.5
<b>Distortion</b>	Low	Med.	Med.	High	High	Low	High	Low	Med.
<b>Precision</b>	High	Low	Low	Low	Med.	Med.	Low	Low	Med.
<b>Dilution [%]</b>	1-5	15-25	15-20	10-50	10-20	5-30	1-10	Low	Med.
<b>Integrity</b>	High	High	High	High	Med.	Low	Med.	Med.	Med.

### 1.3 Applications

Laser cladding is an extremely flexible technique with application in multiple areas from large scale component repair to medical implant manufacture.

As mentioned earlier, it has several different applications. In the following sections, a lot of case studies to adapt the process to different applications are explained.

### **1.3.1 Coating**

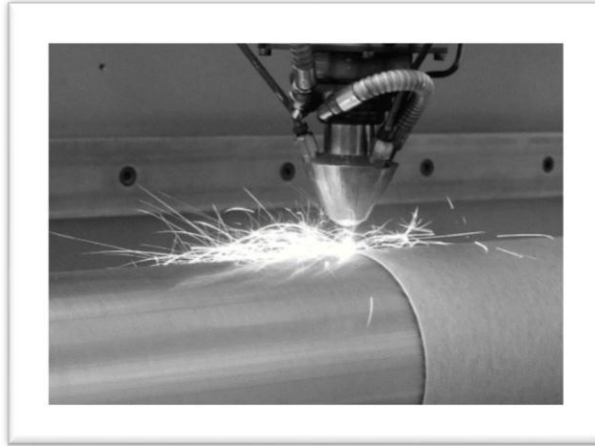
Coating is an overlay deposition process, where the coating material, a powder or wire, is applied on the surface of the base material through a melting process [8].

Laser cladding has the potential to produce coatings with low substrate dilution, minimal distortion and strong metallurgical bonding with the substrate.

Coating results in deposition of a thin layer of material (e.g., metals and ceramics) onto the surface of a selected material. This changes the surface properties of the substrate to those of the deposited material. The substrate becomes a composite material exhibiting properties generally not achievable through the use of the substrate material alone. The coating provides a durable, corrosion-resistant layer, and the core material provides the load bearing capability. There are many coating deposition techniques available. However, selecting the best depends on many parameters such as size, metallurgy of the substrate, adaptability of the coating material to the technique intended, level of adhesion required, and availability and cost of the equipment.

Although laser cladding has the potential for utilization in different industrial divisions for metallic coating, its application to metallic coating is limited due to the high cost and the low process speed. However, with improvement of laser efficiency, reduction in the cost of lasers, and the development of new generation of lasers such as high-power diode and fiber lasers, there is a strong potential for laser cladding to be widely used for coating applications in several major industries. Another indication of the potential of laser cladding for coating of a variety of materials is the increase in the number of published papers and reports concerning the technology in the recent years.

Laser coating of new components gives them surfaces with high resistance against wear, corrosion and high temperatures. It can be prepared on several types of base material. Most commonly the base materials used are unalloyed steels, alloy steels, hardenable steels, stainless steels, nickel or cobalt based alloys. Also various cast irons can be coated successfully by laser process. Laser coating offers a wide range of possible coating materials. Most commonly used laser coatings are various cobalt base hard alloys, e.g. Stellite 6 and 21, nickel based superalloys, e.g. Inconel 625, self-fluxing alloys, e.g. NiCrBSi, and stainless steels [8].



*Fig. 1.2: Laser cladding coating*

Ni-base superalloys are widely used in several industrial sectors, like petrochemical and power generation, due to their high performance in aggressive environment. Because of the high cost of Ni-base superalloy compared to stainless steel, they are reserved for these particular cases where the stainless steels are not suitable or when purity or safety are critically important. D.Verdi et al. [9] deposited a Ni-base superalloy Inconel 625 onto a medium alloy steel by laser cladding using a high-power diode laser.

Surface modification of engineering components for protection against corrosion is a critical field of research in the oil and gas industry. Inconel 625 exhibits high corrosion resistance and high ductility which make it a material of choice for surface modification of oil and gas components, especially those with stainless steel [10]. Laser coating can be regarded as real corrosion barriers, which can protect non-corrosion resistant base materials from corrosion.

The improvement of energy efficiency and power in turbomachines, used in aeronautical industry as well as in power generation industry, is related to the increase of their maximum work temperature, requiring the development of materials with high temperature resistance. A way to achieve high temperature resistance is the development of coatings with good high temperature performance suitable to work as thermal barrier coatings. B. Carcel et al. in order to improve Ti6Al4V high-temperature and its tribological properties, the deposition of TiAl

intermetallic coating on a Ti6Al4V substrate by coaxial laser cladding investigated [11].

Aluminum alloy is the most widely used nonferrous alloy in industrial and engineering fields because of its excellent properties such as high strength-to-weight ratio, high thermal conductivity and easy to shape. Nevertheless, the low hardness and low wear resistance limit the application of aluminum alloy in certain fields where stress and friction are severe. Surface modification technology can enhance the surface properties of metallic materials while retaining the original properties of the bulks and thus has been used extensively in engineering materials processing. Y.S. Tian and R.Ge et.al fabricated coatings containing nickel aluminide on Al alloy 2024 by laser alloying with pure Ni powder [12].

Sp.G. Pantelakis et. Al deposited a coating of Al-clad onto AA2024 for protecting the aircraft aluminum alloy 2024 against corrosion. The effectiveness of Al-cladding for protecting 2024 aircraft aluminum alloy against corrosion has been investigated experimentally by accounting for two different corrosion exposure environments [13].

Recently, the bioceramics coating on titanium alloys was also performed by laser cladding; the coated parts are then used in orthopedic implants with a calcium phosphate layer in order to promote the growth of the bone when the implant is inserted in the body. Laser cladding along with other laser surface treatment methods has also been examined for the production of glassy metallic layers, which provide superior resistance against wear and corrosion.

Laser coating applications include new production, spare part manufacture and as well as maintenance and repair of worn components and equipment. Laser coatings are used to produce surfaces resistant against abrasive, erosive and adhesive wear, wet corrosion, high temperature oxidation and corrosion [8]. Typical applications of laser coatings are:

- Shafts, rods and seals;
- Valve parts, sliding valves and discs;
- Exhaust valves in engines;
- Cylinders and rolls;
- Pump components;
- Turbine components;
- Sealing joints and joint surfaces;



- Tools, blades;
- Moulds.

### 1.3.2 Parts Repair and Refurbishment

The service lifetime of components such as high strength steel crankshafts can be increased significantly by laser cladding reconditioning.

Laser cladding has been applied predominantly to repair of higher value components, including tools worn engine parts such as cylinder heads and torsion shafts, injection moulds and extruder parts, cutting dies and nozzles. In particular the parts of the gas turbine engine need periodical replacement to avoid loss of power, efficiency and eventual breakdown. Among turbine components, the blades suffer from several damages during operation, which limit the overall life of the component: creep, life cycle fatigue and hot corrosion. Therefore, in terms of maintenance requirements, manufacturing difficulties and costs, the blades are the most critical item of today's gas turbines. As a result, blade manufacturing and maintenance companies are looking for repair technologies that not only repair the defected blades superiorly, but also maintain the original mechanical and metallurgical features of the repaired components. Infact, in most cases, repair is a more feasible solution than replacement, as replacement will be very costly.



*Fig. 1.3: Laser cladding repair*

A three-dimensional build-up can be achieved by deposition layer by layer.

This technology has been accepted by leading engine manufactures such as General Electric, Pratt & Whitney, Allied Signal, Rolls-Royce, Allison, Pratt & Whitney Canada, Solar and MTU.

Laser cladding can be used in different repair applications with specific requirements regarding weld bed geometry. In order to repair worn surfaces or to produce a hard facing layer, weld beads with a flat and wide geometry are advantageous. They can be deposited next to each other in order to cover a large surface. The repair of damaged volumes, e.g. tip repair for compressor blades, requires high and narrow weld beads. In order to adjust the laser cladding process for a specific repair task, knowledge about process parameters and their influence on clad bead geometry is necessary.

Conventional methods use welding to retrieve these damaged components; however, these methods are usually destructive due to the highly distributed temperature over the area of repair. This techniques, such as tungsten inert gas, metal inert gas, plasma and electron beam welding, usually cause a large amount of heat during weld metal deposition which results in large temperature increases in the body of the component. The temperature increases above certain limits cause the base alloy to be weakened. This weakening along with component distortion can cause irreversible damage to the part. In contrast to conventional weld repair, the laser cladding process transfers heat only to localized areas, typically using a 0.5 mm diameter laser beam. As a result, heat inputs are at least one order of magnitude lower than the heat input incurred during conventional welding, which results in reduced residual stresses and distortion and a substantially smaller heat-affected zone. Laser cladding can provide a permanent structural repair and refurbishment on many alloys (e.g., aluminum alloys) that are generally considered unweldable by conventional methods. The success of the laser cladding technology in this area is due to the small heat zone, rapid solidification, increased cleanness, lower dilution, and increased controllability over the depth of heat-affected zone.

As already written, one of the most relevant laser-cladding applications focuses on turbine components for aircraft industry. These parts are usually manufactured from thermally resistant superalloys, mainly nickel and titanium-based alloys [14].

B. Graf et al. used a full factorial design to determine the effect of process parameters on the geometric dimensions of the weld bead [15].

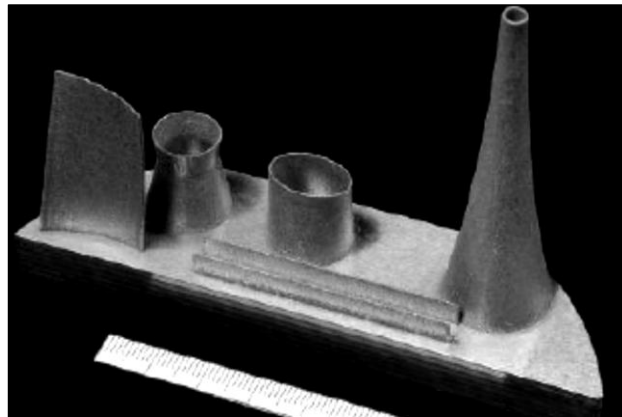
G.Bi et al. investigated a restoration of nickel-base turbine blade knife-edges with controlled Laser Aided Additive Manufacturing (LAAM) [16].

The size of the repair and refurbishment market is immense. The global market of the repair of aircraft engine turbines and compressor blades, used in civil and military applications, has been estimated to be about 1.2 billion dollars per annum [4].

### 1.3.3 Rapid Prototyping and Tooling

Concerning the manufacturing of aeronautic parts by means of the laser cladding technique, it is possible to begin from scratch or from a smaller pre-form, and start adding layers of material up to the final geometry. As no material is eliminated, the amount of necessary raw material is minimized, so the technique results in an environmental impact reduction as well as a moderation in costs, as opposed to competing techniques. Clad overlapping generates layers of added material that build up 3D complex geometries using the so called “layer by layer” method. Therefore, laser cladding can also be used as an additive manufacturing technology, achieving all the advantages of these methods as complete freedom of design, adaptation of the geometry to very complex shapes and very close to the final design, machining volume reduction.

In the figure 1-4 a turbine blade made through laser cladding process is presented.



*Fig. 1.4: Free form parts*

Clad overlapping generates layers of added material that build up 3D complex geometries using the so called “layer by layer” method. Therefore, laser

cladding can also be used as an additive manufacturing technology, achieving all the advantages of these methods as complete freedom of design, adaptation of the geometry to very complex shapes and very close to the final design, machining volume reduction.

A new and major application of laser cladding is in rapid prototyping (RP) and rapid tooling (RT) markets for rapid fabrication of complex components and tools. Rapid prototyping traditionally creates pre-production, three-dimensional parts in materials that are different to the intended production material or with different physical properties. This allows early visualization and evaluation of a part or structure.

Production of tools such as cutting tools, dies and molds, which have traditionally been fabricated by highly-skilled tool and mold makers using CNC and electrical discharge machining, has always suffered from cost problems and slow turnaround times for manufacturers. If tools are fabricated late, market opportunities will be missed, which is often the death knell for a new product. As a result, rapid tooling has received significant attention in recent years from manufacturers looking for technologies that are able to produce high-value tools and components with high integrity, high density, and good surface quality, at low manufacturing costs with a short manufacturing time. Rapid tooling techniques can be divided into two categories: indirect and direct. Indirect approaches use master patterns produced by additive manufacturing to produce a mould or die. There are many processes available, of which the most common are the “soft tooling” techniques, utilizing silicone moulds for plastic parts and as sacrificial models for investment casting of metal parts. Direct approaches produce the actual core and cavity mould inserts. The strength of the process is its ability to fabricate tools with otherwise unrealizable geometries.

The market for RP and RT is significantly large with a significant annual growth. The worldwide tooling market is estimated in the tens of billions of dollars per annum. The market size for RP was approximately \$800 million in 2002, when 4.5 million parts were produced by the available units in the market [4]. The applications of RP in North America are categorized within the following sectors: 25 percent consumer products, 24 percent automotive, 11 percent business machines, 11 percent medical, 8 percent academic, 8 percent aerospace, 5 percent government and 8 percent other. However, many of the customers for RP units are looking for a reliable metallic prototyping machine that will not only be intelligent enough to prototype the components without the need for highly

qualified personnel, but that will also be robust enough to produce the components with high quality [4].

Laser cladding technology has the potential to address the current gap for metallic rapid prototyping. Laser cladding has demonstrated promising capabilities for tools and components fabrication. A recent survey by the National Center for Manufacturing Science (NCMS) revealed that laser cladding could reduce the time of die production by 40 percent, if the process is controllable over the dimensions of the product. It has been reported that for the production of surgical tools, the technology can reduce 62 steps into 7 steps.

#### **1.4 The state of the art**

Laser material processing has been a really important impact for modern manufacturing engineering and a strong influence in the 21<sup>st</sup> century. Among all the laser material processing technologies, laser cladding has attracted a lot of studies over the past 30 years.

The invention of the first working laser by Maiman in the 1960's was a breakthrough in science [4]. Immediately after this invention, scientists claimed that the laser was the answer to a multitude of scientific problems. The first studies on laser cladding is generally considered to have been performed by Gnanamuthu at Rockwell International Corporation in Thousand Oaks of California in the 1970 when commercial multi-kW high-power industrial CO<sub>2</sub> lasers became available. A pre-placed laser cladding method was used to investigate the feasibility of the process in applying dense ceramic cladding to metallic workpieces [17].

At about the same time, several research groups around the world began projects to develop apparatus and systems for development and improvement of the process.

Among these groups, the real impact and precursory research work on laser cladding was performed by William M Steen and his colleagues first at the Imperial College, University of London, and then at Liverpool University, UK, in the 1980. He and his colleague invented the blown powder laser cladding technique [18] (the laser cladding and additive manufacturing method widely used nowadays for research and applications) and developed some fundamental methodologies such as sensors for in-process monitoring [19], calculation of powder catchment efficiency [20], the computer simulation model [21], the triple hopper powder feeder system for variable composition laser cladding [22],

cladding of aluminium alloys [23], surface coating for intergranular corrosion resistance [24], and the principle of layer-by-layer additive cladding for 3D manufacturing.

The other research group, led by Jyoti Mazumder, at the University of Illinois at Urbana-Champaign, Urbana, USA developed models for this process [25] and studied the mechanism of the process [26]. They also applied the technology to many metals and ceramics to investigate their potential for cladability, and also wear and corrosion resistance [27]. Mazumder and his group studied also the laser aided DMD to manufacture 3D component [28] and a closed loop system to control the process [29].

A review of the literature shows that the number of papers and patents related to this technology increased significantly in the 1980's. These papers disclosed the devices for enhancement of the technology, such as development of powder feeders, cooling systems, hemispherical reflecting device for re-absorbing the reflected light, etc. The applications of the technology for wear and corrosion resistant alloys were also reported by many research groups in the 1980's.

The features of this technology received attention from industry in the 1980's as well. Laser cladding was identified as a process with a significant edge over the conventional processes for wear and corrosion resistant coating.

The research projects being conducted by different industries were even ahead of academic projects. The first reported use of the laser cladding by industry was the hard-facing of Nimonic turbine blade interlock shrouds for the RB- 211 jet engine at Rolls Royce in 1981. In 1983, at Pratt and Whitney, the nickel-base alloy turbines of JT8 and JT9 engines were hard-faced using preplaced laser cladding. Hard-facing of turbine blade shroud tips and znotches by laser cladding continued to gain acceptance by different companies.

The technology was being accepted by leading engine manufacturers such as General Electric, Pratt & Whitney, Allied Signal, Rolls-Royce, Allison, Solar and MTU. From a commercialization point of view, several companies, such as Avco Everett Metalworking Lasers Inc. and United Technologies Industrial Lasers Inc. were established in the 1980's to address the needs of industry for metallic coating and repair in North America and Europe. In the automotive industry, laser cladding technology was transferred to the market for the engine valve seat coating by some European and Asian automotive companies, such as Fiat, Toyota, and Mercedes Benz [4].

In the component repair market, laser cladding brought a huge amount of consideration in the 1980's. Laser cladding was successfully utilized for rebuilding and coating of the H-dimension (airfoil section thickness) of worn turbine vanes, the tip of the turbine blades, and turbine bolts. A number of different companies and research groups around the world have utilized laser cladding technology for turbine blade repair, including Huffman Corporation and Gorham Technologies in the USA, Starrag in Switzerland, Sultzer in the Netherlands, SIFCO Turbine Components in Ireland, and many others [4].

The annual number of papers in scientific publications shows an exponential growth from several papers a year in the early 1980's to over 100 a year in recent years.

In a lot of papers laser cladding process is modelled to analyze the influence of the main cladding parameters process, such as laser power, laser speed, powder feeding rate, beam diameter, on the cladding geometric features, defects such as cracks and porosity, and microstructure.

About stellite 6L on SUH600-N base material, it was demonstrated that a short interaction time produces fine microstructures with low dilution, hence, higher hardness compared to a longer interaction time with coarse structure, relatively higher dilution and a lower hardness value. It was also shown that laser-induced thermal effects influence the microstructural evolution, deposition rate and dilution of the clad surface [30].

The solidification behavior and phase transformations occurring during the laser cladding a Ti45Nb coating on mild steel is also been studied. A premixed powder of 55 wt.% Ti and 45 wt.% Nb was used and the processing parameters were set to ensure a laser power density of  $\sim 970 \text{ W/mm}^2$  and an interaction time range of 0.022–0.080 s between the laser beam and the substrate. It was shown that at a constant power density, the interaction time controls the solidification behaviour during the process. For extremely short interaction (ESI) time range,  $0.024 \leq \tau \leq 0.027 \text{ s}$ , crack and pore-free coatings of excellent hardness (up to  $\sim 1000 \text{ HV0.05}$ ) containing  $\beta$  and  $\alpha''$  Ti–Nb based solid solutions and a  $\beta$ +Fe–Ti solid solution eutectic matrix can be made. However, processing at higher interaction times, i.e. at short interaction (SI) time range  $0.030 \leq \tau \leq 0.048 \text{ s}$ , results in the formation of additional brittle intermetallics, including an FeNb  $\mu$  compound and an Fe<sub>2</sub>(Nb,Ti)  $\epsilon$  compound, while only  $\epsilon$  forms at the highest interaction times, i.e. long interaction (LI) time range  $0.060 \leq \tau \leq 0.080 \text{ s}$  [31].

The geometry of the powder flow is also been analysed. The manner with which the composite powder particles injected into the laser formed molten pool decides the deposition quality in a typical laser-based powder deposition of composite material. Since, the morphology and physical properties of nickel (Ni) and tungsten carbide (WC) are different their powder flow characteristics such as the powder particles stream structure, maximum concentration at the converging spot, and the powder particles velocity are noticeably different. In the current study, a computational fluid dynamics (CFD) based powder flow model is established to characterize the coaxial powder flow behavior of Ni–WC composite powders. The key powder flow characteristics such as the stand-off distance, the diameter of the powder stream at the stand-off distance, and the velocity of the powder particles are measured using three different vision based techniques. Both the numerical and experimental results reveal the exact stand-off distance where the substrate needs to be placed, the diameter of the concentration spot of powder at the stand-off distance, and a combination of suitable nozzle angle, diameter, and carrier gas flow rate to obtain a maximum powder concentration at the stand-off distance with a stable composite powder flow [32].

Another group's research developed a model to estimate the clad width, depth and height, having taken into account the process speed and the powder feed rate. For estimation of the clad characteristics the approach was based on the phenomenon of the surface tension, assumed to be dominant in the clad formation. The theoretical approach showed a maximum deviation of 13% for the clad width, 25% for the clad depth and 30% for the clad height for low and medium process speeds. Thus, the analytical model had better accuracy in the estimation of the clad

depth and width. However, the clad height was the least important dimension since it was usually the subject of subsequent conventional machining [33].

To understand the influence of process parameters, deposited layer thickness, micro-hardness, and porosity were analyzed using statistical techniques. The results show that the process window to produce sound samples with dimensional stability and microstructure integrity is very narrow. Micro-hardness data shows that the deposited region generally has uniform distribution of hardness with minimal variation. It was found that with the feedback control of laser power, layer thickness and pore/void are strongly affected by powder mass flow rate. While higher powder feed rate leads higher possibility of pore formation, the analysis result also predicts higher probability of producing actual



layer thickness. The predicted model by the statistical techniques concludes that the interacting effect between layer thickness setting and powder mass flow rate is significant. Dilution, porosity, microstructure, and composition were investigated for the material characteristics of deposited H13 steel. Dilution depth to the substrate is minimal and has few effects on the composition of the final products. The pore interval is very close to the overlap percentage of the process. Optimization of overlap percentage as well as proper control of powder flow rate is essential to reduce the possibility of pore formation. Microstructure shows the difference of dendrite growth between upper and lower zone of sample due to the cyclic heat dissipation. Quantitative chemical composition of deposited steel is almost the same as that of utilized steel powder [34].

An inappropriate combination of laser power, scanning velocity or pre-placed powder height can result in the formation of incomplete fusion interface between the cladding layer and substrate, or reheat cracking along the coarse grain boundary in the heat-affected zone (HAZ) after ageing treatment. The laser-clad layer with required sizes, metallurgical bonding and defect-free can be obtained by optimizing laser power, scanning velocity and pre-placed powder thickness [35].

In order to decrease experimental effort, a design of experiment is used to determine the effect of process parameters on the geometric dimensions of the weld bead. With Nickel based superalloy it is noticeable that a low velocity leads to a larger effect for powder mass flow, therefore a higher increase of bead height when increasing powder mass flow [36].

A large surface can be coated by the overlap of the single clad. A recursive model has been developed for the calculation of the geometry of the coatings formed by the overlap of cladding tracks. Input parameters for the model are geometrical characteristics obtained from the single track experiment. It is a simple model leading to realistic results in practice. The model is based on a couple of physically sound assumptions taking into account the most important characteristics of the cladding process. The model gives an excellent agreement with experimental results for a wide range of parameters and initial conditions of laser cladding. In general the parabolic function shape leads to the most accurate predictions of coating thickness, waviness and cladding angle, although in some cases different functions are also suitable. The model can be easily modified for cladding processes with a changing efficiency of addition of new material in each

step, as well as for 3D manufacturing processes, where the bulk objects are built layer by layer [37].

The importance of laser cladding process is recognized by many industries and research groups. Infact, maintenance, repair and overhaul are required as an alternative to part replacement, to the purpose of cost reduction [15]. In this terms, the potential of this technology is really significant, therefore nowadays a lot of research groups continue to contribute to its growth through research programs and training of students in laser cladding techniques technology.

## Chapter II

# Laser Cladding process

In this chapter, the laser cladding process is analysed in terms of process parameters and responses. First of all a basic description of the process is presented with a classification of the technology: laser cladding technology could be carried out in one step and two steps. The feeding deposited material could be powders, wire or paste.

### 2.1 Laser Cladding Technique

Laser cladding is one of the most important types of laser material processing, in which a laser beam irradiates the cladding materials added and the surface of the substrate moved by a positioning device. As a result of additive material, a thin layer called a “clad” is produced on the substrate. Therefore, for this investigation, the laser cladding process can be defined as a surface treatment process in which a suitable coating material, with the desired properties, is fused onto the surface of a substrate material through the interaction with a laser beam in order to improve the surface properties of the substrate material or to repair a component.

The two main laser cladding techniques are:

1. Two-step process (pre-placed laser cladding)
2. One-step process

In the one-step process, an additive material is fed into the melt pool created by the laser beam. The one step process is more often used in industry due to the higher flexibility of this process. The cladding material is transported by a carrier gas.

The additive cladding material could be feeding in the following different forms:

- Powder
- Wire
- Paste

Among this additive material, powder is the most frequently used. Powder is blown directly into a laser generated melt-pool as it scans across the surface of the substrate. The powder melts and a clad track is built up. Complete coverage is achieved by overlapping the tracks.

In the two-step process the added cladding material is generally in the form of powder. Powder is pre-placed on the substrate until it is melted by the laser beam. Therefore, the first stage consists of a layer of coating material being placed before laser irradiating. It is then melted with the substrate material by the laser beam in the second stage of the process.

The whole process is normally shrouded in an inert gas such as argon.

Powder injection cladding is a more robust method than wire and paste cladding, because there is no direct contact with the melt pool, and the laser beam can pass through the stream of powder particles instead of being obstructed by the wire or paste.

In the following, we analyse the different laser cladding methods with the several issues involved; then we concentrate on laser cladding by powder injection for the rest of this chapter and of the thesis.

### **2.1.1 Two-step process: pre-placed laser cladding**

Pre-placed laser cladding is a simple method used for coating and prototyping. Laser cladding with preplaced powder is the most common two stage cladding method. Several issues are involved in this process. The pre-placed powder particles on the substrate must have not only enough bonding to the substrate, but also enough cohesion to each other. It is necessary to prevent the powder particles on the substrate from removing due to the gas flow during the melting in the second step of the process. To overcome this problem, the powder is usually mixed with a chemical binder to ensure its cohesion with the substrate during the process. The chemical binder evaporates during the process. This can result in some porosity in the clad layer [4].

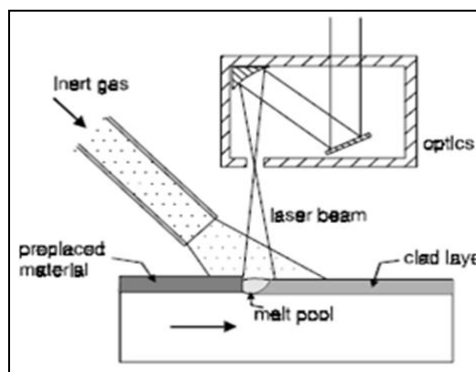
However, the pre-placed layer method is widely applied in current studies of the following advantages [38]:

- A wide range of materials can be easily mixed and used;

- Lower powder loss rate;
- Higher laser absorption rate on the rough surface of the pre-placed layer;
- Less hazardous process.

The bonding method is commonly used to prepare the pre-placed layer using a binder in laboratory investigations because of its simplicity, flexibility and no requirement for equipments.

Xiang et al. [39] produced the pre-placed layer by using the following process: NiCr/Cr3C2 powders and 20% (mass fraction) CaF2 powder were mixed with acetyl cellulose alcohol, which were then pasted onto the substrate surface to form a pre-placed layer with approximate 1.0 mm thickness. Zhang et al. [40] placed the mixed powders onto the specimen surface homogeneously to form the pre-placed layer (around 1.0 mm thick) by using the sodium silicate binder. Wang et al. [41] mixed powders with a small amount of organic binder and prepared an approximately 1.2 mm thick layer on the steel substrate. Wu et al. [42] prepared the pre-placed layer using the following method: the powder was dry-mixed for 2 h in a ball mill, and then applied on a Ni layer of steel substrate surface with the help of a specific quantity of organic binder. Shang et al. [43] mixed a NiCrBSi-type alloy powder (Ni60B, Stellite, Shanghai, China) with a bonding agent (MicroBraz Cement 510) and applied the mixture to the Cr5 steel substrate surface to form a pre-placed layer (approximately 1.0 mm thick). However, a large amount of binder used in the method may decompose into gas, which will deteriorate microstructure and reduce mechanical properties of the coating [44].



*Fig. 2.1 Pre-placed Laser Cladding.*

In the second stage of the process the following phenomena occur:

1. Formation of a melt pool in the top surface of the coating material due to the radiation of laser beam;
2. Expansion of melt pool to the interface with the substrate due to the heat conduction
3. Continued heating ensures that the melt pool is extended to the substrate and that a strong fusion bond is achieved.

The heat input must be well controlled to prevent deep melting of the substrate and the resulting severe dilution on the one hand, and to achieve a strong fusion bond on the other hand.

The two stage methods are particularly useful for parts that can be treated in one single track. It is of course possible to apply several adjacent tracks, but this will result in an increased dilution. Before the first clad track is produced, the entire area is covered by the preplaced material anymore. When the next track is made, the non covered part of the substrate is directly irradiated by the laser beam. Deeper melting of the substrate will occur in this area [45]. The pre-placed layer thickness has a significant effect on the quality of the laser-clad coating. The pre-placed layer thickness has a significant effect on the quality of the laser-clad coating. It determines directly the final thickness of the coating, which affects its service life when applied as an engineering tribological component. Moreover, the pre-placed layer thickness can affect the chemical compositions of the molten pool because of the change in dilution rate. As a result, microstructure and mechanical properties of the coating exhibit the corresponding changes [46].

### **2.1.2 One-step process**

The one-step process starts with the formation of a melt pool in the substrate. Simultaneously added cladding material is fed into this pool and melts; a strong fusion bond between coating material and substrate is achieved immediately.

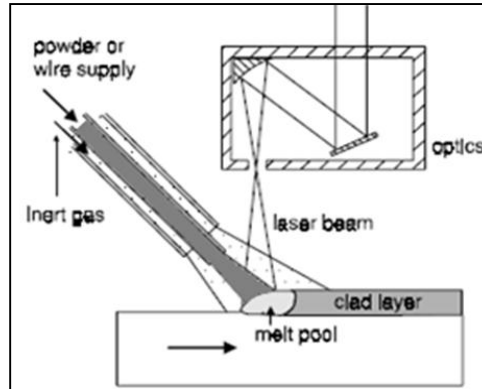


Fig.2.2 One-step proces.

The one-step process has several other advantages over the two step process [45]:

- Larger area which require the application of several adjacent tracks can be produced with less dilution. Contraction of the clad layers on cooling down still occurs, but, because material is fed to the substrate next to the previous track, no part of the substrate is irradiated unnecessarily;
- The coating thickness can be varied on-line by controlling the material feed rate;
- Products with a complex geometry can be treated, because material is fed continuously to the interaction zone. Therefore, flowing out of the molten material by gravitation is not problematic anymore.

One-step laser cladding process can be categorized into three methods:

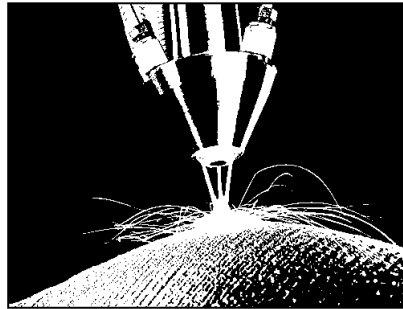
1. powder injection;
2. wire feeding;
3. paste laser cladding.

The common feature of all three methods is the feeding of deposited material in the presence of the laser.

### 2.1.2.1 Laser cladding by powder injection

The injection of powder into a laser generated melt pool is a much more common method compared to other. In laser cladding by powder injection,

powder particles are fed into the heat zone to produce a layer of clad. The method is more flexible: it allows the on-line variation of clad dimensions and clad composition and, many more elements and alloys are available as powder than as wire.



*Fig. 2.3 Laser cladding by powder injection.*

Powder injection cladding is a more robust method than wire cladding, because there is no direct contact with the melt pool and, the laser beam can pass through the stream of powder particles instead of being obstructed by the wire.

Three different concepts of powder injection are possible:

- Off-axis powder injection (a single powder stream is fed lateral into the laser beam);
- Continuous coaxial powder injection (a powder stream cone is produced which encloses the laser beam);
- Discontinuous coaxial powder injection (three or more powder streams are fed coaxial to the laser beam).

This three different powder injection are analysed in the next chapter through a description of the different nuzzles available.

We will address the laser cladding by powder injection process in depth throughout this thesis, in particular in the experimental section.

### **2.1.2.2 Laser Cladding by wire feeding**

In laser cladding by wire feeding the wire is used instead of powder. The wire is usually fed through a ceramic drum containing the desired material wire. Due to the nature of feeding mechanisms, it is essential to use a wire that has been straightened and stored without plastic deformation to ensure stable transport without vibration.





*Fig.2.4 Laser Cladding by wire feeding.*

Wire feeding can be useful for the cladding of rotationally symmetric products that can be clad in one continuous track. The positioning of the wire to the substrate is a critical aspect of the process for two reasons:

- The wire is usually in direct contact with the melt pool in the substrate. In order to not disturb that melt pool the process requires the use of an accurate wire positioning system and an accurate control of the wire feeding rate;
- The substrate is partly shielded from the laser beam by the solid wire. To allow a good quality clad layer, i.e. one with a good bonding to the substrate, flown out and a smooth surface, a ratio between beam diameter and wire diameter of at least a factor three must be used. The wire must be well aligned to the centre of the laser spot to ensure the formation of a symmetrical clad layer.

The use of a rotating wire feeding heads allow cladding with a constant angle between wire and substrate as well as a constant angle between the injection direction and the relative movement of the substrate [18].

However, compared with powder fed methods, laser cladding with wire has the potential to give cleaner process environment, higher material deposition efficiency, improved surface quality and reduced material wastage which serve to improve process economy. The tendency for pore formation as a result of entrapment of air bubbles in the feed powder particles is significantly reduced in wire feeding system. Also, dilution control by increasing material deposition rate can be easily achieved in wire feeding system with negligible material wastage [10].

Moreover, metal wires are cheaper than metal powders, and also wire feeding wastes less material than powder feeding.

In conclusion, we can say that a successful process strongly depends on the process parameters.

### **2.1.2.3 Laser Cladding by Paste**

In laser cladding by paste, a stream of paste-bound material is deposited on a point of the substrate that is usually a little bit ahead of the laser beam. The paste consists of the hardfacing powder with a suitable binder. However, the binder must be dried in a short period of time while the hardfacing material in a compact form is still kept; otherwise powder particles are blown away by the shielding gas.

For this process, a special paste feeding system should be designed. Some researches designed and implemented a paste feeding system along with a cooling system to protect the paste from thermal emissions from the process zone. The shape of paste on the substrate is controlled by paste feed rate and substrate speed. To have a good clad quality, it is essential to optimize these parameters. A poor paste supply or too high process speed causes high dilution and low track height if the laser energy is kept constant. An oversupply of paste on the substrate increases pores formation since evaporation of the binder is inhibited, and it increases the loss of hardfacing material.

High porosity, extreme sensitivity of the process to disturbances, and difficulties in paste feeding mechanism are troublesome conditions of paste laser cladding.

## **2.2 A scheme of the process**

Laser cladding process is influenced by a lot of processing parameters which are also correlated to each other. Therefore, the process results to be really complex so that the relationship between the variables and the effect of the parametric processing on the process results must be analysed and modeled. In the figure the physical and process variables that affect the clad results are shown.

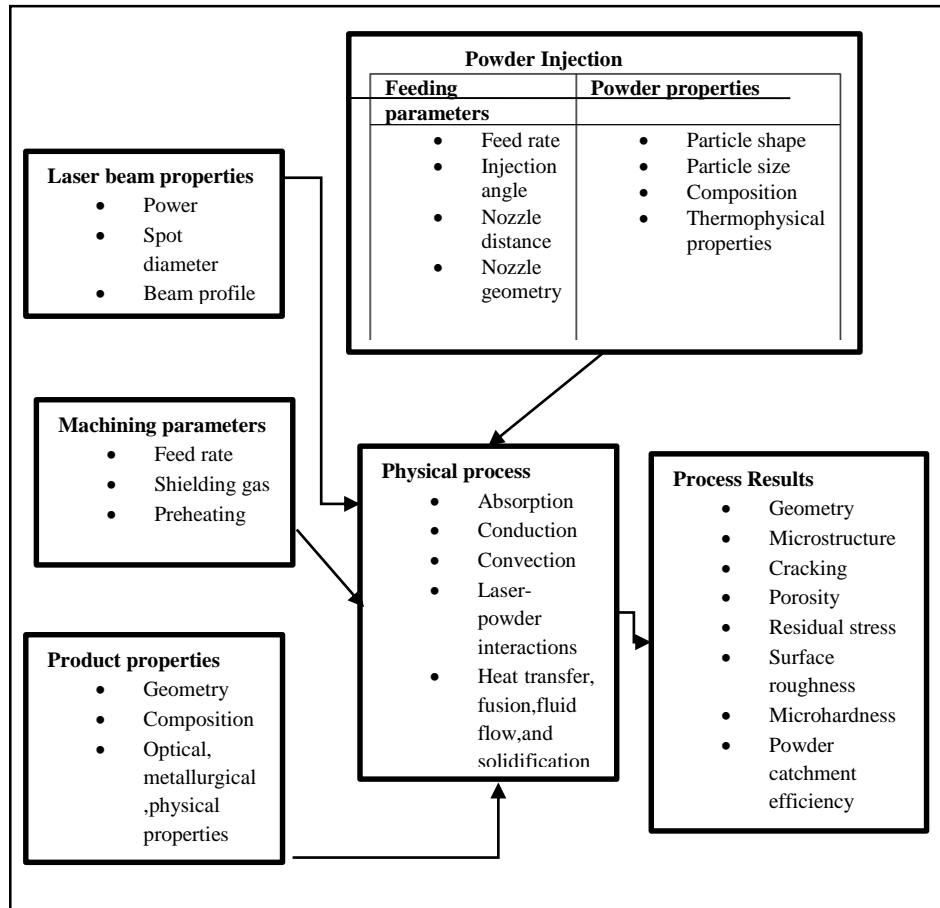


Fig. 2.5 A scheme of the process.

The process parameters regarding the laser beam properties and the machining parameters will be discussed in the next chapter, where the laser cladding equipment is described. The feeding parameters depend on the nozzle configuration, therefore also these variables are presented in the next chapter.

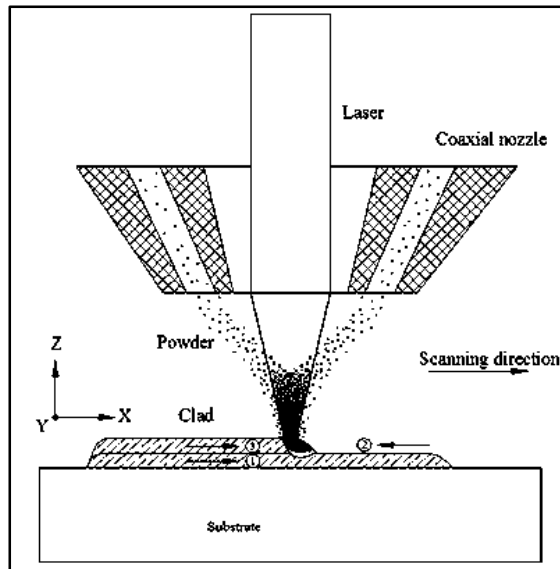
In the next paragraph, the physical process and the most important process responses are analysed.

### 2.2.1 Physical process

Laser cladding is essentially a fusion and solidification process, which involves complicated interactions between the laser beam, metal powders, the base material (substrate), and processing gases.

Contrary to refusion, the cladding process control is difficult because of the interactions between the laser beam, the powder particles and the melted regions. Indeed, even if the greater part of the laser power reaches the workpiece, a fraction is captured by the powder particles, which are thus heated. And only the powder particles that strikes the melted bath are then stucked, whereas the particles that strikes the solid region undergo a ricochet and are then lost.

Considering a coaxial powder injection laser cladding, the melt pool, under the irradiation of a laser beam, is free to deform due to surface tension and other forces. The substrate is stationary in a three-dimensional Cartesian coordinate. A focused laser beam propagating in the negative Z Direction is striking on the substrate and moving at a constant speed in the positive X direction.



*Fig.2.6 Laser and powder interaction.*

The origin is set on the top surface of the substrate and initially coincides with the center of the laser beam. Powders are delivered onto the substrate concentrically with the laser beam [47]. The process can be divided in three phase:

1. The laser beam, when passing through the covered coaxial power stream, loses energy by reflection and absorption on powder particles.

2. A small area of substrate surface under the irradiation of the laser beam gets heated and melted, and forms a molten pool.
3. A clad track is formed solidified from melt pool with the scanning of the laser beam and continuous powder addition.

The physical phenomena produced in the processing zone are essentially the heat conduction, the Marangoni thermocapillary flow, the interaction between the powder and the melt bath, the mass transfers and diffusion, the laser-powder interaction, and the laser-work-piece interaction. Typical physical phenomena in laser cladding include **laser-powder interactions, heat transfer, fusion, fluid flow, and solidification.**

#### **2.2.1.1 Laser-powder interactions**

The absorbed laser power by the workpiece results from the fact that before the laser beam reaches the surface of the workpiece, it crosses the powder flux which reduces a part of the energy which goes in powder particles heating. The total quantity of absorbed power by the work-piece relatively to the laser beam supplied power is given after considering the effect of beam attenuation due to the powder shielding. The particles of powder absorb a part of the attenuated power and restore it to workpiece unless they strike and penetrate the melted bath. The reflected power at the surface workpiece is important and it is also attenuated by the incident particles of powder which absorb a part of the reflected power. The decrease in laser power due to transmission of the laser beam through the powder cloud is not entirely lost. Some of the lost energy heats powder particles and a portion of this thermal energy is returned to the molten pool by particles that are incident on it.

The laser beam when passing through the concentric powder stream from a coaxial nozzle as shown in figure gets attenuated by absorption, reflection, and scattering effects of the particle stream. Meanwhile, powder particles experience temperature rise and even phase changes fusion and vaporization before reaching the substrate.

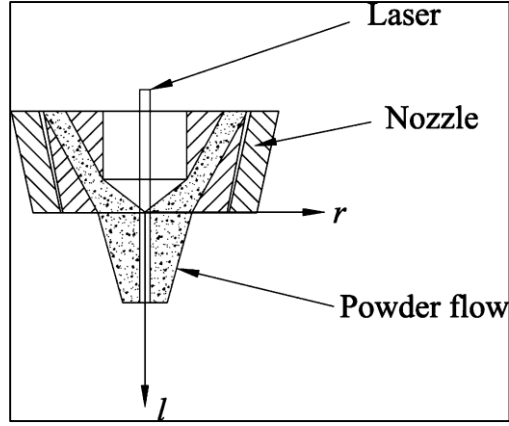


Fig.2.7 Spatial concentration profile of a converged coaxial powder flow.

It has been verified experimentally that the spatial concentration profile of a converged coaxial powder flow can be approximated by a Gaussian distribution as defined in the following equation:

$$N(r, l) = N_{peak}(l) \exp\left(\frac{-2r^2}{R_p^2}\right)$$

where  $N$  is the number of powder particles in a unit volume and is a function of radial distance  $r$  and axial distance  $l$  in an axial-symmetrical coordinate,  $N_{peak}$  is the peak concentration at the center of powder flow (where  $r=0$ ), and  $R_p$  is the effective radius of the powder stream at axial distance  $l$ .

According to the Beer-Lambert law, the attenuation of laser beam intensity after passing through a distance  $l$  in the powder flow can be expressed as:

$$q'_l(r, l) = q_l(r) \exp(-\sigma_{ext} Nl)$$

where,  $q'_l(r, l)$  is the new (attenuated) laser power density,  $q_l(r)$  is the original power density, and  $\sigma_{ext}$  is the mean extinction area of powder particles. Laser power attenuation can be calculated step by step along the axial axis (from nozzle exit to the melt pool surface), where the attenuated laser power density of the upper layer is used as the incident power density of the adjacent lower layer.

The powder particles get heated when absorbing the laser energy. The temperature rise of the powder particles can be calculated with the following heat balance equation:

$$q'_l(r, l) \alpha_p \pi r_p^2 \frac{\Delta l}{v_p} = \frac{4}{3} \pi r_p^3 \rho_p C_p^p \Delta T$$

where  $\alpha_p$  is the absorption coefficient of particles,  $r_p$  is the radius of the particle,  $v_p$  is the particle velocity,  $\rho_p$  is the particle density,  $C_p^p$  is the specific heat of the particle, and  $\Delta T$  is the temperature rise of particles. The temperature rise of particles can also be calculated layer by layer along the axial axis using the attenuated laser power of each layer.

Increasing the powder flow rate or the laser powder interaction distance, nozzle standoff distance, the attenuation of laser power increases. Huan Qi et al. [48] show that the total attenuated laser powers are in the range of 7%–21% of the original laser power with a 6–12 g/min powder flow rate and a 7–10 mm interaction distance. It can be seen also that a portion of the powder flow within the radius of 0.2 mm is already in the molten status when reaching the melt pool. The achievement of the vaporization temperature depend on the powder velocities. At a certain value of powder speed the flying powder particles begin vaporizing upon reaching the melt pool. To maintain powder capture efficiency and avoid undesired plasma formation, the vaporization of the powder should be avoided. Plasma effects can be further minimized through the use of shielding gases, such as helium, for example [48].

According to BY Y. S. LEE et al. with reference to the substrate, the power balance can be expressed as:

$$Q_a = Q_l - Q_{rs} - Q_p - Q_{rp} - Q_{Radi.} - Q_{Conv}$$

where  $Q_a$  is power absorbed by the substrate,  $Q_l$  is total power in the laser beam,  $Q_{rs}$  is incident laser power reflected by the substrate,  $Q_p$  is power absorbed by the fraction of the powder stream that is not included in the clad deposit,  $Q_{rp}$  is power reflected from the powder stream,  $Q_{Radi.}$  is power lost from the substrate by radiation, and  $Q_{Conv.}$  is power lost from the substrate by convection.

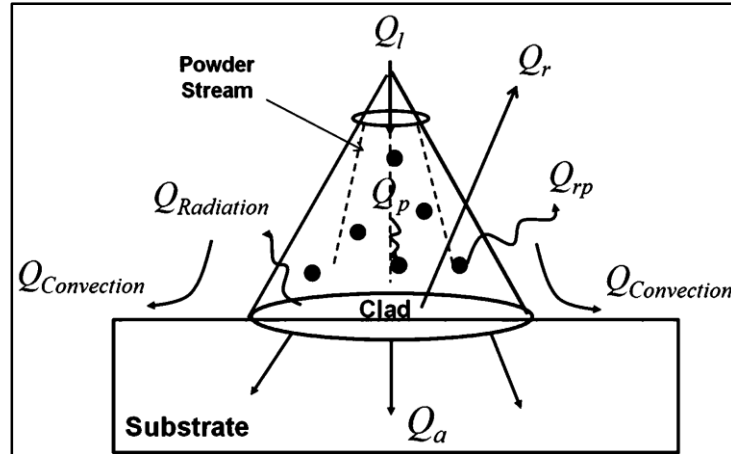


Fig.2.8: Power balance equation.

An experiment measurements of the power losses reported this values: 9% for  $Q_{rp} + Q_p$ , 1% for  $Q_{Radi.} + Q_{Conv.}$ , and 52% for  $Q_{rs}$ . From the values, the fraction of laser power absorbed by the substrate is  $Q_a = 38\%$ . Notice that the reflection from substrate and powder stream are the largest losses from the cladding process.

### 2.2.1.2 Heat transfer, fusion, fluid flow, and solidification.

If the input energy is not enough, only the melted powders are deposited on the cold substrate and solidified instantly. The input energy is not enough to cause a melt pool on the substrate in this case.

When the input energy is increased, the molten pool is formed. Because of the large surface temperature gradient, the liquid in the molten pool flows outwards from the center area. The strong fluid flow inside the molten pool causes the formation of a fluctuating cladding surface. A thin layer of substrate gets melted after the molten pool is fully developed, which makes the fluid flow extend into the substrate. A good metallurgical bonding can be formed in this case [48].

The creation of the **melt pool** during the laser cladding is due to melting of the substrate and the powder impinging on and being assimilated into the melt pool. The melt pool (or molten pool) is the region of superheated molten metal in proximity to the laser/material interface typically in the form of a spherically shaped droplet that moves at the traverse speed. The negative correlation between powder mass flow and melt pool depth can be explained by the thermodynamics of the melt pool. With the increase in powder mass flow rate, the amount of heat



absorbed by the substrate is decreased due to shadowing effect of the powder and the energy required to assimilate it to the melt pool. This causes the decrease in depth of the melt pool inside the substrate. Laser beam melts the surface to a specific depth  $Z$ .

Upon this heating the melted layer affected by the pressure of the transporting gas stream begins to move countercurrent to the scanning direction. When the accelerated melt reaches the opposite solidified side of pool it is rejected from it (combined effect of rejection force and gravity) and returns to the center of melted zone. Here the melt is mixed with a fresh melt and a turbulence flow in the plane parallel to the laser beam scan direction, shown schematically in the figure, is formed.

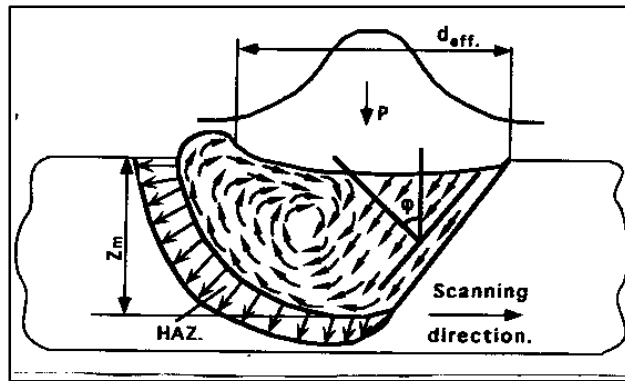


Fig.2.9: Melt pool characterizations.

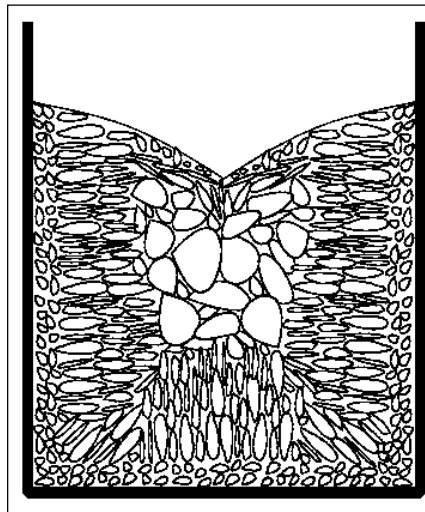
Any formation of porosity resulted from the absorption of gas with the powder particles and turbulence movement of the liquid under the gas jet action. It is very interesting both in scientific and technological aspects to try to estimate the velocity of the liquid within the melt pool. For this purpose the following equation can be used.

$$v_1 = \sqrt{2c_s P / S\rho\lambda}$$

where  $v_1$  is the velocity of the liquid melt motion,  $c_s$  is sound speed in the metal,  $P$  is the power of heating source,  $S$  is the immediate value of effective heated area,  $\rho$  is the density,  $\lambda$  is the specific enthalpy of evaporation.

A thin layer of substrate gets melted after the molten pool is fully developed, which makes the fluid flow extend into the substrate. A good

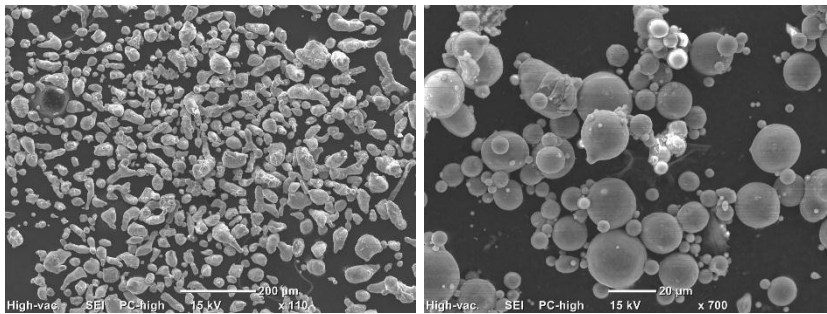
metallurgical bonding can be formed in this case between the substrate and the powder. In metal alloys, it is known that **solidification** morphology is significantly affected by the combination of temperature gradient ( $G$ ) in the liquid at the solidification boundary and solidification rate ( $R$ ). A planar growth mode occurs when  $G$  is very high or/and  $R$  is extremely low value. As  $R$  increases, the solidification morphology can shift to cellular, columnar, and then equiaxed dendritic. Most metal alloys solidify in cellular or columnar dendritic mode. The cellular and columnar growth modes are produced when the growth of crystal structures occurs without formation of any secondary dendrite arms. If additional dendrite arms form, the solidification mode shifts to dendritic. Equiaxed dendritic morphology is possible only when  $G$  is very low. As the cooling rate, which is the product of  $G$  and  $R$ , increases, finer microstructures are produced. Note that high cooling rate results in much closer spacing between cellular or dendrite arms. Eventually, the finer microstructure leads to increased mechanical properties. In general, it is known that cooling rate in laser cladding varies with the processing parameters and is faster than that of conventional casting [49].



*Fig.2.10. Crystal structures as a function of the temperature gradient and rate solidification.*

### 2.2.2 Particles powder

Powders can vary in size and shape and in terms of how they are produced. For most laser cladding applications, the powders are larger in size compared to those used in laser sintering processes. For laser cladding, it is common to see powders range between 10 and 100  $\mu\text{m}$  and are typically spherical in shape. Spherical-shaped particles can reduce any entrapment of inert gas within the melt pool and can thus lead to a final part with less porosity. Powders for alloyed materials will consist of all alloyed constituents as they are produced from the alloyed metal in its molten state. Gas atomization, water atomization and plasma rotating electrode processes (PREP) are typical means for producing powders effective for laser cladding application. The particle feed rate is the average mass of particles leaving the nozzle with respect to time and can range between 1–10 g/min (grams per minute) [50].



*Fig. 2.11: Powders particles: fine and spherical morphology.*

The particle size has a significant effect on the superheating of the blown powder during the laser cladding process. Since smaller particles possess a lower thermal capacitance, they can heat up much quicker. For instance, for coaxial DLD of Ti-6Al-4V, 25  $\mu\text{m}$  diameter particles can achieve a maximum temperature on the order of 1350 K while 45  $\mu\text{m}$  diameter particles only heat up to approximately 900 K [51].

Griffith et al. found that smaller particle sizes ( $-325$  mesh) result in a more stable melt pool for Inconel 625 during DLD [52]. Larger particles with a wider range of sizes ( $-80$  to  $+325$  mesh) were found to provide for an unstable melt pool that was highly agitated confirming the occurrence of free surface

instability. The agitated motion of the melt pool was attributed to the larger momentum inherent to the larger particles resulting in larger displacements in the melt pool and thus oscillations along the free surface.

The particles powder size affect also the dimension of the spot size of the powder flow. Analysis of the powder streams exiting the nozzle, showed that when the coarsest powder was used, the powder focus was greater than 1.5 mm in width. When the finest powder was used, a very small powder focus of approximately 0.5 mm was obtained. Though a very small powder focus was achieved in the powder with the smallest particle size range in this case a low deposition efficiency was found. During observation of the powders exiting the nozzle, it was evident that in this case the powder from appeared to pulse. This could be due to the finest particles which have diameters less than 20  $\mu\text{m}$ , coagulating within the nozzle, due to their large surface area, resulting in the blocking of the nozzle.

Two obvious effects are influenced the efficiency: smaller particle sizes can be focused more easily resulting in better efficiencies and larger deposits. If the particle size is too small however, problems with powder delivery can occur causing a reduction in deposit height and efficiency.

Coarse powder produced high surface roughness values, because of the large powder particle sizes involved [53].

A lower grain size distribution affects the flowability and has an influence on the powder stream stability at the output of the nozzle: the jet was not constant and many construction defects have been observed. Moreover this powder is porous and the manufactured parts showed a large amount of pores [54].

### **2.2.3 Carrier gas**

Powder is delivered to the laser deposition line via a carrier gas. Generally it is an inert gas, Argon or Helium. The pressure and the flow rate have an important effect on the physics of the process.

A high carrier gas flow rate has the effect of increasing the overall depth of the pool, compared to a low flow rate during both pulsed and continuous wave deposition. It can be seen that in continuous wave deposition the area of the melt pool produced with a high carrier gas flow rate is larger than the area produced with a low gas flow rate.

It is also noted that a high velocity of carrier gas flow causes increased surface agitation/disturbance at the melt pool surface and decreased surface roughness. Increased surface disturbance this time assisted by the speed of incoming particles at high flow rates may again increase assimilation reducing surface roughness by reduction of partially assimilated particles.

The effect of carrier gas flow rate on melt pool depth suggest that the increase in carrier gas flow rate increases the speed of powder hitting the melt pool that leads to deeper but shorter melt pool. But this increase in depth of the pool is numerically less significant than the reduction in length of the pool. This can be attributed to the change in powder flow characteristics and ricocheting powder [55].

The main cooling mechanism for mid-flight particles is forced convection with the carrier/shielding gas. The presence of this gas will additionally impact the particle momentum by introducing drag force on the material jet stream and can therefore result in particle deceleration and instability during flight.

Values of the mean surface disturbance in the case of high carrier gas flow rate are almost double the values obtained in the case of low carrier gas flow rate for both modes of laser operation.

The mean surface roughness is higher with a low velocity of carrier gas flow than with a high velocity of carrier gas flow.

A higher value of carrier gas flow rate increases the divergence of the powder stream from the nozzle exit and subsequently reduces the powder concentration.

Not only the carrier gas flow rate, but also the carrier gas pressure has an important effect on the laser cladding process, in particular on the melt pool formation. The main force operating on the melt pool surface is the pressure of carrier gas. The numerical estimations show that surface tension produces a pressure of about  $10^3$  Pa on the melt pool surface. However, the carrier gas delivers a pressure of  $(1-2) \times 10^5$  Pa on the melt pool surface that is several orders of magnitude higher than the pressure provided by surface tension. Obviously, the force affecting the melt pool surface, which are related to the carrier gas, lies in the plan parallel to the laser beam scan direction. The fact that its value is much higher than that of surface tension suggests that melt motion within the pool will occur in the plane of this force action, i.e. in the plane parallel to the laser beam movement direction. Thus, the carrier gas pressure must dominate the vertical flow of melt. Laser beam melts the surface to a specific depth  $Z$ . Upon this heating

the melted layer affected by the pressure of the transporting gas stream begins to move countercurrent to the scanning direction. When the accelerated melt reaches the opposite solidified side of pool it is rejected from it (combined effect of rejection force and gravity) and returns to the center of melted zone. Here the melt is mixed with a fresh melt and a turbulence flow in the plane parallel to the laser beam scan direction is formed.

#### 2.2.4 Process results

The properties of clad layers analysed are:

1. Porosity;
2. Powder catchment efficiency;
3. Surface finish;
4. Surface hardness;
5. Tensile and yield strengths;
6. Residual stress.

It is so difficult to produce a clad layer which meets all requirements. Usually a balance has to be found between several properties. An example is the reduction of crack formation in the clad layer by preheating the substrate. The preheating reduces the cooling rates and the resulting residual stress. Consequently, crack formation is avoided but the hardness is reduced.

In the following, some of this process responses are analysed.

##### 2.2.4.1 Porosity

Pore and void formation is a problem that has been identified in laser cladding process and can be divided into three categories:

- a. Inter-track
- b. Inter-layer
- c. Intra-layer

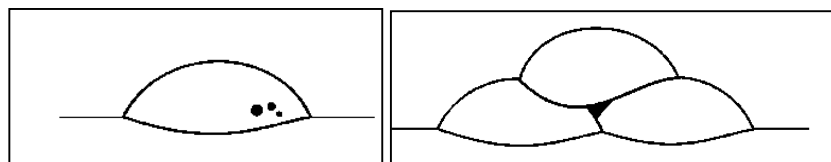


Fig. 2.12: Intra-layer and inter-track pores.

Inter-track porosity is caused by the horizontally aligned or offset tracks of incompatible aspect ratios and forms near the base of deposited tracks.

Inter-layer lack of fusion porosity is caused by incomplete bonding between vertically aligned deposits. Factors that could lead to this include inappropriately low or inconsistent specific energy, misplaced tracks and an oxide layer preventing or hindering fusion.

Intra-layer porosity is often spherical areas of porosity within a layer. It is most commonly attributed to small amounts of trapped gas in the powder particles, but a study of laser welding indicated that it can also be caused by the moisture present in industrial-grade shroud gases.

#### **2.2.4.2 Powder catchment efficiency**

Powder catchment by the melting pool is decided by a number of parameters, and is expressed by catching efficiency  $\eta$ .

$$\eta = \frac{\text{section of the melting pool}}{\text{theoretical section of the powder flow}} = \frac{\frac{\pi}{4} D_s^2}{\frac{\pi}{4} D_p^2} = \frac{D_s^2}{D_p^2} < 1$$

Powder catchment efficiency increases with melt pool diameter and hence tends to increase with beam diameter; an approximately linear relationship between powder catchment and the product of laser power and beam diameter has been identified in the literature. Other experimental results show that catchment efficiency falls with traverse speed and increases approximately linearly with the angle between a lateral nozzle and the melt pool surface when depositing material on an inclined substrate. It has also been noted that reduction in both particle size and stream velocity increase the cladding rate, and by implication the catchment efficiency, so this may not be the whole picture and the melt pool may not always assimilate all the powder that reaches it.

#### **2.2.4.3 Surface finish**

The low feed rate gave smooth surface due to substantial remelting of previous layers, while the high rate gave high roughness and an increases chance of defects due to minimum substrate remelting. Multiple mechanism for unmelted particle attachment also means that smaller particle sizes improved surface finish. Naturally, due to the method of formation, the roughness of the cladding part

varies with direction of measurement and the sidewall roughness in the build direction is normally greater than in the longitudinal direction, particularly for thicker layers. The difference increases with layer thickness, which means that increased deposition rate (and therefore deeper layers) is normally at the expense of greater surface roughness.

Multiple partially overlapping tracks can be deposited to produce horizontal layers, so to effectively increase the height of the substrate. Several studies report on the correlation between processing parameters of cladding and characteristic features of single cladding tracks. Ocelik et al. predict by a model simultaneously the final coating height, surface waviness and final cladding angle from the shape of single track and overlap ratio [37].

#### 2.2.4.4 Surface hardness

Surface hardness is primarily a function of the build material and its microstructure. Microstructure is in turn a function of the thermal gradients and cooling rates during solidification. It has been found that hardness increases with cooling rate. So, hardness has been found to increase with traverse speed but decrease with powder particle size and laser power when substrate and deposition material are the same. Studies on the laser cladding process using dissimilar materials or elemental powder blends indicate that the hardness is primarily determined by the dilution ratio or feed proportions due to those factors determining elemental composition and influencing cooling rate.

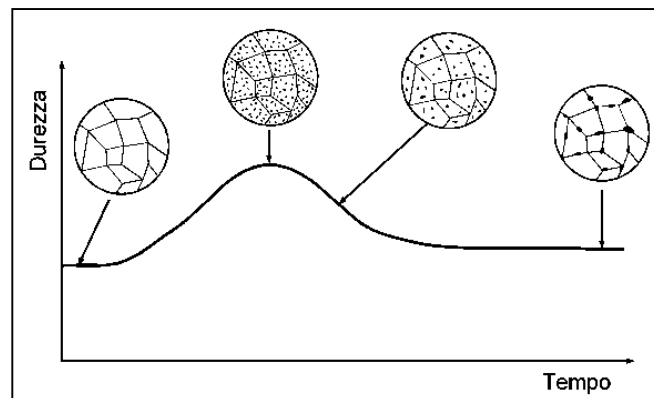


Fig.2.13: Hardness trend as a function of the time.



#### **2.2.4.5 Tensile and yield strengths**

The tensile and yield strengths of a component are related to solidification rates in the same way as hardness. The high cooling rates due to the “self-quenching” effect of unheated material surrounding a highly localized heat flux that occurs in laser cladding process thus explains the superior mechanical properties that can be achieved.

Tensile and yield strengths of the deposited material generally increase with traverse speed and decrease with laser power due to the increased cooling rates parameter changes induce.

Components produced by laser cladding are generally anisotropic due to the directional solidification and residual stresses generated during manufacture. In most cases, yield and ultimate tensile strengths are greater in the horizontal direction, but ductility is lower than in the vertical direction.

#### **2.2.4.6 Residual stresses**

Products produced using laser cladding process contain complex residual stress fields.

The main source of these is the constrained thermal expansion and contraction caused by the transient thermal gradients as the deposited material cools track by track. The stresses are often undesirable from a performance point of view; tensile residual stresses, in particular, can have a detrimental effect on the effective fatigue and tensile properties.

Substrate preheating and process parameters adjustment are possible strategies of regulating cooling rate and melt pool size and hence a means of influencing the residual stress fields generated during laser cladding also showed laser pulse parameters could be used to significantly influence residual stress fields, using a pulse beam significantly increased the level of stress lower in a rectangular test piece and also changed final deposit microstructure.

### 2.2.4.7 Clad Dimensional Characteristics

Several parameters are associated with the clad geometry, which are shown in figure. In this figure,  $h$  is the clad height,  $w$  is the clad width,  $\alpha$  is the angle of wetting, and  $b$  is the clad depth representing the thickness of substrate melted during the cladding and added to the clad region. The aspect ratio is defined as the ratio between the width and the height.

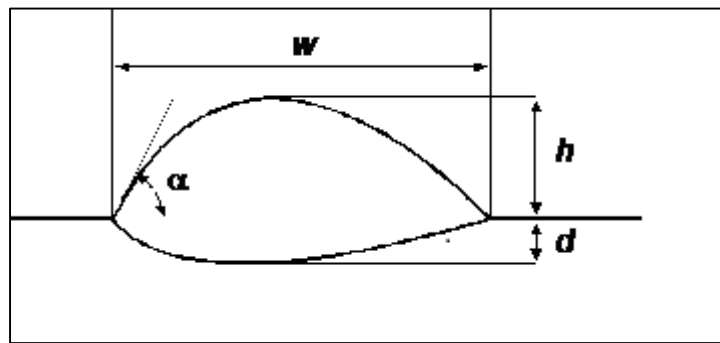


Fig.2.14: Clad geometric characteristics.

The clad dimension are affected by a lot of process parameters.

In particular, the **width** of a single clad on a plane substrate was originally found to decrease linearly with traverse speed, and mathematical models and experiment have shown this also to be true for multiple layer structures. The width of a single track or of a thin wall comprising multiple overlapped tracks increases approximately linearly with laser power and also increases markedly with substrate temperature. The laser spot size has been experimentally established as the most important factor in determining the initial track width on a substrate, provided that the absorbed heat flux is sufficient to induce melting. The width of a thin wall built up from a plane substrate often increases after the first few layers due to a transition from three-dimensional to primarily two-dimensional heat flow. Track width is affected only slightly by power mass flow rate. According to Y.Li et al. the width of single clad was mainly affected by laser power, scanning velocity and diameter of laser spot, and the influence of these processing parameters was similar to those on laser surface melting [56].

The **height** of a single clad decreases with increasing traverse speed but increases with increasing powder mass flow rate. Taking these two results together gives an almost linear relationship between track height and line powder mass.

Some experimental results have shown height to decrease with power, which may be accounted for by a process known as meltdown, excessive melting and flow of the deposition clad. The height of single cladding layer is one of the most important factors for laser rapid forming. Ideally, the height of each cladding layer should be strictly equal to the thickness of the slice sliced from the CAD solid model to ensure the accuracy of the fabricated components. However, there always exist some differences between the height of designed slice and actual cladding layers. Even in the same layer, there were often some height differences resulting from the fluctuation of powder feeding rate, scanning velocity and laser power. Although the height of single cladding layer was affected by many factors, it was indeed determined by the amount of powder which was stuck on the surface of substrate to form a clad, i.e. the more the powder, the higher the height [56].

One of the properties of the clad layer is called **dilution**. Dilution can be defined as the mass of original substrate or previously deposited track melted, divided by the sum of the combined mass of substrate and added material melted. It is an important quality index in laser cladding process: too low a value can indicate insufficient melting of the previous surface and an incomplete fusion bond with the deposited track, while too high a value can indicate excessive remelting. The extent of dilution is highly dependent on the injected powder flux; for a lower powder flux dilution increases and mass deposition decreases, while for higher powder flux the opposite is true. For a given specific energy, dilution of a single-layer cladding track is virtually independent of the laser intensity and traverse speed.

Dilution has two definitions: geometrical and metallurgical. The geometrical definition of dilution is illustrated in figure. According to the specified parameters in the figure, the dilution is:

$$dilution = \frac{d}{h + d}$$

where d is the thickness of substrate that was melted during the cladding process [mm], and h is the height of the clad bead [mm].

Alternatively, dilution may be defined as the percentage of the total volume of the surface layer contributed by melting of the substrate. This method is based on an analysis of the material composition in the clad layer. A comparison is made between the material composition of the pure coating material and the composition of the substrate. According to the composition, dilution is defined as

$$dilution = \frac{\rho_c(X_{c+s} - X_c)}{\rho_s(X_s - X_{c+s}) + \rho_c(X_{c+s} - X_c)}$$

where  $\rho_c$  is the density of melted powder alloy [kg/m<sup>3</sup>],  $\rho_s$  is density of substrate material [kg/m<sup>3</sup>],  $X_{c+s}$  is weight percent of element X in the total surface of the clad region [%],  $X_c$  is the weight percent of element X in the powder alloy [%], and  $X_s$  is the weight percent of element X in the substrate [%].

In laser cladding, either pre-placed or powder injection, **shape angle** is another important parameter that indicate the geometry of the clad. In general, three types of clad cross section may be produced by laser cladding as shown in figure. These cross sections represent the amount of dilution, corresponding shape angle. In practice, the clad angle  $\alpha$  is required to be large enough to avoid porosity creation in the coating, while overlapping individual clad tracks. To avoid the systematic errors and considerable scatter of data, an assumption is often made that the cross section of the laser track lies on a circle [57]. The clad angle  $\alpha$  can be calculated from laser track width  $W$  and laser clad height  $H$  as:

$$\alpha = 180 - 2 \arctan (2H/W)$$

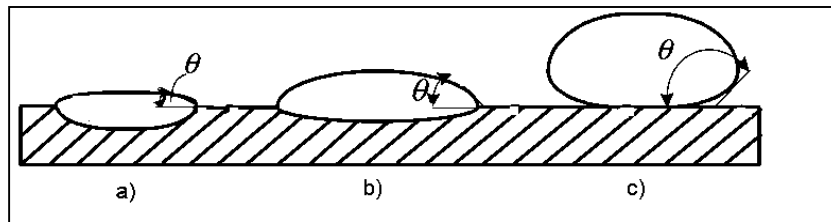


Fig. 2.15: Shape angle  $\alpha$  measurement of dilution.

### 2.3 Physical models

An alternative to the process analysis with experimental methods is to develop models which are based on physical laws. Experiments must be performed to verify the assumptions on which the model is based and to adapt the parameters in it. A good model supports the necessary experimental research for the development of new applications.

A lot of studies have been carried out to predict the geometric characteristics of the clad as a function of the most important parametric processes.

Y. Li et. al found that the height of a single cladding layer was very important for fabrication accuracy and forming stability of components of laser rapid forming because it was affected by almost all processing parameters and was quite difficult to precisely control. For the system with lateral powder feeding pattern, the powder

injection point was the most important factor to the height control of single layer. The variation of the width of single clad, which was mainly affected by laser power, spot diameter and scanning velocity, was similar to that in laser surface melting [56].

J.Choi et.al analysed the relationships between laser cladding process variables and the product characteristics using statistical techniques. The results show that the process window to produce sound samples with dimensional stability and microstructure integrity is very narrow. Micro-hardness data shows that the deposited region generally has uniform distribution of hardness with minimal variation. It was found that with the feedback control of laser power, layer thickness and pore/void are strongly affected by powder mass flow rate. While higher powder feed rate leads higher possibility of pore formation, the analysis result also predicts higher probability of producing actual layer thickness. The predicted model by the statistical techniques concludes that the interacting effect between layer thickness setting and powder mass flow rate is significant. Dilution, porosity, microstructure, and composition were investigated for the material characteristics of deposited H13 steel. Dilution depth to the substrate is minimal and has few effects on the composition of the final products. The pore interval is very close to the overlap percentage of the process. Optimization of overlap percentage as well as proper control of powder flow rate is essential to reduce the possibility of pore formation. Microstructure shows the difference of dendrite

growth between upper and lower zone of sample due to the cyclic heat dissipation. Quantitative chemical composition of deposited steel is almost the same as that of utilized steel powder [34].

P.Balu et al. established a computational fluid dynamics (CFD) based powder flow model to characterize the coaxial powder flow behavior of Ni–WC composite powders. The key powder flow characteristics such as the stand-off distance, the diameter of the powder stream at the stand-off distance, and the velocity of the powder particles are measured using three different vision based techniques. Both the numerical and experimental results reveal the exact stand-off distance where the substrate needs to be placed, the diameter of the concentration spot of powder at the stand-off distance, and a combination of suitable nozzle angle, diameter, and carrier gas flow rate to obtain a maximum powder concentration at the stand-off distance with a stable composite powder flow [32].

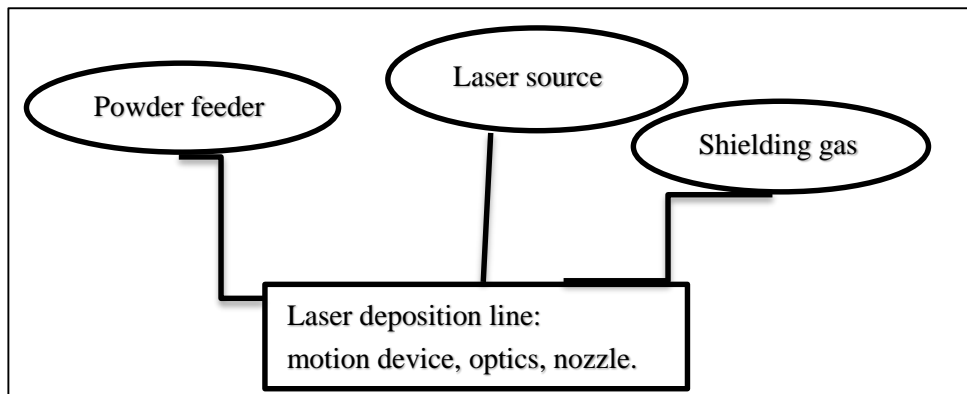
## Chapter III

### Laser Cladding Equipment

In this chapter the items of the Laser cladding equipment are presented. In particular, the process requires the following equipment:

- Laser source
- Powder feeder
- Laser deposition line: motion device, optics, nozzle.

The following scheme show how this components are connected.



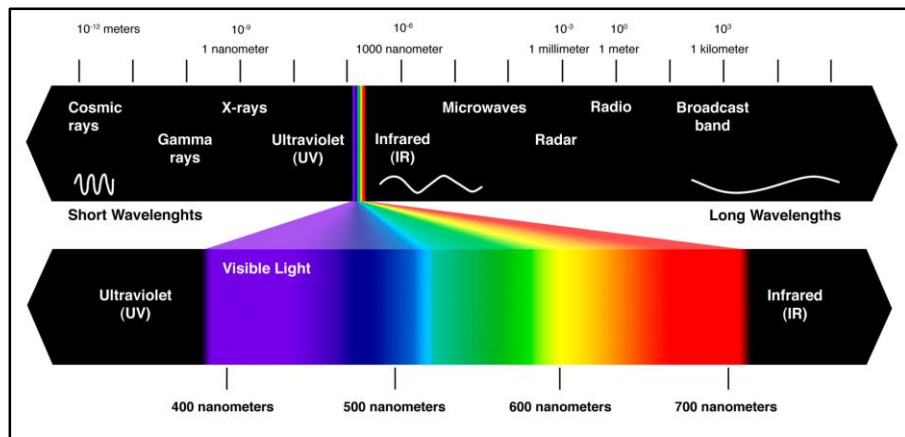
*Fig. 3.1: Laser cladding equipment components.*

It is essential to understand the construction of these devices and their performance under different working conditions for the laser cladding process to be successful.

This chapter provides a comprehensive comparison of available lasers, powder feeders, and nozzles to demonstrate their potential and suitability for use in laser cladding technology. It is very important to know the field of application of the different configurations, which depend on the particular condition and use.

### 3.1 Laser source

The word LASER is an acronym for Light Amplification by Stimulated Emission of Radiation. Stimulated emission of radiation is a natural process first identified by Einstein. It occurs when a beam of light passes through a specially prepared medium and initiates or stimulates the atoms within that medium to emit light in exactly the same direction and exactly at the same wavelength as that of the original beam.



*Fig.3.2:Electromagnetic spectrum.*

A typical laser device consists of an amplifying or gain medium, a pumping source to input energy into the device, and an optical cavity or mirror arrangement that reflects the beam of light back and forth through the gain medium for further amplification. A useful laser beam is obtained by allowing a small portion of the light to escape by passing through one of the mirrors that is partially transmitting.



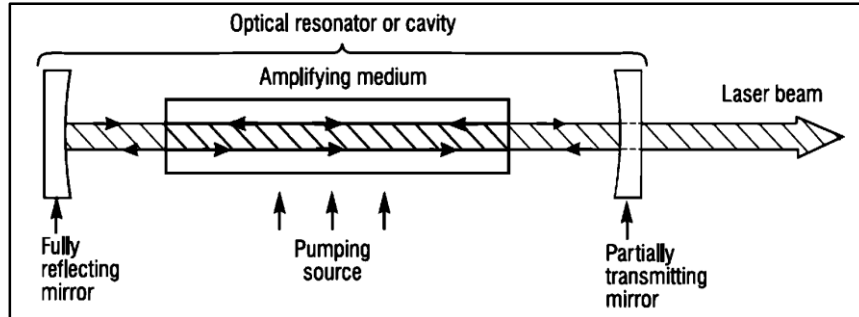


Fig. 3.3: A typical laser device.

All the lasers are produced as a result of electrons jumping from an excited energy level within a radiating species to a lower-lying energy level and, in the process, radiating light that contributes to the laser beam.

### 3.1.1 Construction of a laser

A laser consists of an active laser material, a source of excitation energy, and a resonator or feedback mechanism to perform the three stages of laser action. The general construction of a laser is shown in figure.

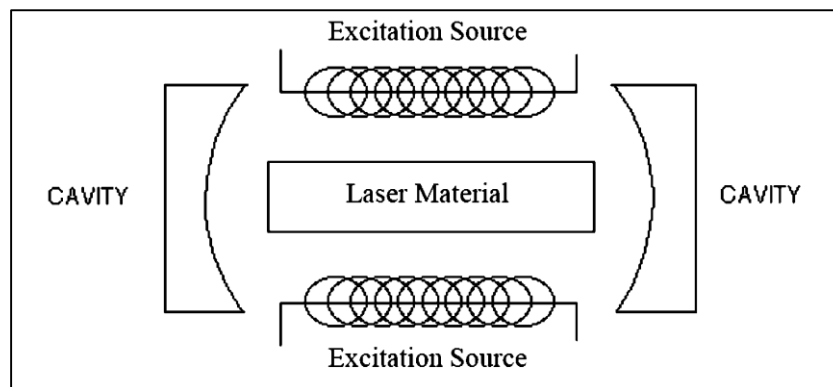


Fig.3.4: General construction of a laser.

**Laser material:** the lasing material can be a solid (Ruby, YAG and glass lasers), liquid (Dye lasers), gas (Helium-neon, argon and carbon dioxide) or a semi-conductor (InGaAIP). A material is said to be in “Normal State” if the number of atoms in the lower energy level is more than the number of atoms in

the higher energy level. The material is said to be in an excited state if population inversion has been achieved. The laser material is one in which population inversion is possible. The downward transition from the excited to the normal state is triggered by stimulated emission. The lasers are classified depending on the number of energy levels used for the excitation and the stimulated emission process. Commercial lasers are 3 level and 4 level system, while the simple 2 level system is not used in practice, as it is difficult to achieve population inversion in a 2 level system.

**Excitation source:** population inversion is achieved by “pumping energy” from an external source. Depending on the external source, the excitation process is called as optical pumping or electrical pumping. In electrical pumping, an AC or DC electrical discharge is used for excitation. Gas lasers and semiconductor lasers are usually excited using electrical pumping. In optical pumping, light is the source of energy and is used for most of the solid-state and dye lasers.

**Resonator:** a cavity that has a pair of mirrors, one of each end of the laser is used as a resonator in most lasers. One of the mirror is completely reflective while the other mirror is partially transparent. The reflection of the laser beam between the two mirrors results increased power. The beam is reflected back for amplification, until a specific threshold power is reached. The portion of the laser with the necessary power is coupled as output through the partially transparent mirror.

### **3.1.2 Lasers their types and characteristics**

The first laser action was demonstrated in a ruby crystal by Maiman, in 1960. Since then, a large number of materials in various media have been found to give laser action at wavelengths in the visible, ultraviolet and infrared regions.

These include various gases, solids, liquid, glasses, plastics, semiconductors, and dyes. In addition to the ruby crystal, many other crystals doped (introduced as an impurity) with rare earth ions have light been found to give extremely good laser output. The crystals are grown in specially designed furnaces with the desired compositions and then cut and polished into cylindrical laser rods with the faces optically flat and parallel to each other. The numerous types and designs of lasers are steadily increasing and can be broadly classified according to their production techniques.

**Ruby Laser:** Ruby laser is historically the first one to be discovered; it gives laser radiation on a pulsed length ( $1 \text{ nm} = 10^{-9} \text{ m}$ ).

It consists of a ruby rod xenon flash tube, a suitable cavity to reflect the light from flash tube to the ruby rod, and a high voltage power supply to give electrical energy to the flash tube. During his experiment, Maiman found that the ideal composition for the ruby crystal is five atoms of chromium for every ten thousand atoms of aluminum, i.e., a concentration of 0.05 percent. The ruby rod used was 4 cm long and 1/2 cm in diameter and the ends were ground to a high degree of flatness and parallelism. One end was silvered making it a mirror (almost 100 percent reflective) to reflect all the rays of light striking it. The other end of the rod was partially silvered; the laser beam was emitted through that end. The ruby rod was surrounded by a helical xenon flash lamp and both of them were held inside a cylindrical cavity, coated with a reflective material. The light from the xenon flash tube was focused by the cylindrical cavity onto the ruby rod, thereby exciting the chromium atoms which were responsible for the laser action. The ruby laser is a three-Level system since only three energy levels are involved in the process of stimulated emission. The depopulation of the ground state for population inversion is achieved by exciting the atoms of the ruby crystal with intense light from a xenon flash lamp. Thus the atoms are excited from the ground state (level 1)

to an upper state (level 3) by means of absorption. From the energy level 3, the atoms are transferred to energy level 2 without emitting radiation (non-radiative transfer). The energy level 2 is called metastable level since the atoms stay at this level for a longer interval of time. Finally, the atoms return to the ground state from the metastable level through the process of stimulated emission giving rise to an intense laser light at 6943Å. The laser beam comes out in the form of a pulse of very short duration (about a millisecond). The continuous wave operation of the system is very difficult to achieve.

Only 1 to 2 per cent of the input is utilized to obtain the laser action. The rest is dissipated as heat and is therefore wasted. In Q-switched mode, the power up to 500 MW has been achieved. Since this laser requires considerable input energy to give laser action, it is now being used only for limited applications in the areas of holography, high speed photography, etc.

**Nd: YAG Lasers:** YAG is formed from a mixed oxide system having a composition of  $\text{Y}_3\text{Al}_5\text{O}_{12}$ . Using Czochralski method, the crystal is grown in a

specially designed furnace by dipping a rotating seed into a crucible of molten material and withdrawing it at a constant speed.

Iridium crucible is used because of high melting point of YAG (1910-1970°C). The optimum concentration of neodymium in YAG is about one percent.

The YAG crystal growth difficulties limit the size of the laser rods to approximately 1 cm in diameter. However, the YAG host has the advantage of having a relatively high thermal conductivity to dissipate the heat generated, thus allowing these crystals to be operated at high repetition rates of the order of many pulses per second. With a continuous source of excitation like tungsten lamp or krypton arc lamp, continuous laser output of about 1 kW power could be obtained.

Due to these excellent properties, Nd:YAG laser is extensively used in many industrial applications like drilling of holes in solid objects, welding of metals and alloys, etc, and also in medical applications like eye surgery, treatment of cancer, etc.

**Liquid (Dye) lasers:** liquid lasers are similar to the solid-state lasers in that they consist of a host material (in this case a solvent such as alcohol) in which the laser (dye) molecules (such as rhodamines or coumarins) are dissolved at a concentration of one part in ten thousand. Dyes exhibit a very high degree of fluorescence, i.e., when the dye is exposed to ultraviolet light, it glows with characteristic colour depending on the nature of the material. Different dyes have different emission spectra or colours. As a result, dye lasers cover a broad wavelength range from the ultraviolet at 320 nm to the infrared at about 1500 nm. A unique property of dye lasers is the broad emission spectrum (typically 30-60 nm) over which the gain occurs. When this broad gain spectrum is combined with a diffraction grating or a prism as the cavity mirrors, the dye laser output can be a very narrow frequency beam (10 GHz or smaller). Frequency tuning over even larger ranges is accomplished by inserting different dyes into the laser cavity. Dye lasers are available either in pulses (up to 50-100 MJ) or as continuous output (upto a few watts) in systems that are pumped by either flash lamps or other lasers, such as frequency-doubled or tripled YAG lasers or argon ion lasers. Since the dye degrades slightly during the excitation process, most of the dye lasers are arranged to have the dye circulated from a much larger reservoir.

The dye lasers are used mostly for applications where tunability of the laser frequency is required either for selecting a specific frequency that is not available from one of the solid-state or lasers or for studying the properties of a material when the laser frequency is varied over a wide range. Therefore, the dye laser

becomes an important tool for spectroscopy, photochemistry, pollution monitoring, Isotope separation, etc. Another important application of dye lasers is for producing ultra short optical pulses by a technique known as mode locking. In this process, the longitudinal modes of a dye laser (as many as 10,000) are made to oscillate together (in one phase) causing the individual pulses as short as 50 femtosecond ( $5 \times 10^{-14}$  s) to emerge from laser. These short pulses find application in studying very fast processes in solids and liquids and perhaps also in optical communication. The dye lasers are less expensive than the solid-state lasers and are relatively easy to maintain for regular operation.

**Gas Lasers:** The gas lasers have a gas or a mixture of gases as their light-amplifying substance. Helium-neon, argon ion, and carbon dioxide lasers are the most widely used gas lasers. Javan, Bennett and Herriott succeeded in demonstrating the first gas laser towards the end of 1960-a few months after the Maiman's discovery of the ruby laser. They used a helium-neon mixture (90 per cent helium and 10 per cent neon) as the active material. In most cases, the gas is contained in a glass or quartz tube about 25-100 cm long and the gas molecules are excited in an electric glow discharge. With a few exceptions, these lasers receive their energy input via collisions of gas atoms with high-energy electrons.

This energy is provided by applying a high voltage between electrodes located within the gaseous- medium to accelerate the electrons to the necessary high energies. The gas lasers are of continuous type and normally have high coherence. But, they are considerably less powerful as compared to the pulsed solid-state lasers.

**Semiconductor lasers:** the semiconductor or diode lasers are the smallest of all the known lasers; they have a size of a fraction of a millimeter. The laser consists of a semiconducting crystal, such as gallium arsenide, lead selenide, etc, with parallel faces at the ends to serve as partially reflective mirrors. The entire laser package is very small and can be incorporated into an integrated circuit board, if required. A semiconductor, as the name implies, is half-way between a conductor and an insulator (non-metal), so far as its electrical conductivity is concerned. The semiconducting materials containing gallium and arsenic compounds have been found to generate infrared rays when the current is passed through them. This implies that these semiconductors convert electrical energy into photons. But, these were ordinary incoherent light rays and were not produced by the laser action.

However, when the gallium arsenide crystal is through it, the laser action does take place. Many semiconductors serve as laser materials and they have been made to 'lase' under the stimulation of electricity instead of light which is used for the other solid-state lasers.

There are two types of semiconductors, viz., n-type and p-type. To understand the functioning of these devices, it is necessary to know the nature of the electronic energy states in a semiconductor. A typical semiconductor has bands of allowed energy levels separated by forbidden energy gap region. In an intrinsic semiconductor, there are just enough electrons present to fill the uppermost occupied energy band (valence band) leaving the next higher band (conduction band) empty. In an n-type semiconductor, a small amount of impurity is added intentionally so that the material is made to have an excess of electrons, which thus becomes negative. On the other hand, by adding a different type of impurity in a p-type semiconductor, the material can be made to have an excess of holes (vacancy of electrons), which thus becomes positive.

The semiconductor laser consists of a tiny block (about one square millimetre in area) of gallium arsenide. When the p- and n-type layers are formed in an intimate contact, the interface becomes a p-n junction. When direct current is applied across the block, the electrons move across the junction region from the n-type material to the p-type material, having excess of holes. In this process of dropping of the electrons into the holes, recombination takes place leading to the emission of radiation. The photons travelling through the junction region stimulate more electrons during the transition, releasing more photons in the process. The laser action takes place along the line of the junction. Due to the polished ends of the block, the stimulated emission grows enormously and a beam of coherent light is emitted from one of the two ends. With a gallium arsenide laser, a continuous beam of a few milliwatts power is easily obtained.

The semi conducting lasers are also called junction lasers or junction diode lasers because they produce laser energy at the junction of two types of impurities in a semiconductor. They are also called injection lasers because electrons are injected into the junction region. The technology of semiconductor lasers has undergone considerable development with the important goal of achieving room-temperature operation, low threshold energy, high output powers, wavelength diversity and long lifetimes. In 1969, continuous operation at room temperature was achieved in a (gallium aluminium arsenide) double heterostructure laser. With further improved developments, device lifetimes of

tens of years were obtained with output in the range of tens of milliwatts and with operating wavelengths

from 0.7 to 1.8 microns (1 micron =  $10^{-4}$  cm). By constructing a row of p-n junctions positioned next to each other, all the separate gain media can be forced to emit together in a phased array to produce an effective combined power output. In this way, gallium aluminium arsenide diode lasers have been operated continuously at room temperature with output in the range of several watts. In addition, electrical to optical power conversion efficiencies of greater than 50 per cent have been obtained.

The semiconductor lasers, being simple in construction and light in weight with compact units and requiring little auxiliary equipment, are very suitable for applications where high powers are not required. They are primarily used in the area of communication in which the near-infrared laser beams can be transmitted over long distances through low-loss optical fibres. In addition, they have found a large market as reading devices for compact disc players.

### 3.1.3 Characteristics of laser beam

In the following we address the physical quality of radiation emitted by the lasers.

*Monochromaticity:* the frequency emitted by the laser is given by the difference in energy between the energy levels for which there is radiation emission. It is given by Planck's relationship:

$$\nu_0 = \frac{E_2 - E_1}{h}$$

where:  $h$  is the Planck's constant;  $E_2$  – upper level energy;  $E_1$  – lower level energy. The two energy levels between which laser radiation emission occurs are stable. Thus a single frequency is emitted and amplified in the optical cavity. This means that laser radiation has a single wavelength. This means that the radiation emitted by the laser is monochromatic. Laser with Nd: YAG emits radiation with wavelength of 1.06  $\mu\text{m}$ .

*Coherence.* Coherence of electromagnetic radiation means maintaining a constant phase difference between two points of wave front of the wave. Coherence is of two types: spatial and temporal. Spatial coherence is limited to a given area and the temporal coherence is limited to a certain time. Laser radiation

have high spatial and temporal coherence compared with conventional light sources.

*Divergence and directionality.* The propagation and directionality of radiation is described by diffraction theory. Maximum intensity of radiation is limited by the angle of divergence. In the laser medium will be amplified only radiation propagated on direction of optical cavity axis. Construction of optical cavity leading to a low beam divergence which means a high directionality.

The laser beam is described by a converging and symmetrical hyperboloid of revolution that defines the beam focus. If  $z$  to be the propagation direction, the beam geometry is given by the equation of caustic:

$$D^2(z) = D_0^2 + z^2 \theta^2$$

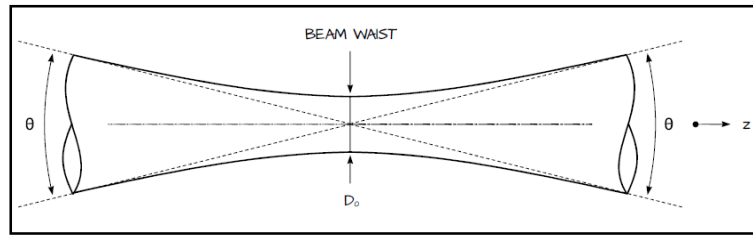


Fig.3.5: Laser geometry.

In the far field, the equation became:

$$\frac{D(z)}{2z} = \tan \frac{\theta}{2} \quad \Longrightarrow \quad D(z) = \theta z$$

The intersection of a generic plan and the laser beam produces, in any proportion, the spot. In particular, if the plane pass through the belly the focal spot is obtained, whose diameter is the minimal diameter and is generally defined as  $D_0$ .

The power of the electromagnetic radiation per unit area is called irradiance, and is not uniform in the spot due to the architecture of the source. You can then refer to a distribution of irradiance, identified by transverse electromagnetic mode,  $TEM_{lm}$ . The notation has two subscript indicating the number of minimum values of the distribution of irradiance encountered



proceeding along orthogonal directions. Possible irradiance profiles are obtained as solutions of Hermite-Gauss equation of electromagnetic propagation.

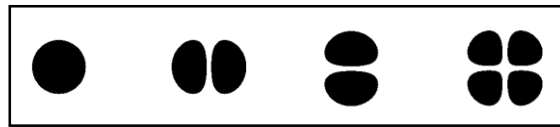


Fig.3.6: Transverse electromagnetic mode,  $TEM_{lm}$

$TEM_{00}$        $TEM_{10}$        $TEM_{01}$        $TEM_{11}$

The product between the diameter  $D_0$  of the minimal spot and the divergence angle of the beam  $\theta$  is a constant and is a function of:

$k$  = characteristic parameter of the distribution of irradiance

$\lambda$  = wavelength of the radiation emitted

$N$  = index of refraction of the material through which the beam propagates (about 1.0003 for the air)

$$D_0 \theta = \frac{K\lambda}{N}$$

The Gaussian beam is characterized by a value of  $K$  as following:

$$K_g = \frac{4}{\pi}$$

The non-Gaussian beams are characterized by characteristic parameters  $k > k_g$ . At equal active means ( $\lambda$ ) and focal diameter ( $D_0$ ), according to the product characteristic it results that the divergence of the beam is minimal if the distribution is Gaussian irradiance:

$$\theta_g = K_g \frac{\lambda}{D_0} = \frac{4\lambda}{\pi D_0}$$

The focal length  $f$  is the distance between the optical center of a lens and the focal plane. Among collimating lens and the focusing lens there is provided a region in which the beam is collimated and the wavefront is flat.

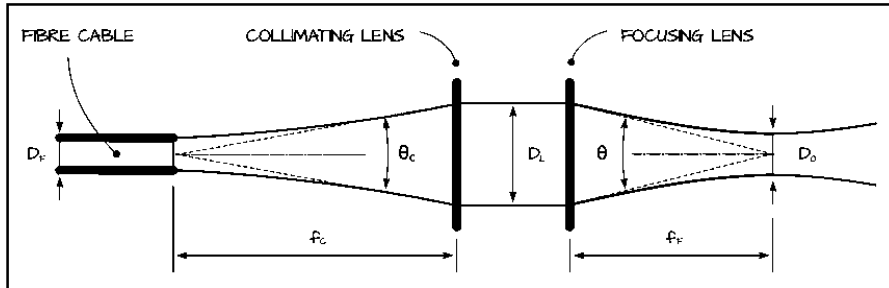


Fig.3.7: Collimating and focusing lens.

In the far field, upstream and downstream of the collimation, you have:

$$D_L = f_c \theta_c \quad D_L = f_f \theta$$

According to the product constance between neck diameter and angle of divergence, between upstream and downstream of the region of collimation relation applies:

$$D_f \theta_c = D_o \theta$$

It is reached in this way the equation to calculate the focal diameter depending on the diameter of the fiber of transport:

$$\frac{D_o \theta}{D_f \theta_c} = 1 \quad \Longrightarrow \quad \frac{D_o f_c}{D_f f_f} = 1 \quad \Longrightarrow \quad D_o = D_f \frac{f_f}{f_c}$$

It is necessary to introduce a parameter to describe the change in diameter of the beam in the near field. It is considered, starting from the neck of the beam and along the direction of propagation, the distance within which the diameter remains less than a threshold value  $D_h$ :

$$D_h = h D_o$$

The corresponding distance  $z_h$  identifies the depth of field and is obtained from the equation of the caustic:

$$z_h = \frac{D_0}{\theta} \sqrt{h^2 - 1}$$

The most common value for calculating the depth of field is  $h = \sqrt{2}$ . You get the Rayleigh distance beam and reformulates the equation of the caustic:

$$z_{\sqrt{2}} = \frac{D_0}{\theta} \quad D(z) = D_0 \sqrt{1 + \left(\frac{z}{z_{\sqrt{2}}}\right)^2}$$

Narrow depth of field are inadequate for certain processes. Large depth of field, however, permit greater distance machining and machining reproducible regardless of control of the focal position.

At equal active medium and focal diameter, the maximum Rayleigh distance is the one associated with the distribution of Gaussian irradiance:

$$z_{\sqrt{2G}} = \frac{D_0}{\theta_G} = \frac{D_0}{\frac{4\lambda}{\pi D_0}} = \frac{\pi D_0^2}{4\lambda}$$

There are several ways to assess the quality of the laser beam, but they all refer to measures that identify "what" the beam can be focused with limited divergence.

- *Beam parameter product (BPP)*
- *Beam propagation parameter ( $M^2$ )*
  - *Brightness*

The BPP is the product of the minimum radius of the spot that can be realized and the semi-amplitude of the angle of divergence:

$$BPP = R_0 \alpha = \frac{D_0}{2} \frac{\theta}{2} = \frac{D_0 \theta}{4} = \frac{K\lambda}{4}$$

$$BPP_g = \frac{K_g \lambda}{4} = \frac{\lambda}{\pi}$$

higher the value of BPP is, lower the beam quality is.

The distribution of irradiance in real beams deviates from Gaussian form: to quantify the difference between a theoretical distribution is introduced and a real factor  $M^2$ .

$$M^2 = \frac{BPP}{BPP_g} = \frac{\pi BPP}{\lambda}$$

The higher the factor  $M^2$ , the lower the beam quality, because the greatest divergences are obtained.

For some industrial applications, it is not expressly required high power; is required, rather, high brightness.

$$B = \frac{P}{A_0 \Omega}$$

P = beam power

$A_0$  = extension of the focal spot

$\Omega$  = solid angle in the far field

High brightness is so synonymous with high power supplied high quality.

### 3.1.4 High power disk lasers

The principle of the disk laser operation is based on the use of an active element in the form of a disk with a cooled surface. High cooling efficiency of the laser medium is provided by a large area of the disk surface, which is important from the point of view of the heat transfer process. Therefore, the average power in the beam can reach quite high values. It is important to note that due to effective heat transfer within the disk area there is no thermal lens effect, characteristic of 'rod' and 'slab' (optical range) geometries of the active element. In this case, cooling is performed through a side surface of the active element; a two-dimensional heat flow, forming a parabolic profile of thermal distortion, propagates through this side surface.

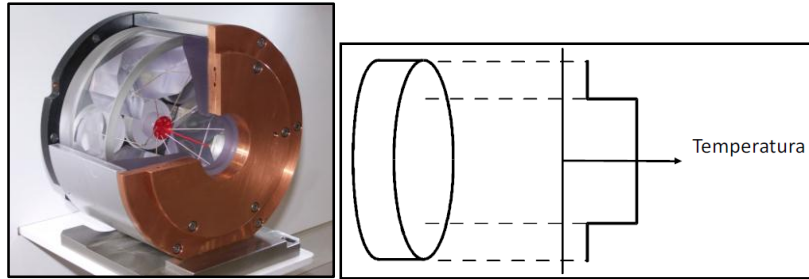


Fig. 3.8 Disk laser component.

The temperature dependence of the refractive index in this case leads to the emergence of a strong thermal lens effect. Such a lens deteriorates the directivity of the output and significantly limits the effectiveness of its action. The thin disk, in contrast, is cooled through a thin contact region on one side and generates a one-dimensional axial heat flow on the other side. As a result, the temperature gradient is distributed parallel to the laser beam, which does not result in the thermal lens effect. In practice, a thin laser element in high-power disk lasers is either connected to a porous heat sink or is cooled by forced convection [58].

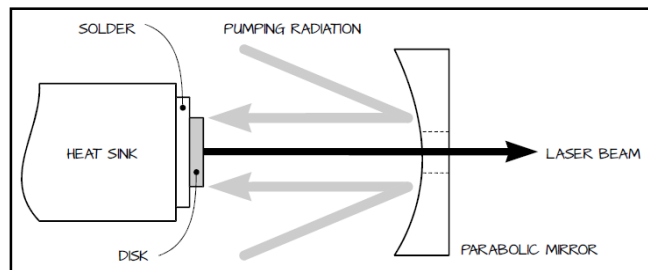


Fig. 3.9: Disk laser configuration.

At a constant temperature of the active laser element, the average output power achieved is directly proportional to the area of the pump zone and, consequently, to the cross-sectional area of the laser beam on the disk. This is a unique feature of disk lasers, which allows one to change the power density at a constant energy of the beam on the disk. This property is particularly important for multi-kilowatt sources, because it makes it possible to adjust the value of the peak output power without changing many other parameters that affect the performance of the overall system [59].

The power of disk lasers is limited not only by the power of the pump and overheating of the medium but also by the losses due to the ASE and the background radiation losses in the resonator. To avoid overheating, the size of the active medium should vary in accordance with the law of power scaling. Then, to avoid large losses caused by their exponential growth during the ASE, amplification of radiation corresponding to transverse round trips should not be large. This requires a reduction in gain  $G$ . Gain is determined by the reflectivity of the output mirror and disk thickness. Amplification of radiation per round trip, however, should not be substantially greater in magnitude than the radiation loss per round trip along the same optical path.

The power of the laser disc can be scaled by acting on the diameter of the bundles of pumping; the beam quality is not affected.

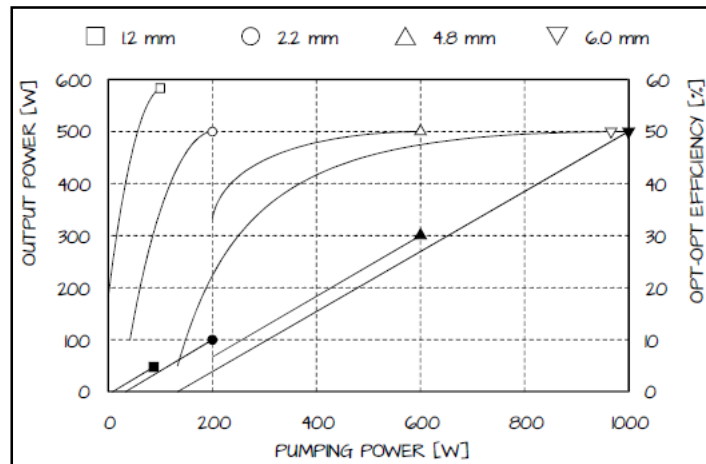


Fig.3.10: Efficiency as a function of pumping power.

The difference between the gain and losses per round trip of radiation determines the optical energy that is coupled out from the laser cavity. Reduction of the gain at this loss level requires an increase in the disk thickness. In this case, at a certain critical size, the disk becomes optically too thick and cannot be pumped above the threshold without overheating. To reduce the effects of the ASE, it was proposed to use an optical cover consisting of an undoped material on the surface of the laser disk. This cover allows the spontaneously emitted photons to escape from the active layer and prevents their resonance in the bulk of active material. Rays cannot be reflected from the surface, as in the case of an open disk.

This allows the maximum power achievable by the disk laser to be increased by an order of magnitude. Reflection of the ASE from the disk edge should also be suppressed. This can be done through the absorbing layer at the generatrix of the disk cylinder. In the regime when output power is close to maximal, much of the energy is used in the ASE; therefore, the absorbing layers must also have radiators accumulating heat. In the case of the maximum pump density of the disk laser its efficiency is quite low: most of the pump power is used in the ASE and is absorbed at the edges of the device. In this case, the distribution of the pump energy between several disks can significantly improve the performance of the laser system. Indeed, lasers, consisting of several modules with disk elements in a single cavity, have been repeatedly reported.

In conclusion the disk lasers advantages are:

- Active medium in almost three levels;
- Pumping diode;
- Limited effect of thermal lens;
- Reduction of losses in the resonant cavity;
- Reduction of parasitic effects;
- Higher efficiency compared to traditional laser (25% wall-plug, 65% opt-opt);
- Possibility to increase the power by expanding the diameter of the pumping;
- Low values of BPP in combination with acceptable values of  $M^2$ ;
- Rayleigh distances higher compared to Nd: YAG laser

### **3.2 Powder feeder**

The powder feeder system chosen to transport powder greatly affects the powder flow. Typical feed systems used can be categorized into the following groups based on operation principles:

- Gravity-based
- Mechanical wheel
- Vibrating

Many powder feeders incorporate a combination of these methods, which provide a more steady powder flow.

Gravity-based feed systems rely on the weight of the powder, and the wall angle of the hopper to deliver powder. As long as the flowability is high enough for the powder being used, a steady flow of powder should be easily obtained. In order to increase the controllability of gravity-based powder feeders, different devices such as a metering wheel can be integrated into the powder feeder. Also, a back pressure can be supplied on the powder funnel to increase the stability of the powder stream, which can be affected by the change in the height of powders in the funnel. Adding the external component for the measurement of powder is an essential device for obtaining a feed rate with high precision. Therefore, many feed systems of this type incorporate a metering wheel at the base of the hopper that regulates the powder deposition into a more even and steady flow. The following figure, below, shows a schematic of a typical gravity fed powder feeder incorporating a metering wheel [4].

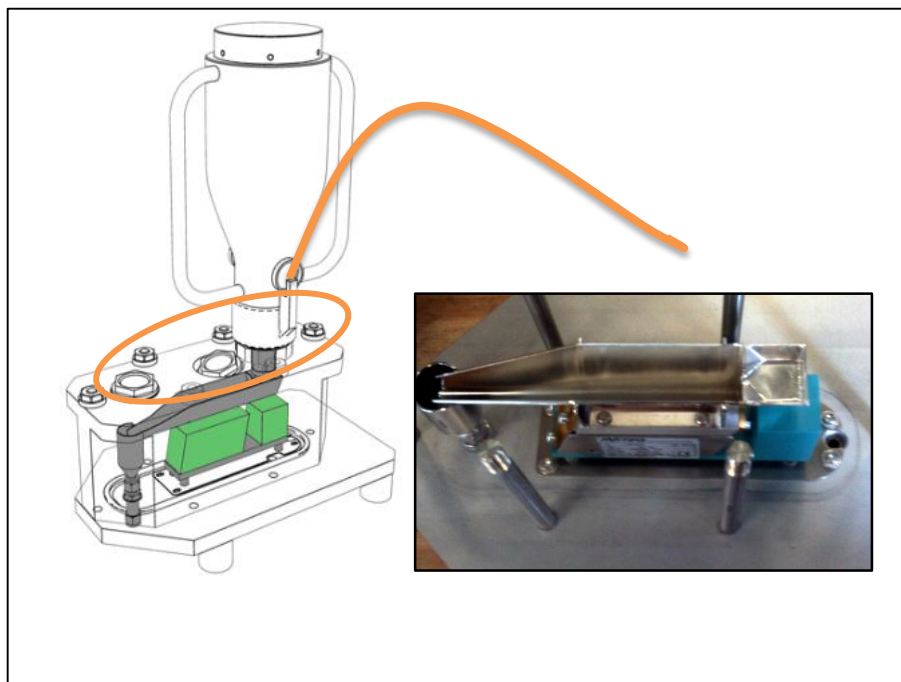
Mechanical wheel feeders use a rotating helical rod to pull powder from the hopper and deposit it into the feed outlet some distance away. There are many rod configurations that promote steady flow at different feed rates, however, due to high friction between the powder and rod, these feed systems are generally avoided [4].



*Fig.3.11: Mechanical wheel powder feeder.*



In the vibrating feeder the quantity of delivered powder is determined based on the vibrational frequency of the conveyor. A relation must be found to express the mass flow as a function of input voltage inducing vibration to the conveyor [4].It wil be described in the four chapter.



*Fig.3.12: Vibrating powder feeder.*

### **3.3 Laser deposition line**

The laser deposition line is composed of a motion device and a laser head.

The **motion device** could manipulate the laser cladding head or/and the workpiece.

The movement axes allow the handling to physically perform the process on the surface required. A good cell treatment should be able to permit the motion

of the head on three axes of translation and at least two axes of rotation, so as to cover the volume necessary to treat components of a defined size.

The laser head could be moved into the working area by a robot or an automatic shuttle handling system.

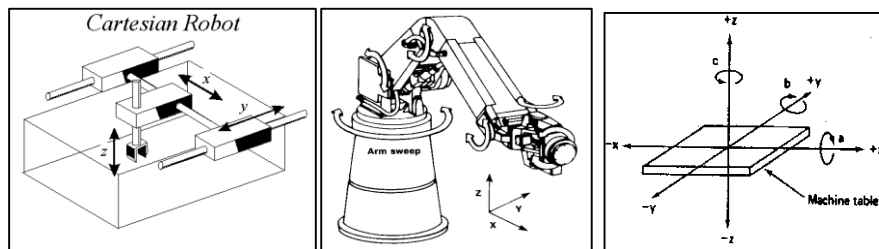


Fig.3.13: Laser cladding motion device.

It is also appropriate to provide, in addition or alternatively, a handling both rotational and translator, also of the component.

The choice to move the head or the component has to be evaluated for each application.

In order to perform complex part, the use of 5-6 continuous axis kinematics is necessary.

**Laser cladding head** is composed of of an optical system, with a collimator and focus lens, and a nozzle to focuses the powder in the melt pool. The laser beam, as produced in the resonator of a laser system, must be transported and manipulated by an optical system. The laser beam must be focused into a spot with the required shape and power density on the workpiece. The powder flow has to be focused onto the workpiece by a nozzle.

In the following figure a scheme of the laser cladding head is shown.

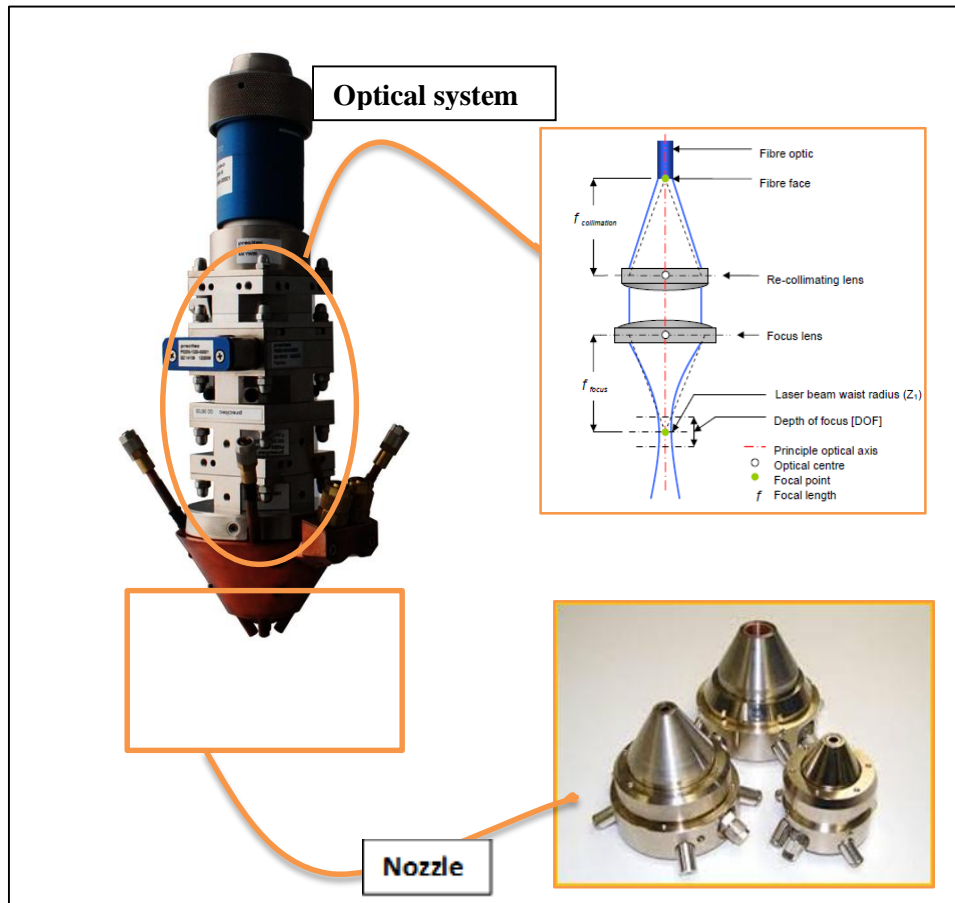


Fig.3.14: Laser cladding head: optical system and nozzle.

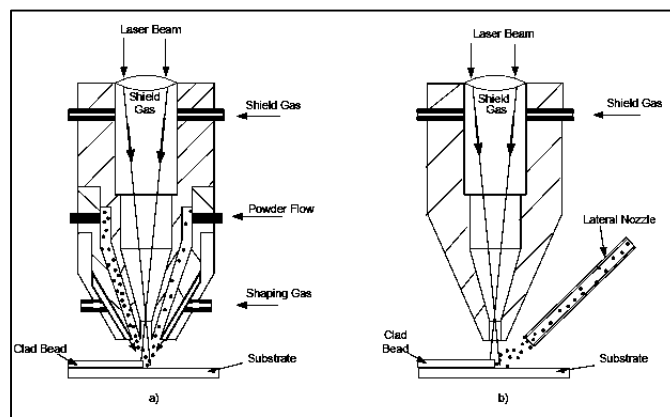
**The optical system** head contains optics that generally consists of a collimating lens, located in the collimator, and a focusing lens located in the processing head.

The purpose of the collimator lens is to re-collimate the laser beam as it exits from the fibre optic and the purpose of the focal lens is to focus the laser beam to the desired diameter.

In laser cladding by powder injection, the powder delivery nozzle can have

two different configurations, coaxial or lateral. Nozzles can be divided into two categories, depending on the orientation of the nozzle work axis relative to the optical axis of the laser beam. For off-axis nozzles, the nozzle work axis lies at an angle relative to the optical axis of the laser beam while for coaxial nozzles the work axis and optical axis coincide.

As known, laser cladding, in contrast to laser cutting or welding, requires a large laser spot. This is realized by working out of the focal plane. If a lateral nozzle (see the following text) not integral with the head is used, laser beam defocusing by head motion is possible. If a coaxial nozzle is used, the laser beam defocusing is achieved by a mobile collimator lens. This process is described in the four chapter.



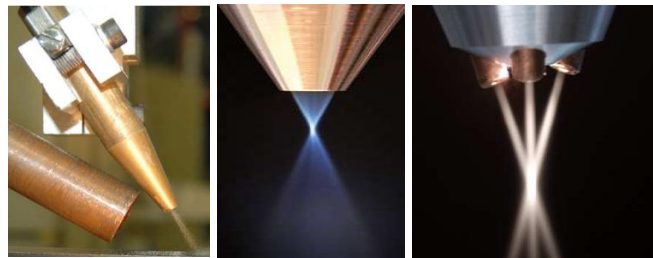
*Fig.3.15: Coaxial and lateral powder injection.*

**The nozzle** is responsible for shaping and directing the powder stream into the shallow melt pool created on the substrate surface.

One of the advantages of a coaxial nozzle is its independence from the direction of motion; however, experimental work has shown that its powder efficiency, which is the ratio between the deposited powder on the substrate and the delivered powder by the powder feeder in a specified period, is significantly less than that of the lateral nozzle. In both types, the powder can be preheated when it passes through the nozzle to increase efficiency.

With respect to the two kind of nozzle described above, three different concepts of powder injection can be investigated [60]:

- Off-axis powder injection (a single powder stream is fed lateral into the laser beam);
- Continuous coaxial powder injection (a powder stream is produced which encloses the laser beam);
- Discontinuous coaxial powder injection (three or more powder streams are fed coaxial to the laser beam).

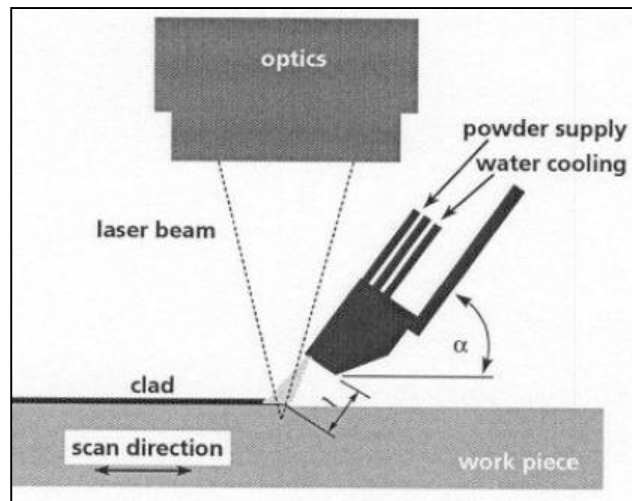


*Fig. 3.16: Off-axis powder injection, continuous coaxial powder injection and discontinuous coaxial powder injection.*

### **3.3.1 Off-axis powder injection**

In off-axis powder injection the nozzle is positioned lateral to the laser beam. The position is determined by the angle between nozzle and work piece ( $\alpha$ ) and the distance between nozzle tip and work piece ( $l$ ) as shown in figure. Since the powder stream diverges when leaving the nozzle  $l$  should be as small as possible to achieve a high powder efficiency (= weight of clad track per unit length versus powder amount fed per unit length). Typical values of  $l$  range from 8 to 12 mm. An increased of the angle leads to a decreased cross section of the powder stream on the work piece and thus the efficiency increases. The decrease at  $70^\circ$  is due to an increased value of  $l$ . The displacement was necessary to avoid collision between nozzle and laser beam. Another parameter determining the efficiency is the direction of injection. When the flow direction of the particles is the same as the moving direction of the work piece (dragging injection) a higher efficiency is achieved as for the opposite situation (stinging injection). In case of dragging injection more powder is injected directly into the melt than during

stinging injection. From this result it is clear that off-axis powder injection is not suitable for 3D-cladding. Figure 6 shows an off-axis nozzle with adjustment unit. Size and geometry of the nozzle opening can be varied depending on the width of the clad track. For a track widths between 0.5 and 5 mm a circular cross section of the opening with a diameter of 1.5 to 3.5 mm is adequate. Cladding of wider tracks (5 - 25 mm) requires a rectangular cross section of the opening (e.g. 1.5 x 15 mm<sup>2</sup>). Since the nozzle is positioned close to the melt pool it is exposed to laser beam reflections. Therefore the nozzle should be water-cooled to ensure long-term operation without any damage [60].



*Fig.3.17: Off-axis powder injection configuration.*

### **3.3.2 Continuous coaxial powder injection**

In continuous coaxial powder injection a powder stream cone encloses the laser beam. Figure 7 shows a coaxial powder injection. For long-term operation it is essential that the nozzle is water-cooled. The powder stream cone is produced as follows: the powder stream of the powder feed unit is split into three identical streams which are fed into a ring-shaped expansion chamber inside the nozzle. In this chamber a homogenous "powder cloud" forms which then is fed into a cone-shaped slit. Eventually the powder leaves the nozzle in the form of a hollow cone. The geometry of the powder stream cone is mainly determined by the apex angle  $\beta$  of the cone respectively of the cone-shaped slit.

Other parameters which determine the core diameter  $d_p$  of the powder stream focus are the distance  $f_p$  between nozzle tip and focus point, the slit size, the powder feed rate and the powder particle size. With increasing value of  $f_p$  the core diameter  $d_p$  increases due to the divergence of the powder stream.  $d_p$  increases significantly with increasing slit size. The same effect is observed when the powder feed rate is increased. Reducing the particle size leads to a smaller powder stream focus diameter. The typical powder stream focus diameter of a coaxial powder injection nozzle lies in the range of 1 to 3 mm. For given values of beam diameter on the work piece,  $\beta$ ,  $f_p$  and  $d_p$  the powder efficiency depends on the distance  $l$  between nozzle tip and work piece. The highest efficiency is achieved when  $f_p$  equals  $l$ . For the given ratio of the core diameter of the powder stream (1.8 mm) and the laser beam diameter on the work piece (2.7 mm) of 0.67 the maximum efficiency is about 50 %. However, it should be noted that values up to 90 % can be achieved for smaller ratios.

The major advantage of coaxial powder injection compared to off-axis powder injection is the potential for 3D-cladding. However, tilting of the nozzle is restricted. Since the homogeneity of the powder stream cone depends on the powder distribution inside the expansion chamber of the nozzle it is clear that gravity will effect the powder stream when the nozzle is tilted.

Experiments have shown that a maximum tilt angle of approx. 20° can be accepted without significant effects on the geometry of the clad layer [60].

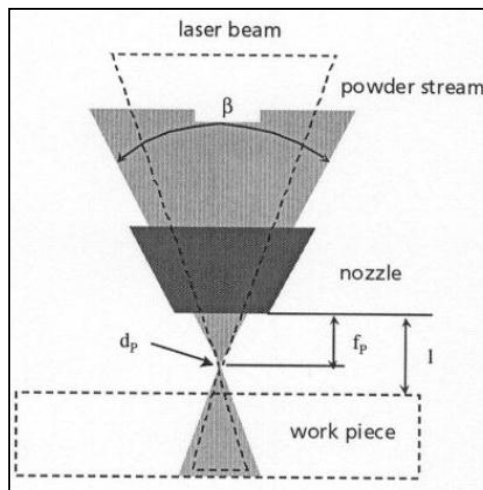


Fig.3.18: Continuous coaxial powder injection.

### 3.3.3 Discontinuous coaxial powder injection

In discontinuous coaxial powder injection several individual powder streams are distributed around the laser beam, thus forming a powder stream focus.

The core diameter of the powder stream focus depends on the angle between the individual powder streams  $\beta'$  (analogous to  $\beta$  for coaxial powder injection), the diameter of the nozzle holes, the distance between nozzle tip and powder stream focus, the powder feed rate and the particle size. The effects of these parameters are similar to those already discussed for coaxial powder injection. For given values of beam diameter on the work piece,  $\beta'$ ,  $f_p$  and  $d_p$  the powder efficiency depends on the distance  $l$  between nozzle tip and work piece. The highest efficiency is achieved when  $f_p$  equals  $l$ .

Compared to the coaxial powder injection nozzle the efficiency decreases significantly when  $l$  is smaller or larger than  $f_p$ . This is due to the divergence of each of the individual powder streams. The typical core diameter of the powder stream focus lies in the range of 2.5 to 4 mm (note: 1-3 mm for coaxial powder injection nozzles). For the given parameters the maximum efficiency is similar to the value measured für the coaxial powder injection nozzle (approx. 48 %). However, values up to 90 % can be achieved for an appropriate ratio of powder stream area and laser beam area on the work piece.

The major advantage of the three way nozzle is the potential für 3D-cladding including the potential to tilt the nozzle. The powder stream focus is only slightly affected. The maximum tilt angle actually tested successfully is  $90^\circ$  [60].

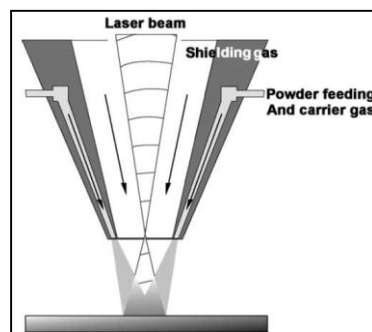


Fig.3.19: Discontinuous coaxial powder injection.



## Chapter IV

### **Laser cladding station and process tuning**

In this chapter details of the laser cladding station and of the experimental setup used in this research are presented.

This chapter starts presenting the laser deposition line with all the components that differentiate a welding station from a cladding station. In the following section, the laser source, the head of laser cladding, the robot and the feeder powder system are described. One of the most important and at the same time critical aspect of the process is about the steadiness and regularity of the powder flow. Therefore, it has been necessary to complete the station with a flow monitoring system to ensure a constant flow rate during testing. This system, developed in UNISA laboratory, is also presented. The last section of this chapter describes the process tuning.

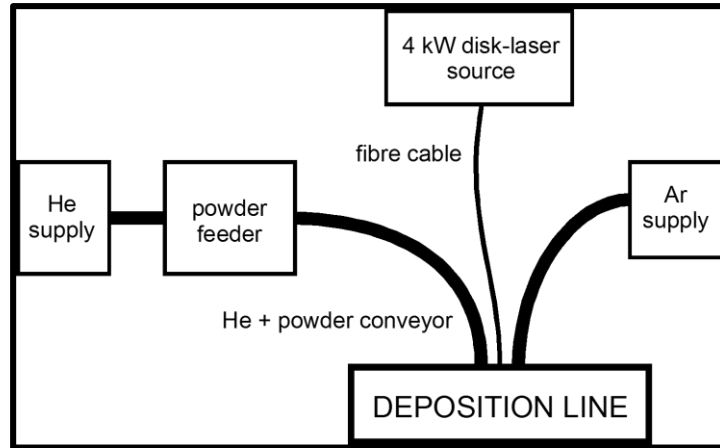
#### **4.1 Laser deposition line**

As known in the second chapter, a laser deposition line is generally a complex system where a number of components are required.

The laser cladding station setup in UNISA is composed of the following components:

- Laser source;
- Head of laser cladding;
- Manipulate system;
- Powder delivery and monitoring system.

In the following picture a scheme of the station is presented.



*Fig.4.1: Laser cladding deposition equipment.*

Powder is mixed with the carrier gas (in this case Helium) and delivered to the laser deposition line via the powder conveyor. Shielding gas is required to prevent oxidation during fusion and solidification.

In the follow, a description of each component is given. Moreover, some information about the connections of all the parts is also analysed.

#### **4.1.1 Laser source**

The experimental work described in this thesis is performed using a Yb:YAG disk-laser source with a continuous wave emission. The wavelength of 1030 nm is well suited for transport by optical fibers cable of 300  $\mu\text{m}$  diameter, which is an advantage for situations where a flexible beam delivery system is required.

The main technical features are given in Table.

*Tab. 4-1: Laser source technical features.*

<b>Maximum output power [kW]</b>	4.0
<b>Laser light wavelength [nm]</b>	1030
<b>Beam Parameter Product [mm × mrad]</b>	12.0

#### **4.1.2 Laser Cladding head**

Laser cladding head is composed of an optical system, with a collimator and focus lens, and a nozzle to focuses the powder in the melt pool.

As known, laser cladding, in contrast to laser cutting or welding, requires a large laser spot. This is realized by working out of the focal plane. In particular, the cladding head is equipped with a motorized (mobile) collimator lens, which changes the beam profile. A voltage set drives the movement of the lens as described in the following section.

In according to the description of the previous chapter, the collimator length is the distance between the end of the fibre cable and collimator lens position, instead the focal length is the distance between the focal lens and the point of minimum spot laser diameter. In this research the focal length of the lens and the focal length of collimation are respectively 200 mm and 100 mm.

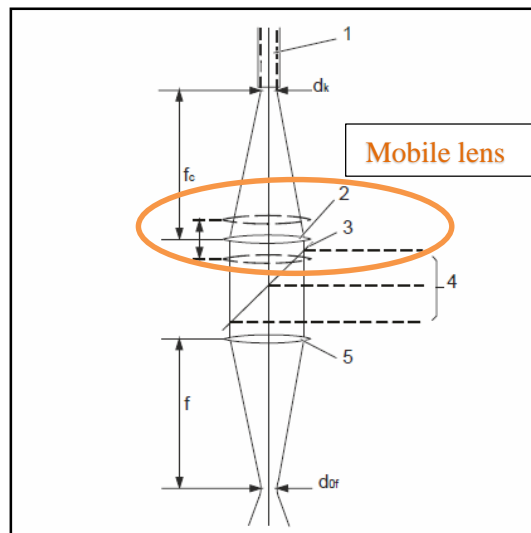


Fig.4.2 Collimating and focusing lens.

The minimum spot laser diameter is called focal diameter  $d_{of}$  and depends on the diameter of the fiber, the used collimator and focusing lens, in according to the following relation:

$$d_{of} = \frac{f}{f_c} d_k$$

where

$d_{of}$ : focal diameter [mm]

$f$ : focal length [mm]  
 $f_c$ : collimating length [mm]  
 $d_k$ : fibre cable diameter [mm]

The minimum laser spot diameter in this work is:

$$d_{of} = \frac{200}{100} \cdot 0.300 = 600 \mu m$$

The laser cladding head of UNISA station is also composed of a three-beam nozzle to blow the powder on the base substrate in the deposition line: namely, three stream cones of metal powder are provided coaxially around the laser beam; each stream is injected by a separate inert gas conveying flow, then the powder meets the laser beam in the cladding area on the top surface of the substrate. The nozzle used is the model SO12, with *stand off* distance of 12 mm, corresponding to a powder flow diameter onto the surface base material of 2.5 mm. The highest laser power which could be employed with this nozzle is 3 kW.



*Fig.4.3: three-beam nozzle.*

### 4.1.3 Manipulate system

A six-degree of freedom industrial robot (ABB IRB 2400 M2400) with a dedicated controller is used to manipulate the laser beam over the cladding substrate. Its characteristics are given in the following table:

*Tab. 4-2 Manipulate system technical characteristics.*

<b>Model</b>	IRB2400/16 Type B
<b>Carrying capacities</b>	16 kg / 1.55 m
<b>Speed</b>	100 ÷ 1000 mm/s
<b>Absorption</b>	0.37 ÷ 0.67 kW



*Fig.4.4: six-degree of freedom industrial robot.*

### 4.1.4 Powder delivery and monitoring system

The powder delivery system consist of a hopper powder feeder from MEDICOAT.



*Fig.4.5: Vibrating powder system.*

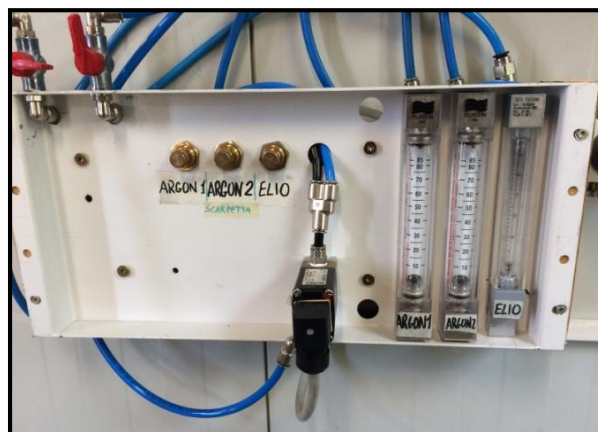
This kind of feeder is based on the volumetric control of the powder flow, which is continuous fed into a hopper through an oscillating channel as shown in the following figure.



*Fig.4.6: Oscillating channel.*

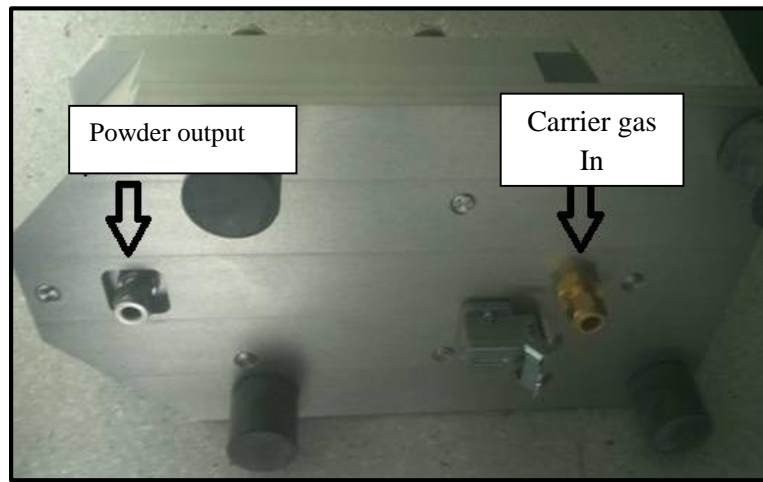
The quantity of delivered powder is determined based on the vibrational frequency of the conveyor. A relation must be found to express the mass flow as a function of input voltage inducing vibration to the conveyor by a command and control unit Reovib 168. The voltage signal changes in the range 0-10 V.

As known for the transport of the powders the use of a carrier gas is needed. In this case, we use Helium which must be delivered to the power supply system of the powder with a defined flow and pressure. Therefore, a ball valve regulator to set the carrier and the shielding gas flow is required.



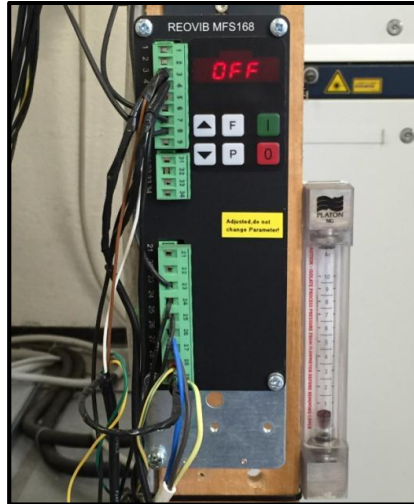
*Fig.4.7: Ball valve regulator of Helium and Argon gas.*

As you can see in the following figure, the carrier gas input is the fitting close to the plug, brass fitting. It is connected with a 3/8" tube or pipe. A similar pipe is used for the powder output, connected to a stainless steel fitting. Since the metal powder could cause the formation of electrical discharges, the cable for the powder carrier have to be antistatic.



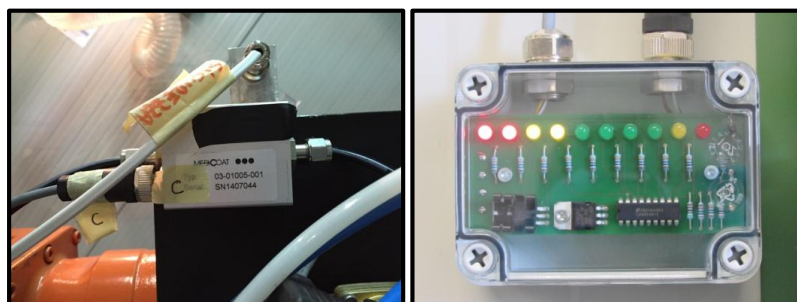
*Fig.4.8: Gas and powder fitting.*

Medicoat imposed some technological limits: it is recommended to use for the shielding gas a variable flow rate in the range of 0-10 l / min and the maximum pressure should not exceed 6 bar. The powder feeder, as already mentioned, is connected to a frequency converter REOVIB MFS 168 which is used for controlling vibratory feeders. It is a command and control system which generates an output frequency independent of the mains supply parameters, in particular the set output frequency corresponds to the frequency of mechanical oscillation of the conveyor, thus allowing regulation of the powders flow. This frequency may be set manually or automatically, but for our use it is set manually. The setting of the vibration is adjust through an external control voltage variable between 0 and 10 V given to the REOVIB.



*Fig.4.9: Drive unit component.*

In order to check the steadiness of the powder flow, a flow watch sensor connected to a led display unit is used in the process. These components check if the powder rate is constant during the process to ensure the proper execution of the process. The flow watch supervises the powder flow needed for the coating application. It is very important because hidden defects into the coating could be the result of a disturbed powder flow. To measure the whole powder line, the flow watch has been connected as near as possible to the powder line output. This is then connected with the LED display that indicates precisely the trend based on the number of LEDs turned on. We have a total of 10 LEDs that are proportional to the powder flow from 0 to 100%.



*Fig. 4.10: Flow-watch and display unit.*



## **4.2 Process tuning**

The laser cladding process tuning has been carried out in according to the next steps:

- Carrier and shielding gas setting;
- Powder mass flow setting as a function of the drive unit voltage and setting of the head position in order to focuses the powder onto the workpiece;
- Laser spot diameter as a function of the collimator lens position setting by a voltage signal.

As already written, laser cladding process requires the use of two inert gas:

- shielding gas, in order to protect the clad on the surface of the workpiece from the air of the external environment;
- carrier gas, to transport the metal powders from the conveyor to the nozzle.

In this case we use Argon as shielding gas and Helium as carrier gas. Moreover, in order to facilitate the process analysis influenced by a lot of parameters, the carrier and shielding gas have been defined at a constant value of pressure and mass flow.

### **4.2.1 Powder mass flow setting**

The quantity of delivered powder is determined based on the vibrational frequency of the conveyor. Therefore, a relation must be found to express the mass flow as a function of input voltage inducing vibration to the conveyor by a command and control unit Reovib 168. The voltage signal changes in the range 0-10 V.

After setting the carrier gas flow rate, a lot of trials are carried out changing the voltage signal. Each trial last 5 minutes and the container, used to

collect the powder, is weighed before and after the trial to calculate the powder flow rate. Helium as carrier gas has been set at 3,5 bar and 8 l/min.

AA2024 aluminum powders with mean particle size ranging from 20 to 60  $\mu\text{m}$  has been used. The feeding powder has been preliminary dried at 100 °C for one hour.

In the next table, the value of the parameters are shown.

Tab. 4-3: Powder mass flow as a function of the voltage.

Voltage [V]	Powder mass flow [g/min]
3	0,4
4	0,8
5	2,5
6	4,2
7	5,9
8	7,9
9	9,6
10	12,1

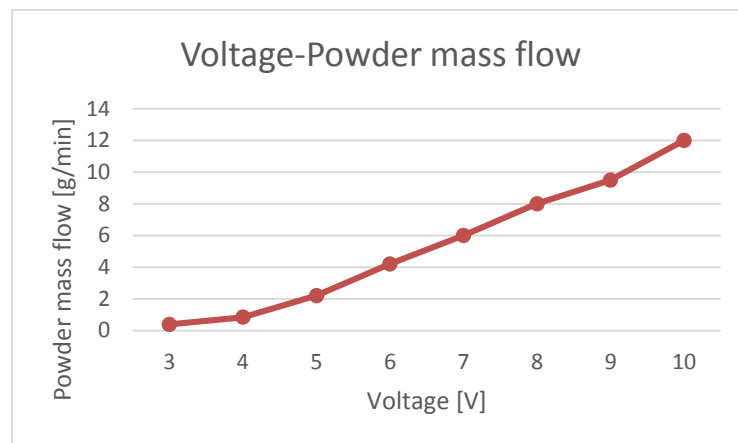


Fig.4.11: Powder mass flow as a function of voltage.

After the setting of the powder mass flow, it's necessary to set the position of the head so that the laser beam and the powder flow are focused onto the

surface. With a three nozzle the distance between the end of the nozzle and the workpiece must be 12 mm.

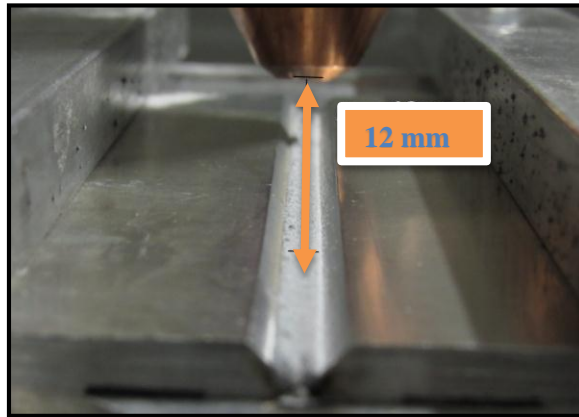


Fig. 4.12: Position of the head.

#### 4.2.2 Laser spot diameter setting

Since the focal beam diameter is 0,6 mm and a laser spot of 3-5 mm is needed, the laser beam must be defocused. As already written, the defocusing of the beam is achieved through a mobile collimator lens which changes the beam profile. Defocusing the laser beam through the handling of the laser head is not possible, because, in this way, the powder beam profile changes too and the powder flow in not focuses onto the workpiece.

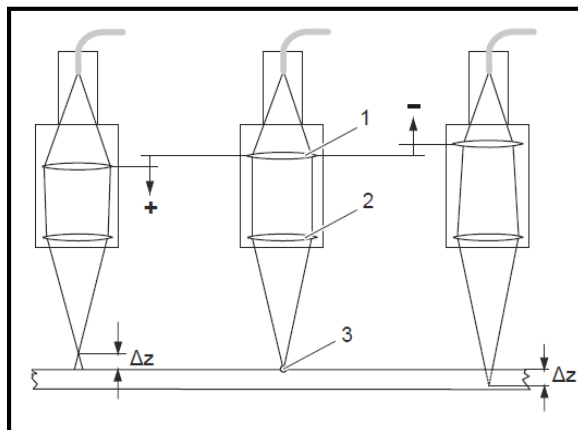


Fig.4.13: Setting of the collimator lens.

Before analyzing the relationship between the voltage and the focal position  $\Delta z$ , we have to define the  $\Delta z$  as a function of the spot laser diameter onto the surface.

To investigate the distribution of the spot diameter as a function of the  $\Delta z$ , the beam characteristics and the laser beam caustics have been analysed.

In particular the Rayleigh distance and the angle of divergence are defined as follow:

$$z_R = \frac{d_0^2}{4 * \frac{BPP}{1000}} = 7,5 \text{ mm}$$

$$\vartheta = \left( \frac{4 * BPP}{d_0 * 1000} \right) = 0,08 \text{ rad} = 4,6^\circ$$

From the caustics equation we know that:

$$d(z) = d_0 \sqrt{[1 + \left(\frac{z}{z_R}\right)^2]}$$

In the following graphic the relationship between the laser spot diameter and the  $\Delta z$  is given.

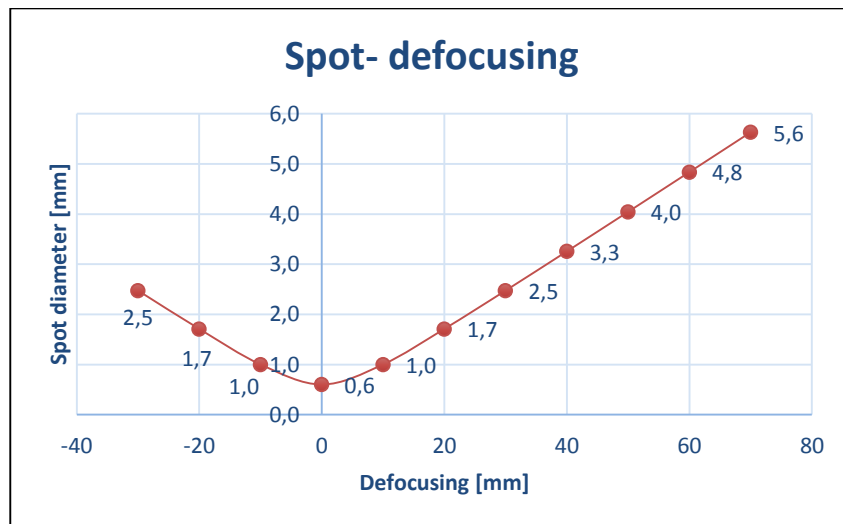


Fig.4.14: Spot diameter as a function of defocusing.

A correlation between the position of the focal spot and the voltage of the collimator lens can be define. In particular the focal position in the entire control range is proportional to the setpoint voltage. The setpoint voltage to be entered is calculated according to the following calculation formula:

$$V = \frac{\Delta z - B}{A}$$

Where:

Tab. 4-4 Setpoint voltage and focal position.

Parameter	Description	Unit
V	Setpoint voltage	V
$\Delta z$	Focal position	mm
	$\Delta z = 0$ Focal point is on the workpiece surface	mm
	$\Delta z > 0$ Focal point is above the workpiece surface	
	$\Delta z < 0$ Focal point is in the workpiece	
A	Coefficient A	mm/V
B	Coefficient B	mm

Depending on the focal length of the lens and the focal length of collimation the following values are given for the coefficients A and B.

Tab. 4-5: Coefficients for the Setpoint voltage calculation.

Focal lengths	A	B
$f=200$ mm $f_c=100$ mm	4,82 mm/V	21,03 mm

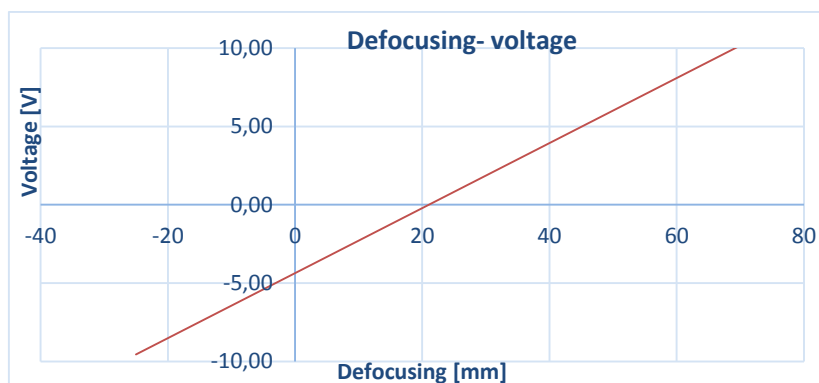


Fig.4.15: Voltage as a function of laser beam defocusing.

### 4.3 Trials execution

First of all, the powder is preheated at a temperature of 100 ° C for a time of about one hour to remove the moisture. After the pre-heating and after waiting a sufficient time to cool, the powders are filled in the powder supply system. The next step is to clean the edges of the specimen with acetone in order to remove any powder or residual dirt from the previous processing. The cleaned samples will be clamped on the worktable with a clamping system in order to keep the plates in a fixed position so to prevent displacement during the execution of the test, and above all to limit the distortions of the plates.

Then we set the following processing parameters:

- voltage of the collimating length;
- voltage regulating the powder flow rate;
- laser power;
- laser speed;
- the path that the robot must perform;
- the ignition timing of the laser and the initial delivery of the powders;
- switching on the laser and the powder delivery system.

The path that the robot must perform is taken automatically by the system and is controlled via a camera set on the laser head. In this way we check if the path is correct.

At the beginning it is necessary to check and ensure that the system is clean, so it is necessary that a cleaning operation is carried out. The powder flows for a time required to remove the remaining powder in the cable and nozzle, then power off the dispenser of powder and gets out only helium in order to eliminate the residual powder. This process is repeated at the end of the work.

A cleaning operations with vacuum and compressed air is carried out to eliminate the residual powder not fused on the track which could cause entrainment air among the clad.

## Chapter V

### Experimental test

In this chapter, the experimental tests and the final analyzes for each experimentation are discussed.

The first one is a test of single deposition on a AA2024 aluminum alloy plate carried out in order to understand the alloy characteristics for this process and to analyze the most important responses of the Laser cladding process. The effect of the most significant parameters is analysed in terms of main effect and interaction plots by Minitab statistic software.

The second one is a about a filling milled grooves through laser cladding for repair applications. In particular a pre-machined V-grooves on AA 2024 aluminum plates has been repaired by the laser cladding process with AA 2024 aluminum powders alloy. The respect for the company constraints is checked in terms of structure, defects such as porosity and cracks, microhardness.

In order to analyse the process for another aluminum alloy, the same groove has been milled and filled on A357 aluminum alloy plates.

With respect to AA2024 alloy, A357 alloy has a good corrosion resistance and excellent castability thanks to Si particles presence. Moreover, this alloy exhibits a relatively high flowability, which is preferred for Additive Manufacturing processes. It is a precipitation-hardenable A357 alloy, so in conclusion an analysis pre and post heat treatment is carried out.

## 5.1 Single clad deposition on AA2024 plates

A systematic approach has been taken in this study to investigate the effects of the main governing parameter. Taking into account that laser cladding is aimed to fix any damaged component using materials with same or similar features with respect to the base metal, AA 2024 powder has been considered to produce clads on AA 2024 plates. Inspections have been conducted in terms of clad geometry in the transverse cross-section. In particular, the possible formation of micro-pores has been discussed. Moreover, the microstructure in the clads and in the heat affected zone has been investigated via both optical and electron microscopy and energy dispersive spectrometry [61].

### 5.1.1 Test sample and powder features

AA 2024 powder has been considered to produce clads on AA 2024 plates.

Among all of the commercial high-strength heat-treatable and age-hardenable aluminum alloys, AA2024 is widely diffused in a wide range of applications and manufacturing areas, especially in the automotive, military and aerospace industries, thanks to excellent plasticity, corrosion resistance, electric conductivity and strength to weight ratio. Nevertheless, it is known that the response of this alloy to the laser beam is hindered by reflectivity, high thermal conductivity and excessive fluidity, as well as affected by significant tendency to pore formation. In addition, vaporization and loss of alloying elements may result in reduced strength as a consequence of rapid heating and cooling thermal cycles.

The chemical composition is given in the table 5-1. 5 mm thick AA 2024 plates have been used as substrate material. Prior to each test, the samples were cleaned with acetone and a clean cotton cloth to remove any aluminium dust or dust particles on its surface.

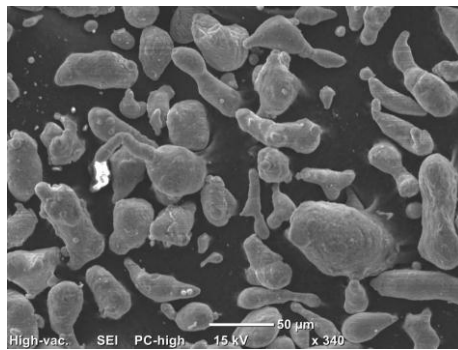
*Tab. 5-1: AA 2024 aluminum alloy chemical composition in weight percent.*

<b>Cu</b>	<b>Mg</b>	<b>Mn</b>	<b>Si</b>	<b>Fe</b>	<b>Zn</b>	<b>Ti</b>	<b>Cr</b>	<b>Al</b>
3.80 ÷ 4.90	1.20 ÷ 1.80	0.30 ÷ 0.90	0.50	0.50	0.25	0.15	0.10	Balanced

The aluminum powder alloy used in this study is a gas atomized one produced by LPW.

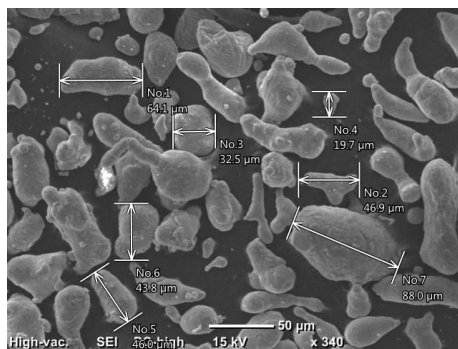


AA 2024 powder with mean particle size ranging from 20 to 60  $\mu\text{m}$  has been considered. As a steady feed rate must be provided, the feeding powder has been preliminary dried so to flow properly in the powder conveyor. As you can see in the picture 5.1, the powders has not a regular shape.



*Fig.5.1: AA2024 powder particles morphology.*

The powders have been produced by argon gas atomization. Compared to the process of atomization in water, the process in inert gas should allow a more spherical shape. The irregular morphology observed may be due to an excess of oxygen present in the chamber of the atomizer which compromised the formation of protected atmosphere. The dimensions measured are consistent with the defined range as shown in the figure 5.2.



*Fig.5.2: AA2024 powder particles size.*

A micrograph of the particles taken using a scanning electron microscope (SEM) is shown in figure. The microstructure of the powder particles varied but

generally consisted either of a coarse Al-Cu eutectic structure or an Al-Cu eutectic structure with copper crystals dispersed in it as can be seen in figure 5.3.

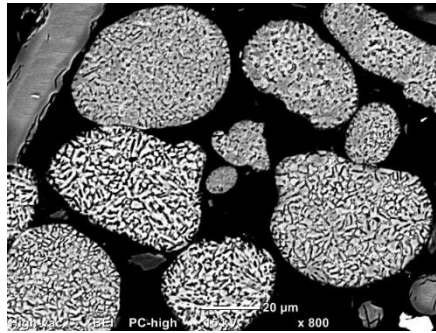


Figura 5.3: AA2024 powder particles cross section.

The composition in weight percent is given in the following table.

Tab. 5-2: Particle powder chemical composition.

<b>Cu</b>	<b>Mg</b>	<b>Mn</b>	<b>Si</b>	<b>Fe</b>	<b>Zn</b>	<b>Al</b>
5.03	1.42	0.16	0.32	0.19	0.25	Balanced

A puntual analysis has also been performed in order to evaluate the difference of composition between the black and white zone.

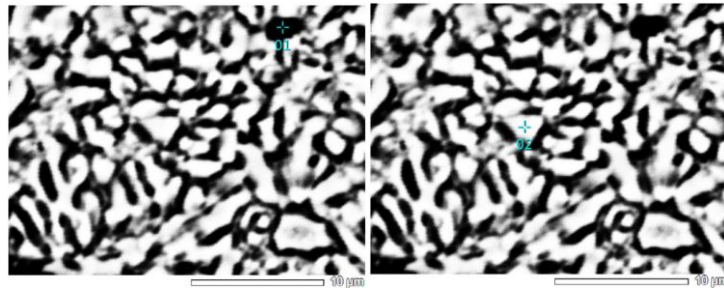


Fig.5.4: AA2024 SEM analysis of powder particles.

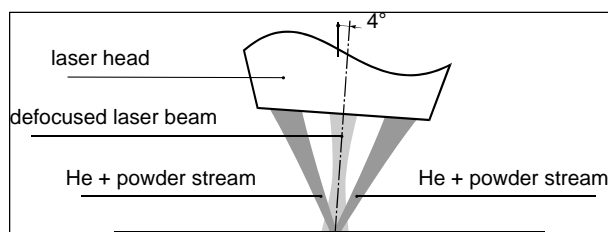
Tab. 5-3 SEM punctual analysis of powder particles.

	<b>Mg</b>	<b>Al</b>	<b>Si</b>	<b>Mn</b>	<b>Fe</b>	<b>Cu</b>
<b>01</b>	1.18	90.65	0.12	0.67	0.52	6.86
<b>02</b>	1.35	96.55	0.28	0.20	/	1.55

## 5.1.2 Experimental procedure

### 5.1.2.1 Laser deposition line

Argon flowing coaxially to the laser beam has been considered to shield the melt pool from the ambient, whereas helium has been preferred as carrier gas to transport the powder from the feeder to the processing nozzle. Different gases have been considered to these purposes; as carrier argon would disrupt the inert atmosphere above the pool. Since tilting of the laser head in the order of few degrees is common practice to process highly reflective metals such as aluminum and copper in order to prevent back reflections from entering the optics train [62], a tilting angle of  $4^\circ$  has been used. Powder laser cladding by means of a three-beam nozzle has been investigated



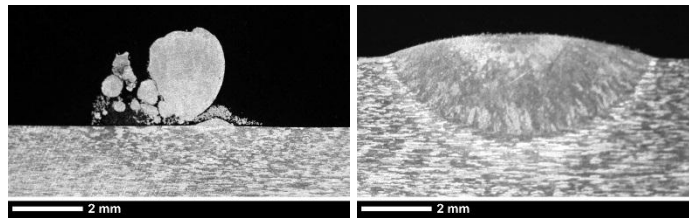
*Fig.5.5: Scheme of the three-beam nozzle; not to scale.*

### 5.1.2.2 Design of Experiments

Since many variables are involved in laser cladding, a systematic approach has been taken in order to investigate the process. A defocused beam has been considered in order to match the spot of the powder stream cones; furthermore, lower irradiance is benefited to the purpose of reduced depth of fusion and dilution in turn. The spot size of the laser beam on the substrate has been set to 5 mm. The flow rate for both helium and argon has been found based on preliminary trials and has been taken as a constant, 8 and 10 l/min, respectively. The effects of laser power  $P$ , laser scanning speed  $s$  and powder feeding rate  $m$  have been discussed.

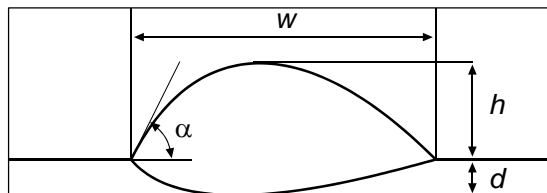
The processing levels have been chosen according to the literature, then adjusted based on preliminary trials. Detachment, lack of clad or excessive

dilution may result from improper conditions as shown in the figure 5.6. In this frame, with respect to power and speed, it must be taken into account that part of the beam irradiation for diffusion bonding and surface melting is lost in absorption in the powder stream; the remaining energy then suffers from scattering and reflection on the work-piece. Moreover, scanning speed must be taken below a threshold value so to promote homogenization of the interface between the clad and the substrate. Based on these assumptions, and given the technical constraint on maximum deliverable power to the nozzle, the processing window for power, speed and powder feeding rate has been found.



*Fig.5.6: Improper cladding conditions: lack of clad and excessive dilution.*

A full factorial, 2-level experimental plan has been arranged to investigate the process in the form of single clad deposition for an overall length of 100 mm. At a first stage analysis, the choice of a factorial plan with two levels is consistent with the literature [63], [15]. The levels for each leading factor are given in Table 5-4; eight processing conditions result. Three runs have been planned for each of them in order to check the statistical significance of the responses; a random test procedure has been considered. Consistently with the literature [63] [36] [64] [65], the main geometrical responses to be measured are clad width  $w$ , clad depth  $d$  and clad height  $h$ . Furthermore, the shape angle  $\alpha$  at both sides is worth investigating, being it related to dilution [4]: one may assume that shape angles below or above  $45^\circ$  are distinctive in conditions of high dilution or non wetting, respectively.



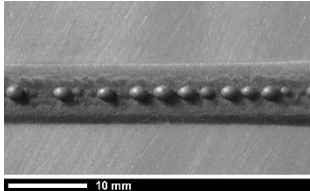
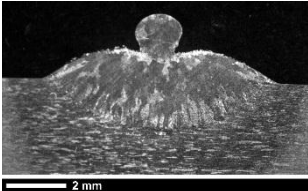
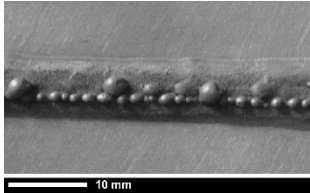
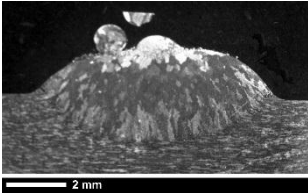
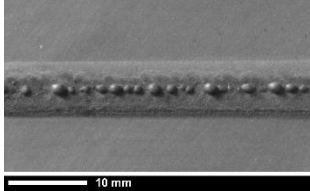
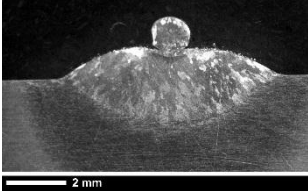
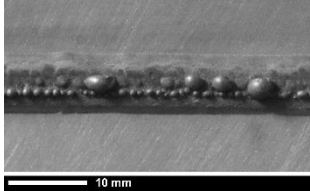
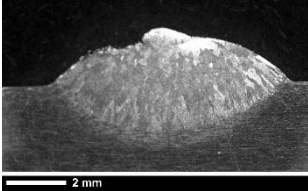
*Fig.5.7: Main geometrical responses to be measured in the clad cross-section.*

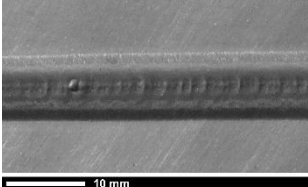
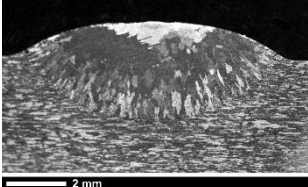
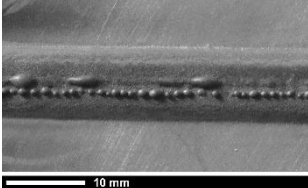
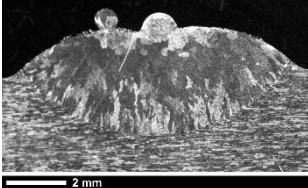
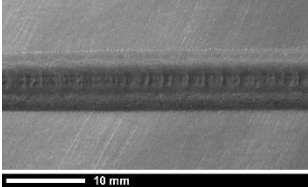
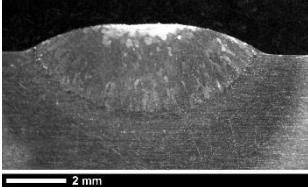
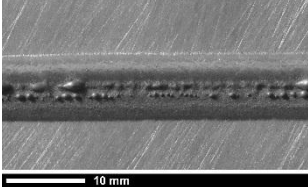
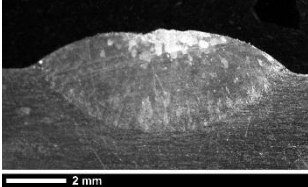
Tab. 5-4 Levels for each governing factor.

Level	Power $P$ [W]	Scanning speed $s$ [mm min <sup>-1</sup> ]	Powder feeding rate $m$ [g min <sup>-1</sup> ]
-	2500	150	5
+	3000	200	7

The measurements have been conducted upon transversal cut. In addition, since hardness is intended to be a measure of strength, its trend in the cross-section has been discussed. The microstructure has been investigated via optical and electron microscopy and energy dispersive spectrometry (EDS).

Tab. 5-5 Clad aspect and random cross-section for each processing condition.

Condition	Clad aspect	Transverse cross-section
<p><b>1</b></p> <p><math>P = 2500</math> W  <math>s = 150</math> mm min<sup>-1</sup>  <math>m = 5</math> g min<sup>-1</sup></p>		
<p><b>2</b></p> <p><math>P = 2500</math> W  <math>s = 150</math> mm min<sup>-1</sup>  <math>m = 7</math> g min<sup>-1</sup></p>		
<p><b>3</b></p> <p><math>P = 2500</math> W  <math>s = 200</math> mm min<sup>-1</sup>  <math>m = 5</math> g min<sup>-1</sup></p>		
<p><b>4</b></p> <p><math>P = 2500</math> W  <math>s = 200</math> mm min<sup>-1</sup>  <math>m = 7</math> g min<sup>-1</sup></p>		

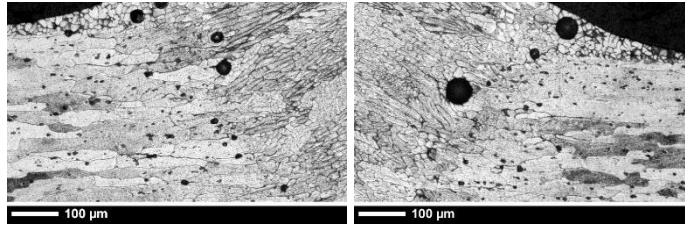
Condition	Clad aspect	Transverse cross-section
<p><b>5</b></p> <p><math>P = 3000 \text{ W}</math>  <math>s = 150 \text{ mm min}^{-1}</math>  <math>m = 5 \text{ g min}^{-1}</math></p>		
<p><b>6</b></p> <p><math>P = 3000 \text{ W}</math>  <math>s = 150 \text{ mm min}^{-1}</math>  <math>m = 7 \text{ g min}^{-1}</math></p>		
<p><b>7</b></p> <p><math>P = 3000 \text{ W}</math>  <math>s = 200 \text{ mm min}^{-1}</math>  <math>m = 5 \text{ g min}^{-1}</math></p>		
<p><b>8</b></p> <p><math>P = 3000 \text{ W}</math>  <math>s = 200 \text{ mm min}^{-1}</math>  <math>m = 7 \text{ g min}^{-1}</math></p>		

### 5.1.3 Results and discussion

#### 5.1.3.1 Defects and geometric analysis

The aspect of the track and the corresponding macrographs are shown in the table 5-5. All of the processing conditions of the experimental plan provided consistent outcome. Nevertheless, a number of micro-pores, ranging from 15 to 60  $\mu\text{m}$  on average have been found, mainly at clad boundaries. One may assume rejection of processed parts at quality checks is prevented; the usual specifications for quality in laser welding [66] have been borrowed. Even tighter requirements are matched when considering specific customer regulations for aerospace. It is widely accepted that micro-pores in AA 2024 as a consequence of fusion bonding [62] [67] are ascribed to hydrogen and other common gases. Indeed, high temperatures as experienced in the melt pool, allow a large amount of hydrogen

to be absorbed: as hydrogen solubility in solid metal is lower compared with solubility in liquid state [68], hydrogen exceeding the solubility limit at room temperature and not escaping from the solidifying clad results in pore formation.



*Fig.5.8: Micro-pores at clad boundary; condition 7*

Based on measurements in the cross-sections, the average values for each chosen response are given in Table 5-6 and have been discussed in terms of main effects plots with respect to clad geometry.

*Tab.5-6 Average values of the responses for each condition of the experimental plan.*

<b>Condition</b>	<b>w [mm]</b>	<b>d [mm]</b>	<b>h [mm]</b>	<b>Left <math>\alpha</math> [°]</b>	<b>Right <math>\alpha</math> [°]</b>	<b>Dilution [%]</b>
1	8.50	1.51	1.04	31.6	30.4	59.2
2	8.94	1.52	2.07	40.2	44.0	42.4
3	8.05	1.50	1.05	29.6	28.5	58.8
4	8.66	1.63	1.90	35.3	42.9	46.1
5	8.62	2.42	1.16	23.4	28.3	67.6
6	9.41	2.61	1.53	38.7	32.9	62.9
7	8.05	2.43	1.01	26.5	24.2	70.8
8	8.86	2.41	1.34	34.6	33.2	64.2

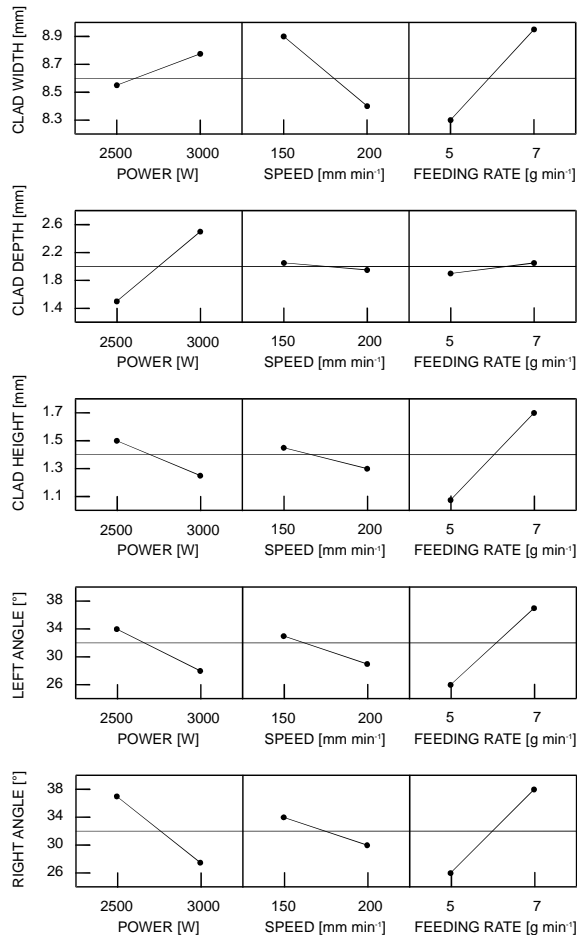


Fig.5.9: Main effects plot for geometric responses in the clad cross-section.

Being the dilution a combined parameter of depth and height, it has not been analysed. Some considerations will be carried out about depth and height respectively.

As expected, clad width increases for increasing power, increasing powder feeding rate and decreasing speed. Consistently with similar findings in the literature on aluminum cladding [64], an increase in power also yields an increase in clad depth since the available energy to melt the substrate is increased; the effect of both the scanning speed and the powder feeding rate is far less



significant. As regarding the clad height, power and scanning speed have mild effect instead. On the other hand, an increase of powder feeding rate results in increased clad height, provided that an adequate power level is set in order to effectively melt the powder particles. Nevertheless, it has been shown [65] that improper processing conditions with even higher power level may result in vaporization of powder before cladding, with consequent reduction of the overall clad dimensions, as the laser energy is lost in melting the substrate although producing the track. Moreover, an increase of power results in width increase, shape angle decrease and consequently a decrease of height. Both right and left wetting angle have a common trend as a function of the governing factors; in particular, the same trend of clad height is noticed. Therefore, the same reasons apply.

The interaction plots have been drawn. Only slight interactions are in place within the investigating domain. Similar findings are reported in the literature [15].

#### **5.1.3.2 Microstructure and micro-hardness**

As clearly shown in the macrographs, an heat affected zone (HAZ) is formed between the base metal and the fusion zone. Optical and electron microscopy observations, Vickers micro-hardness tests and EDS inspections have been conducted in the transverse cross-section to further discuss the evolution of microstructure.

The trend of micro-hardness, as resulting from an indentation pattern at approximately 0.5 mm from the surface of the plate, is discussed as a function of the distance from clad centre (Figure 5.10). Common trends and values have been found, irrespective of the processing conditions. Namely, moving from the base metal toward the clad, micro-hardness slightly increases in the primary HAZ, then decreases in a tight belt which can be referred to as secondary HAZ; a further drop is noticed in the fusion zone. The overall thickness of the substrate is involved in the primary HAZ, as suggested by the trend of micro-hardness resulting from a suitable vertical indentation pattern starting from the top surface along the centre line of the track (Figure 5.10).

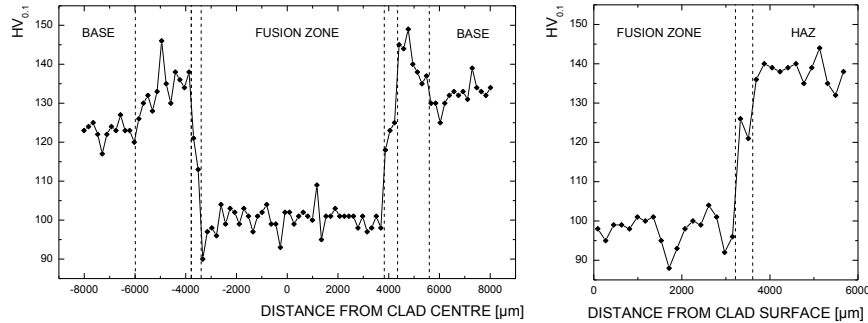


Fig.5.10: Hardness along longitudinal (left) and transverse (right) patterns; condition 7

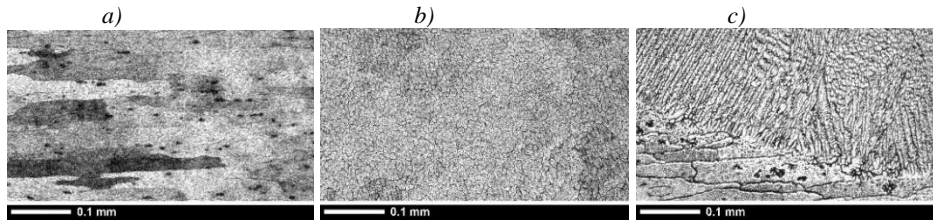


Fig.5.11: Microstructure of base metal a), core of the clad b) and HAZ interface c); condition 7.

Base average hardness is 125 HV0.1 in the base metal, which is solution-heat treated and naturally aged to stable condition, with elongated grains in both the longitudinal and long transverse direction (Figure 5.11 a). A steep decrease in micro-hardness to 98 HV0.1 on average is noticed in the fusion zone. Finer grains are formed in the core of the clad (Figure 5.11 b); a pronounced columnar structure, which is usually referred to as feather crystals [69], is produced instead at the interface with the HAZ and is driven by the direction of the thermal gradient (Figure 5.11 c).

As regarding the HAZ, the evolution of microstructure depends on both temperature and time, as in thermal aging. The material is hence expected to follow different responses based on the experienced thermal cycle. Namely, a higher cooling rate is in place in the primary HAZ where an average value of 137 HV0.1 is measured.

In this frame, backscattered electron imaging is helpful to investigate the microstructure in the cross-section. Initial dissolution of soluble phases in the base metal (Figure 5.12 a) is affected by the laser inducing fine precipitation of dispersoids in the primary HAZ (Figure 5.12 b), with consequent increased

hardness. Dispersoids move toward the grain boundary in the secondary HAZ, where the response follows overaging as a consequence of a lower cooling rate, thus giving reasons for lower hardness. Phase constituents are found at grain boundaries in the fusion zone (Figure 5.12 c): bright clusters of typical intermetallics such as S-phase,  $\theta$ -phase and  $\alpha$ -phase are deemed to mark dark aluminum grains. To support these assumptions, areal and punctual inspections have been conducted via EDS for the aluminum matrix and the grain boundaries, respectively (Figure 5.13). The corresponding quantitative analyses are given in Table 5-7, in comparison with the average values as obtained in the base metal. The chemical composition in punctual inspection at grain boundaries depends on the site of interest, thus suggesting that a compound of intermetallics is formed.

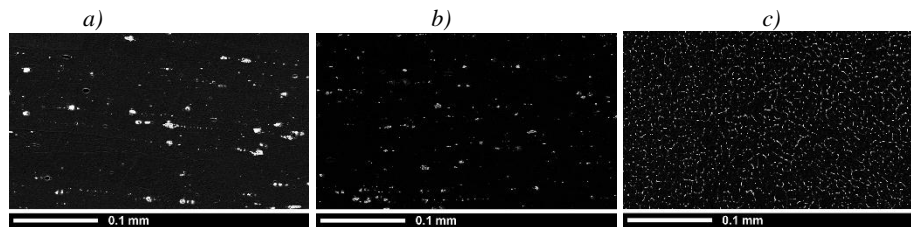


Fig.5.12: BEI scanning: base metal a), primary HAZ b) and fusion zone c); condition 7.

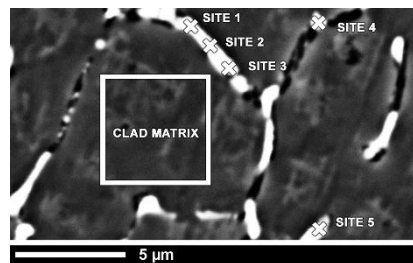


Fig.5.13: EDS inspection: sites of interest in the fusion zone; condition 7.

Tab. 5-7 Average weight percentages of the main elements, as resulted from EDS inspections in the corresponding sites of interest

Site	Cu	Mg	Mn	Si	Fe	Al
Clad matrix	0.93	1.17	0.30		0.02	97.45
Grain boundary – site 1	26.42	2.16	0.25	0.17	0.14	70.33
Grain boundary – site 2	23.57	1.71	0.29	0.22	0.32	73.88
Grain boundary – site 3	18.20	1.60	1.81	0.56	3.68	74.15
Grain boundary – site 4	27.03	1.51	0.10	0.20	0.12	70.29
Grain boundary – site 5	30.82	2.09	0.12	0.49	0.20	66.27
Base metal	3.35	1.85	0.35	0.22	0.10	94.01

#### 5.1.4 Adjustment of the process conditions

The results of the deposition experimentation are:

- Symmetry of the deposit dimension;
- Adequate metallurgical bonding between the coating and the base material;
- No macro-pores and cracks in the surface layer.

Nevertheless, all of the experimental conditions are affected by:

- High dilution;
- Large width.

Therefore, other experimental condition have been test in order to reduce the value of dilution.

##### 5.1.4.1 Experimental conditions

In order to decrease the value of dilution, as a function of depth and height, and to achieve a narrower clad, in according to the main effects of the first experimentation, other trials have been conducted with the following changes:

- smaller laser spot on the surface (3 mm instead of 5 mm);
- decrease of power and increase of laser speed in order to reduce the thermal input.

In particular the aims of this trials are: a narrower clad, reducing the laser spot on the surface; decrease of geometric dilution by reducing heat input.

Moreover, the effect of the powder feeding rate is also been analysed

In the following table, the process parameters are given:

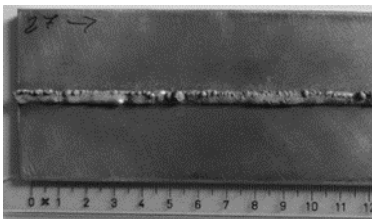
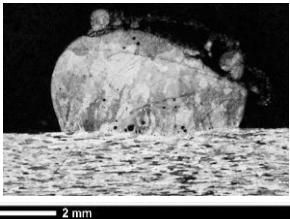
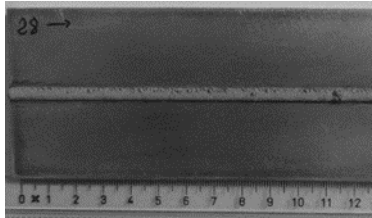

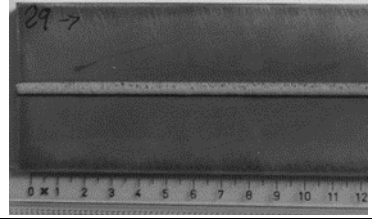
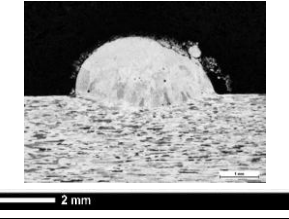
Tab. 5-8 Conditions of the second experimentation.

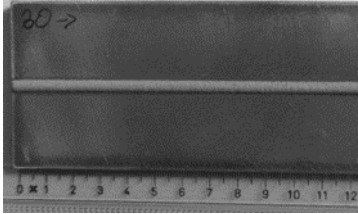
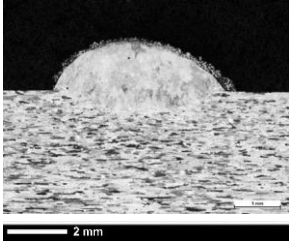
Conditions	Power $P$ [W]	Scanning speed $s$ [mm min <sup>-1</sup> ]	Powder feeding rate $m$ [g min <sup>-1</sup> ]
1	1500	400	10
2	1500	400	8
3	1500	400	6
4	1500	400	4

### 5.1.4.2 Results and discussion

In the table 5-9 clad aspect and cross-section for each processing condition are given.

Tab. 5-9 Results of the experimentation.

Condition	Clad aspect	Transverse cross-section
<p><b>1</b></p> <p><math>P = 1500</math> W  <math>s = 400</math> mm min<sup>-1</sup>  <math>m = 10</math> g min<sup>-1</sup></p>		
<p><b>2</b></p> <p><math>P = 1500</math> W  <math>s = 400</math> mm min<sup>-1</sup>  <math>m = 8</math> g min<sup>-1</sup></p>		
<p><b>3</b></p> <p><math>P = 1500</math> W  <math>s = 400</math> mm min<sup>-1</sup>  <math>m = 6</math> g min<sup>-1</sup></p>		

Condition	Clad aspect	Transverse cross-section
<p><b>4</b></p> <p><math>P = 1500 \text{ W}</math>  <math>s = 400 \text{ mm min}^{-1}</math>  <math>m = 4 \text{ g min}^{-1}</math></p>		

In the following, the geometrical characteristics as a function of the powder flow rate are reported.

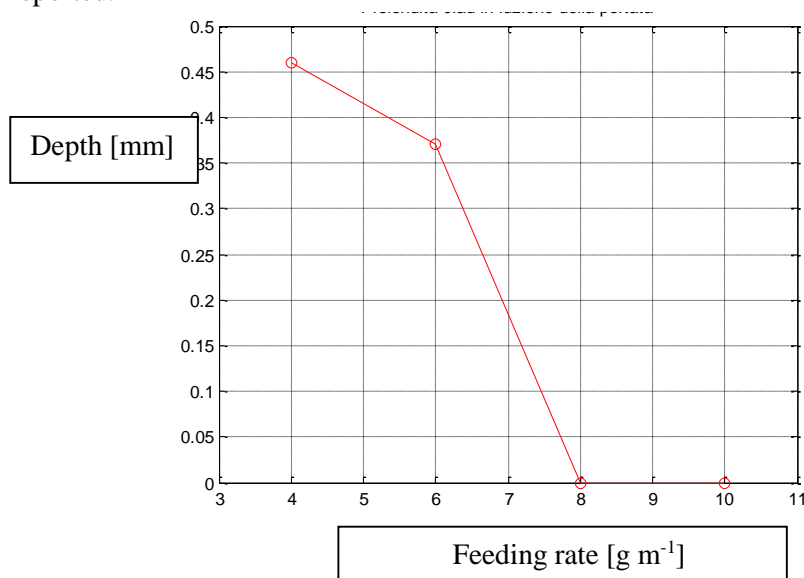
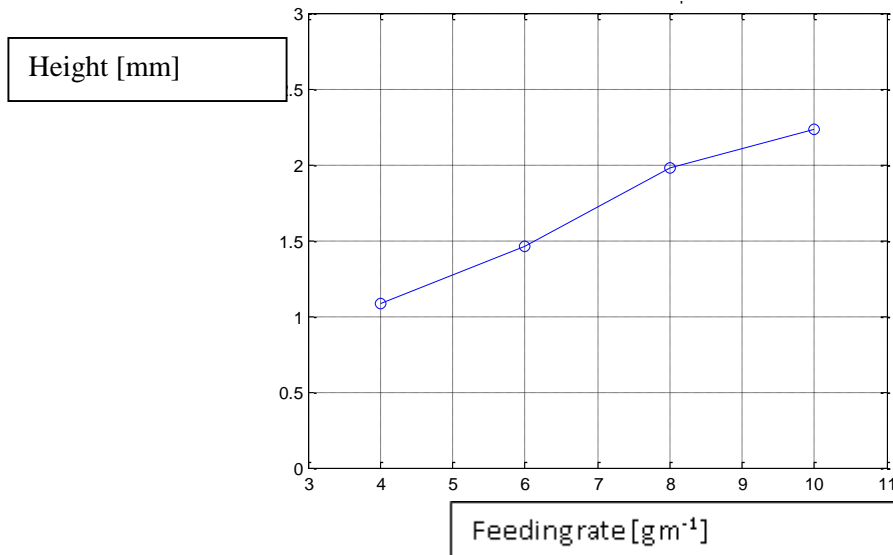


Fig.5.14: Clad depth as a function of feeding rate.



*Fig.5.15: Clad height as a function of feeding rate.*

As you can see in the graphs, an increase of the powder flow rate causes an increase of the height and a decrease of the depth. Not all the trials are satisfactory for our aim, in particular in the first and second trials there is not a good bonding between the clad and the base material and there are a lot of pores in the clad. Instead the other two conditions have a good adhesion, no pores and a low value of dilution. Conditions 3 and 4 have good adhesion, no pores and a low value of dilution. In particular dilution, which was about 70% in the previous experimental plan, is now restrained to 20% on average. The 4 condition, will be taken in account for the next experimental test.

## 5.2 Laser cladding into a pre-machined V-groove of AA2024 aluminium alloy

Laser cladding process has been established in several industrial applications. It is used for hard facing or repair purposes as reported in the first chapter.

In a repair process damaged areas or cracks can be removed by milling and subsequently be reconditioned with new material deposition. For this purpose the use of laser cladding has rarely been studied. In the literature there are some researches on the welding with filler material in a V-groove. Weld has been made by joining two pipe coupon tests by means of Gas Tungsten Arc Welding (GTAW). The configuration of the joint groove was V-shaped and the weld was completed in four passes using a filler metal. A metallographic studies and mechanical tests were made to determine microstructure evolution and mechanical properties of weld joint [70]. The microstructure and mechanical characteristics of joints welded with Gas Metal Arc Welding (GMAW) procedure, made of plates of 6082-T6 alloy with V-groove shape are also been investigated [71].

G. et al investigated the use of laser cladding to repair a damaged areas. The material has been deposited into different groove shapes, using both stainless steel and Ti-6Al-4V [72].

In this work a V-grooves on AA 2024 aluminum plates has been repaired by the laser cladding process with AA 2024 aluminum powders alloy.



*Fig. 5.16: V-groove aluminum plate.*

The dimensions of the specimens are shown in figure 5.17.



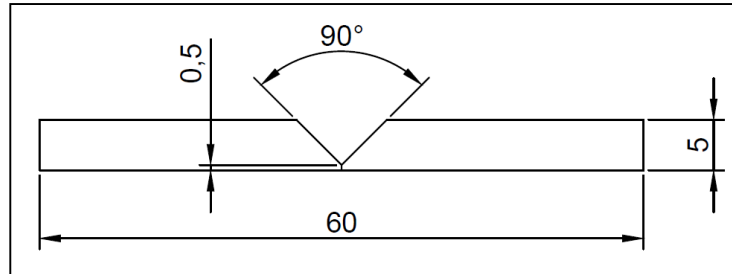


Fig. 5.17: Aluminum plate geometric characteristics.

The aim is to fill this groove, as shown in the figure, with a set of parameters in order to achieve low input, and consequently low distortion and dilution, in according to some company requirements about defects and microhardness. This research is part of a full project conducted by the department of industrial engineering of the University of Salerno in cooperation with Avio Aero.

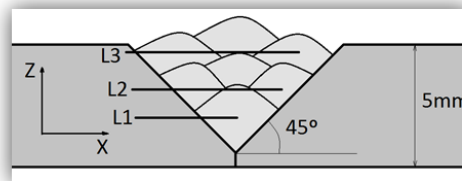


Fig.5.18: V-groove filling.

The dilution has to be minimized and the distortion controlled so that a subsequently milling to remove the jointed unmelted metal at the bottom and the overlap material at the top will be possible.

The company requirements are:

- The interface between the base material and the filler material, has to be clean in order to provide a proper metallurgical bonding between the base material and the filler;
- Some requirements apply for the porosity content: 0.5 mm  $\times$  0.5 mm max pore size; 3% max of total clad area;
- Microcracks are not allowed in the base material neither in the heat affected zone;
- A difference in Vickers microhardness of 100 HV maximum between the base material is allowed.

The parameters of the 4 condition tested on the plate surface of the specimen have been used for rebuilding the groove in a preliminary test.

### 5.2.1 Preliminary test

The clad tracks are deposited layer by layer. Each layer is composed of multiple adjacent tracks characterized by the same process parameters. After each layer deposition, the powder nozzle is raised to a defined distance, in order to deposit the next track at the same condition of laser focus.

The origin of the reference system is defined at the base of the groove, so that the first track will be processed at coordinates  $\Delta x = 0$  and  $\Delta z = 0$ .

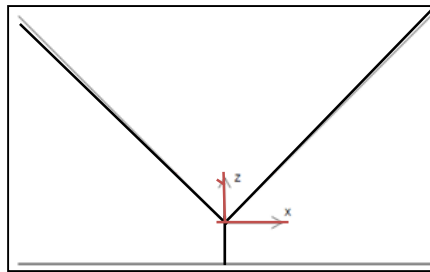


Fig.5.19: Origin reference system.

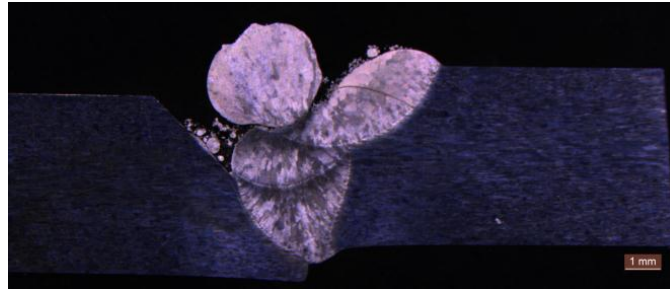
The height of the clad is measured by a calipers after each deposition. The  $\Delta z$  value will be set to the this. The  $\Delta x$  value is set to the radius of the laser beam spot, in this case 1.5 mm. The number of clads for each layer and the number of layers are decided by visual analysis during the trials.

In the following table the process parameters are given.

Tab. 5-10 Process parameters for each layer.

Parameters	LAYER 1	LAYER2	LAYER3
Power [W]	1500	1500	1500
Scanning speed [mm/min]	400	400	400
Powder feeding rate [g/min]	4	4	4
Offset [mm]	1) $\begin{cases} \Delta x = 0 \\ \Delta z = 0 \end{cases}$	2) $\begin{cases} \Delta x = 0 \\ \Delta z = 2.2 \end{cases}$	3) $\begin{cases} \Delta x = -1.5 \\ \Delta z = 3.5 \end{cases}$ 4) $\begin{cases} \Delta x = 1.5 \\ \Delta z = 3.5 \end{cases}$

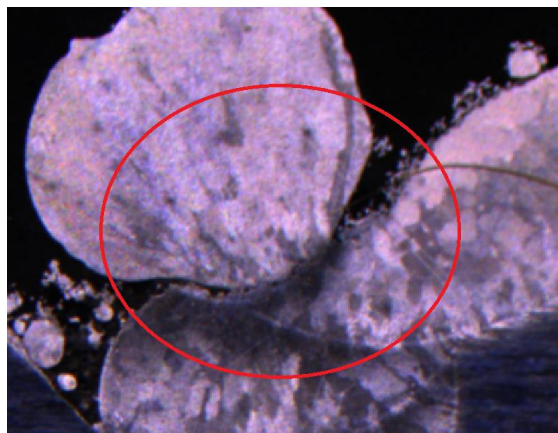
As shown in the following picture, the trial has not completely carried out since a lot of issues were presented.



*Fig.5.20: Clad cross section.*

In particular, we can observe:

- Agglomerates of unmelted powders on the surface of the clad. Probably, the thermal input is not adequate to this powder rate;
- Not acceptable metallurgical bonding between the 2nd and 3rd layer;
- Buckling of the base plates.



*Fig. 5.21: Clad issues.*

Therefore, we can say that the parameters for single track clad can not be used to fill the V-groove, since the geometry is different. Moreover, parameters have to be changed layer by layer.

It was also decided to go on with an analysis strategy layer by layer: after the deposition of each layer the specimen is analyzed by cross section and by

microscope to evaluate the geometry assumed by the clad and to calculate the displacement  $\Delta x$  and  $\Delta z$  of the laser head. This analysis is important also to measure the dilution and the plates distortions layer by layer.

### **5.2.2 Analysis strategy layer by layer: process parameters**

In order to resolve the issues of the preliminary test, the following changes are carried out:

- A decrease of powder feeding (3 g/min instead of 4 g/min) to prevent unmelted powder delimited by the walls of the groove;
- A change of parameters layer by layer: in particular the power will be increased layer by layer to improve the metallurgical bonding of the clads;
- Manually removal of the residual powder out of the groove since the residual powder in the groove would negatively affect the cladding process.
- After each deposition, the clad will be cutted in order to evaluate its quality by a microscope and measure the  $\Delta x$  and  $\Delta z$  displacement.

For the first layer, in order to reduce the distortion and the deformation of the plates, the interaction time between the laser beam and the base material has to be reduced so the laser speed is increased equal to 1000 mm / min. However, to ensure an adequate heat input to melt the powder and part of the base material, a power increase is necessary. The maximum value of power which we can use with the three beam nozzle is 3000 W, and this is the value used for the first layer deposition.

For the other layers, in according with the last paragraph, the following changes are carried out: power increase with respect to the preliminary test, and variation of the power layer by layer. In particular, the values will be 2000 W, 2200 W and 2400 W, respectively, for the 2nd, 3rd and 4th layers.

The parameters that will not be changed with respect to the preliminary filling are:

- Helium flow rate: 8 l / min (3.5 bar);
- Argon flow rate: 10 l / min (5 bar);
- Spot size of the laser beam on the surface: 3 mm;

- Laser speed of 400 mm / min;
- The origin of the reference system.

The following table gives the process parameters.

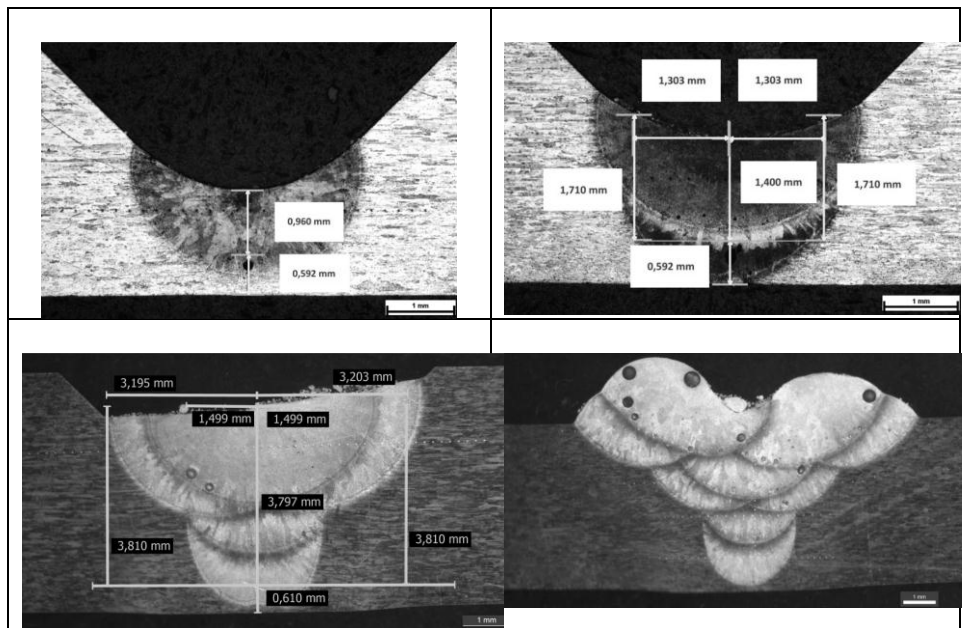
Tab. 5-11 Process parameters for each layer.

PARAMETRI	1° LAYER	2° LAYER	3° LAYER	4° LAYER
Power [W]	3000	2000	2200	2400
Scanning speed [mm/min]	1000	400	400	400

After each deposition, the clad has been cutted in order to evaluate the quality by a microscope and measure the  $\Delta x$  and  $\Delta z$  displacement.

In the following a cross sections with the relative measurements for each layer are shown.

Tab. 5-12: Cross section for each layer.



In order to define the  $\Delta x$  displacement, a measurement for each layer has been made taking into account the original edges of the V-groove as shown in the following picture.

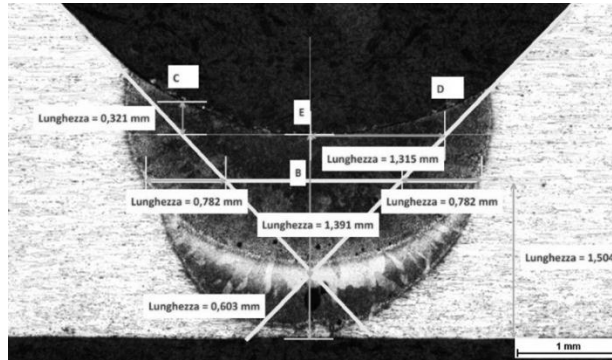


Fig.5.22: Displacements measurement.

In conclusion, the layer have been deposited in according to to the strategy shown in the picture below. The table shows the process parameters used for the deposition of each layer.

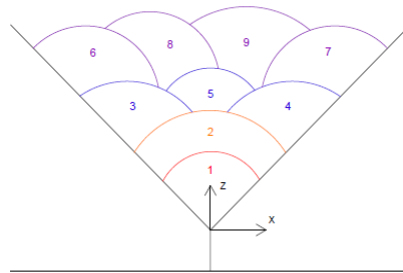
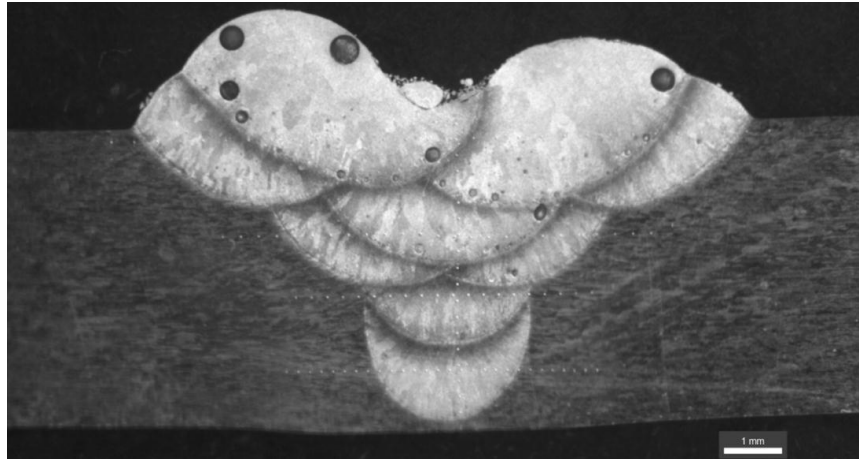


Fig.5.23: Strategy of deposition scheme.

Tab. 5-13 Process parameters for each layer.

PARAMETERS	LAYER 1	LAYER2	LAYER 3	LAYER 4
Power [W]	3000	2000	2200	2400
Laser speed [mm/min]	1000	400	400	400
Powder feeding [g/min]	3	3	3	3
Offset [mm]	1) $\begin{cases} \Delta x = 0 \\ \Delta z = 0 \end{cases}$	2) $\begin{cases} \Delta x = 0 \\ \Delta z = 0,96 \end{cases}$	3) $\begin{cases} \Delta x = -1,3 \\ \Delta z = 1,7 \end{cases}$ 4) $\begin{cases} \Delta x = 1,3 \\ \Delta z = 1,7 \end{cases}$ 5) $\begin{cases} \Delta x = 0 \\ \Delta z = 1,4 \end{cases}$	6) $\begin{cases} \Delta x = -3,2 \\ \Delta z = 3,8 \end{cases}$ 7) $\begin{cases} \Delta x = 3,2 \\ \Delta z = 3,8 \end{cases}$ 8) $\begin{cases} \Delta x = -1,5 \\ \Delta z = 3,8 \end{cases}$ 9) $\begin{cases} \Delta x = 1,5 \\ \Delta z = 3,8 \end{cases}$

A cross section of the filled V-groove is shown.



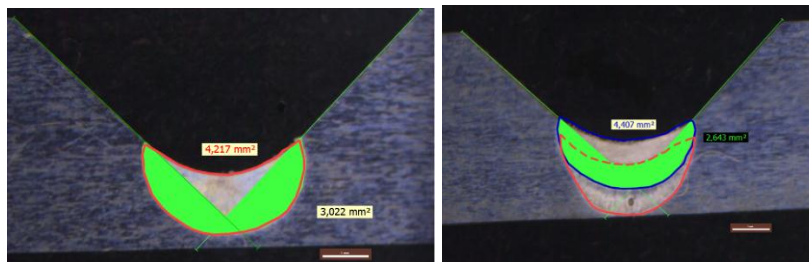
*Fig.5.24: Filled V-groove cross section.*

### 5.2.3 Buckling, deformation and dilution analyzes

In order to evaluate the melted material both of the base material and of the pre-deposited clad, outlining the reference of the V-groove is necessary. The dilution has been analyzed as the ratio between the melted area of the substrate and the area of the clad.

$$dilution = \frac{A_{melted\ substrate}}{A_{clad}} * 100$$

In the following pictures this measures are shown.



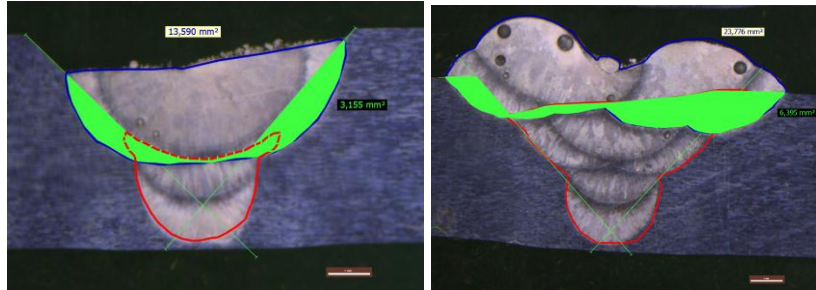


Fig.5.25 Dilution measurements.

In the following table the values of dilution for each layer are shown.

Tab. 5-14: Dilution measurements.

	Dilution [%]
1° layer	72
2° layer	60
3° layer	23
4° layer	27

The third and fourth layer value of dilution is adequate for this kind of process. Instead, the dilution for the first and second layer could seem excessive, but it is necessary to melt the substrate so that the weld of the two plates is achieved.

In order to evaluate the buckling and deformation of the specimens, some measures are made pre and post deposition.

In particular, the following characteristics are analyzed:

- a: juxtaposition thickness of the plates;
- b: width of the plates;
- c: maximum distance of the V-groove;
- $\alpha$ : distortion of the plate.

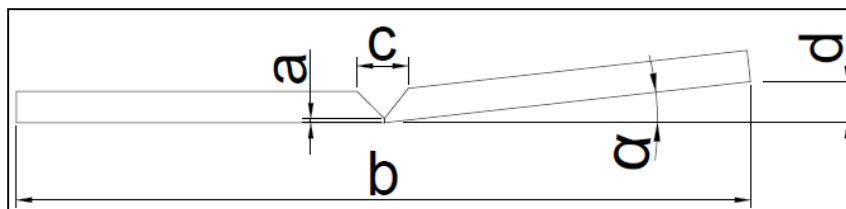


Fig.5.26: Buckling measurements.



Since a milling has to be made to remove the unmelted material at the bottom and the overlap material at the top, the deformation (reduction of the width) must not exceed the 2% value while the buckling must not exceed 1,50 °.

In the following table the measurements before and after deposition are shown for both the individual layer and the complete filling.

*Tab. 5-15 measurements before and after deposition.*

	a [mm]	b [mm]	c [mm]	b <sub>i</sub> [mm]	b <sub>u</sub> [mm]	c <sub>i</sub> [mm]	c <sub>u</sub> [mm]	α <sub>i</sub> [°]	α <sub>u</sub> [°]
1° layer	0.59	117.66	8.89	117.50	117.43	8.47	8.40	/	/
2° layer	0.59	117.68	8.65	117.45	117.38	8.48	8.39	/	/
3° layer	0.61	117.64	8.63	116.73	116.55	7.53	7.48	0.64	0.67

	a [mm]	b [mm]	c [mm]	b <sub>i</sub> [mm]	b <sub>u</sub> [mm]	α <sub>i</sub> [°]	α <sub>u</sub> [°]
4° layer	0.50	117.77	8.95	116.55	116.38	1.38	1.46

The distortion of the plate for the deposition of the 1st and 2nd layer is negligible, instead it becomes more significant in the 3rd and 4th layers. Moreover, as the number of depositions increases, the deformation grows; in particular in the complete filling there is a reduction of the width of 1,04% with respect to the original size and a distortion greater than 1°. However the requirements are always respected.

In the following paragraph the microscope and SEM analyses are given in order to analyze the defects and the distribution of the alloy constituents in the substrate and in the clad. Finally, a microhardness analysis is presented.

### 5.2.4 Results and discussion

The following analysis are conducted:

- Defects analysis: by the use of the optical microscope in order to identify and analyze the defects such as pores and cracks, inclusions or any separations between clad and material basis;
- Metallurgical analysis: by means of optical microscope and scanning electron microscope (SEM), in order to investigate the structure of the base material and the clad, distinguishing the

composition of the phases by means of the analysis EDS (energy dispersive spectrometry);

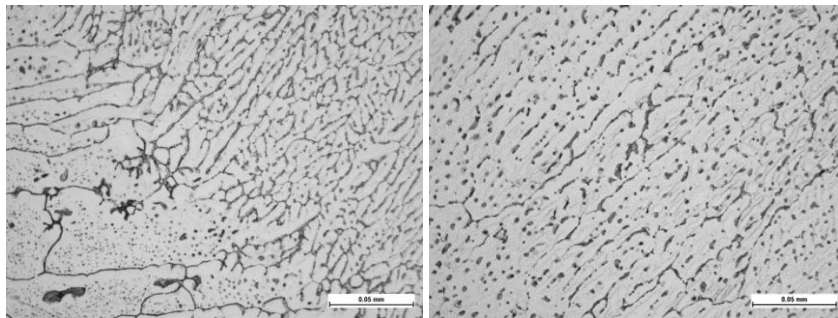
- Mechanical Analysis: analysis of Vickers microhardness, to determine the hardness in various locations along the transversal section of the groove.

This analysis have to be conducted to check the compliance of the company requirements given in the last paragraph.

#### 5.2.4.1 Defects analysis

The interface between the base material and the filler material, in this case the clad must be clean and representative of a metallurgical bond between the base material and the filler. Defects extended for a maximum of 2%, and at the interface with single length of 0.2 mm can be accepted (cold joints, porosity, delamination, etc.). Voids, pores and cavities within the filler material should be evaluated and reported as porosity and documented by photo. The maximum level of porosity must be less than 0.5 x 0.5 mm. Any levels of porosity exceeding this limit may be accepted but must still be documented. Microcracks are not allowed neither in the base material not in the heat affected zone. Microcracks are allowed to a maximum of 0.5 mm only on the filler material.

As shown in the following pictures, there is a good metallurgical bonding between base material and clad. Moreover, there are no defects in the cladding interface.

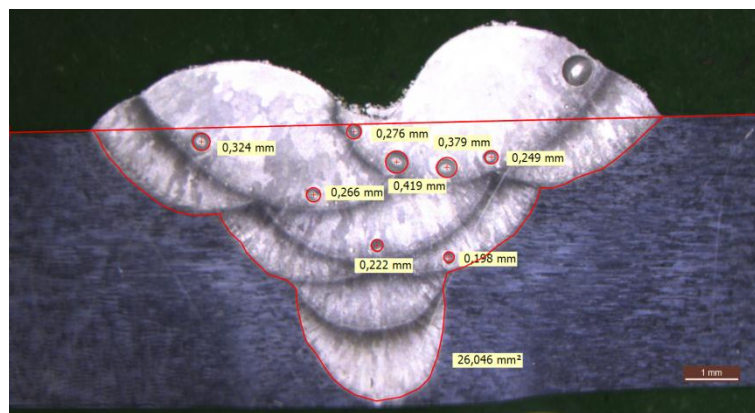


*Fig 5.27: Haz (on the left) and clad interface (on the right).*

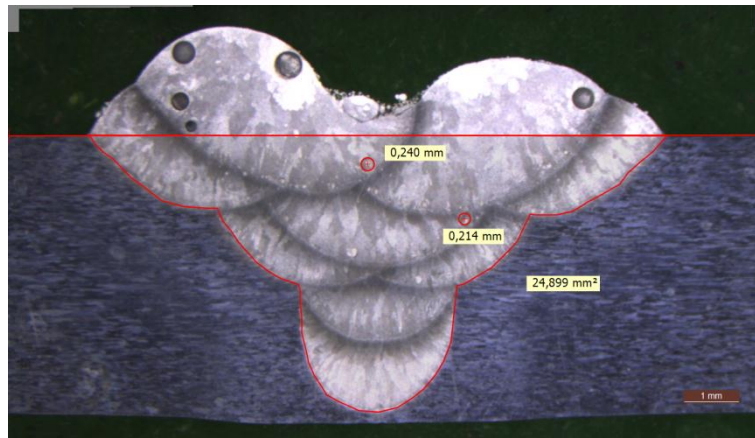
The analysis shows the presence of pores within the clad and in the overlap material on the top of the surface. These pores have a spherical shape, which suggests that they are caused by dissolved gases. It could be a problem of

supersaturation that the solidified metal may have against the gas previously absorbed from the liquid phase. Unlike other metals, the aluminum absorbs almost exclusively hydrogen.

In the following pictures the measurements of the pores are given to check if the dimension respect the company requirements and if the ratio of the void total area and the clad is less of 3%. Two cross section are given being the first one the section with the maximum extension and the second one the section with the minimum extension.



*Fig. 5.28: Pores measurements first cross section.*



*Fig. 5.29: Pores measurements second cross section.*

The pores respect the requirement, having all a size smaller than 0.5 x 0.5 mm.

Moreover, the total area of the pores has been calculated as the sum of each pore  $A_i$ , and it has been related to the total area of the clad  $A_f$ .

$$A_{\%} = 100 \cdot \frac{\sum A_i}{A_f}$$

Pore first section [mm<sup>2</sup>]

0,08  
0,06  
0,11  
0,05  
0,06  
0,14  
0,04

Pore second section [mm<sup>2</sup>]

0,045  
0,036

Area clad first section [mm<sup>2</sup>]

26,05

Area clad second section [mm<sup>2</sup>]

24,89

Porosity percentage first section [%]

2,18

Porosity percentage second section [%]

0,33

The total porosity in both section is less than 3%, therefore the company requirement is observed.

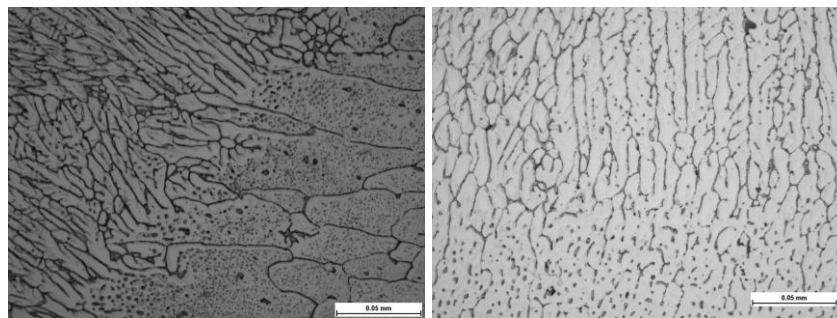
#### 5.2.4.2 Metallurgical analysis

Metallurgical structure of the material has been investigated. The base material is characterized by elongated grain structure typical of the rolling process used to machine the plate. The following picture shows the presence of the fine precipitates (black point) in the aluminium matrix.



*Fig. 5.30: Base material, aluminum matrix.*

The microstructure of cladding in the interface zone shows a columnar growth traversing the cross section in according to the direction of heat evacuation.



*Fig. 5.31: HAZ clad and substrate (left), HAZ third and fourth layer (right).*

Dispersoids move toward the grain boundary in heat affective zone and phase constituents are found at grain boundaries in the fusion zone as shown in the following.

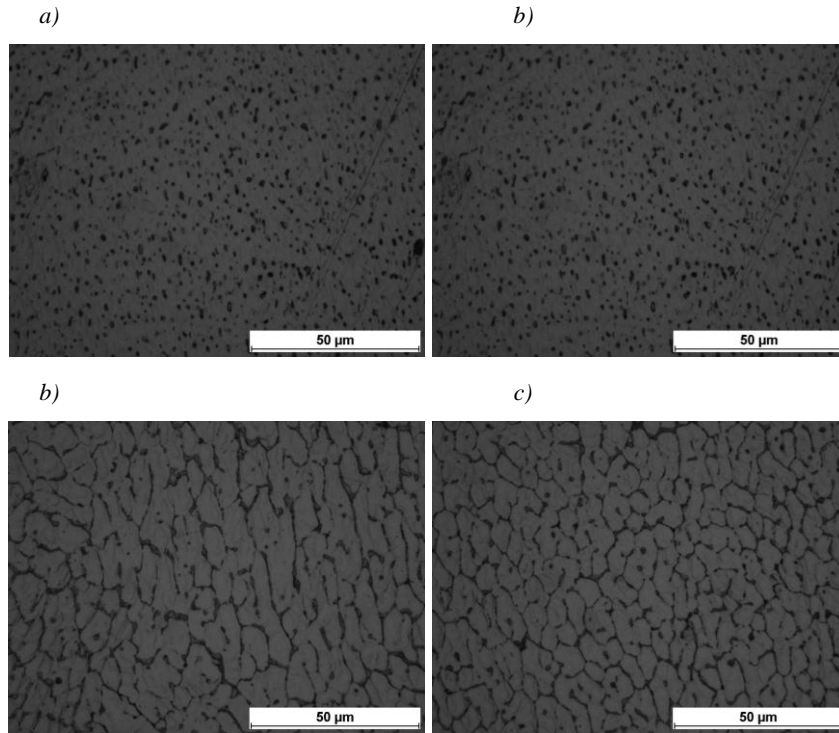


Fig.5.32: a)1° layer, b)2° layer, c)3° layer, d)4° layer microstructure.

In the following the grain size, calculated as the average of the grains contained in four segments having a length of 50 μm and directed at angles of 0°, 45°, 90° and 135° is shown.

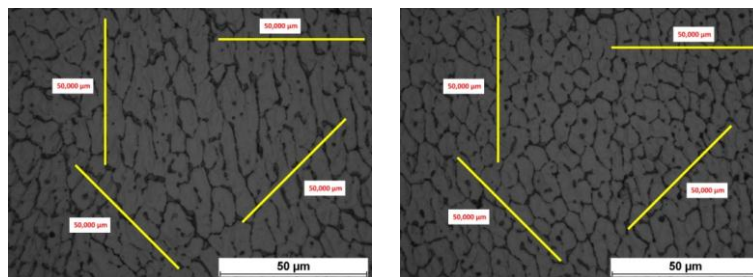


Fig.5.33: Grains size measurement 3° layer (left) e 4° layer (right)

This measurement has not been performed for the first and second layer because the precipitates are not at the grain boundary, therefore the grain are not well defined.

Tab. 5-16: Grain size measurements.

Grain size 3° layer			Grain size 4° layer		
Number of grains in 50 $\mu\text{m}$	Avarage number of grains in 50 $\mu\text{m}$	Average size of the grain [ $\mu\text{m}$ ]	Number of grains in 50 $\mu\text{m}$	Avarage number of grains in 50 $\mu\text{m}$	Average size of the grain [ $\mu\text{m}$ ]
5	6.5	7.69	5	6.8	7.41
7			7		
8			8		
6			6		

The fourth layer is characterized by smaller grains since it is subjected to a faster cooling and is not subjected to successive heatings.

In the following an analysis on the first layer is shown.

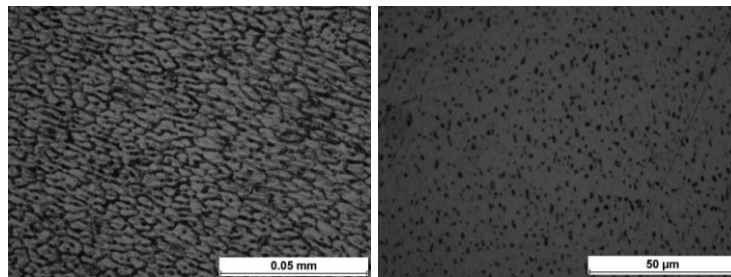


Fig.5.34: 1° layer microstructure: reference sample (left), full filling (right).

Comparing the first layer of the reference sample, where only the first layer has been deposited, with the first layer of the full filling is possible to observe in the second one a dispersion of the precipitates since it is subjected to successive heating due to the deposition of subsequent clad.

### 5.2.4.3 SEM examination

The SEM image of the base material shows the matrix of aluminium (black region) with the precipitates dispersed within (grey points).

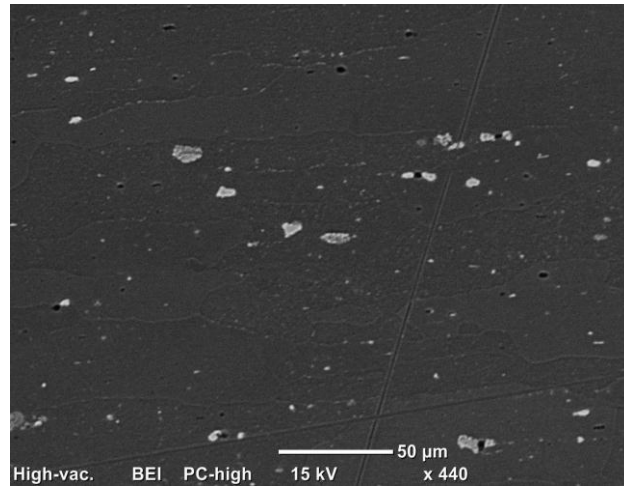


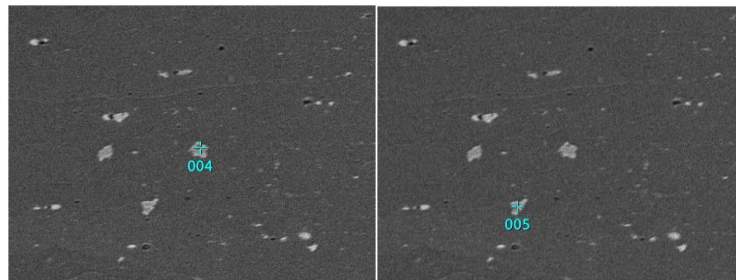
Fig.5.35: Base material: SEM analysis.

The EDS analysis in the base material confirms the alloy composition as given in the following table.

Tab. 5-17: EDS analysis in the base material.

	Mg [%]	Al [%]	Si [%]	Mn [%]	Fe [%]	Cu [%]
<b>Lega</b>	0.33	92.76	0.06	0.63	0.17	4.54

The compositions of the intermetallic particles in the base material highlighted in the following pictures have also been determined by EDS analysis.





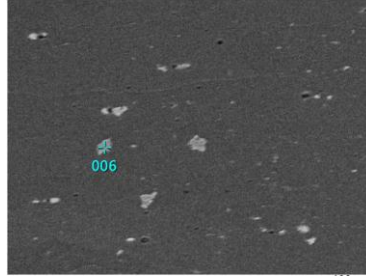


Fig.5.36: Intermetallic particles.

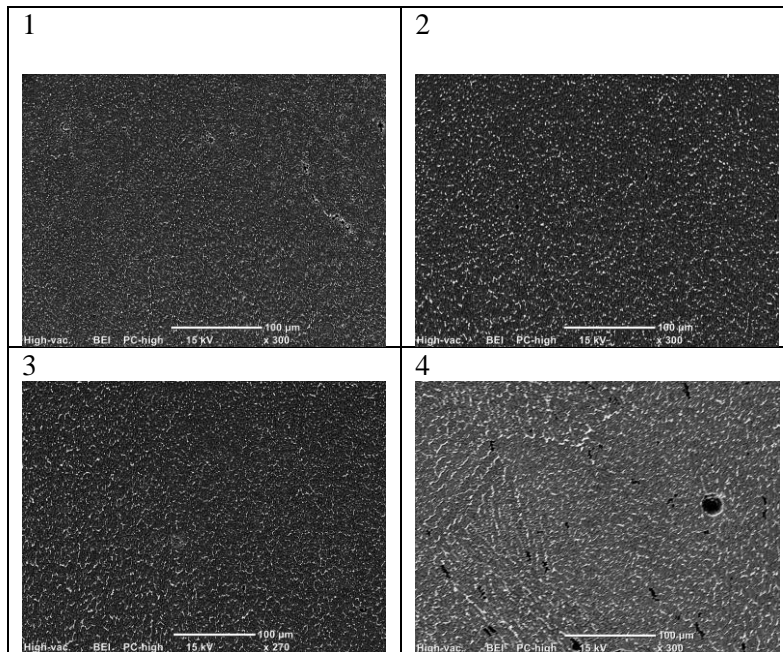
Tab. 5-18 EDS punctual analysis in the base material.

	Mg [%]	Al [%]	Si [%]	Mn [%]	Fe [%]	Cu [%]
<b>004</b>	1.02	69.94	1.83	2.60	6.31	18.30
<b>005</b>	0.79	64.73	1.94	1.04	6.12	25.39
<b>006</b>	1.02	69.94	1.83	2.60	6.31	18.30

As you can see in the table, the intermetallic particles are mainly of aluminium and copper.

The same analysis has been performed in the clad for each layer.

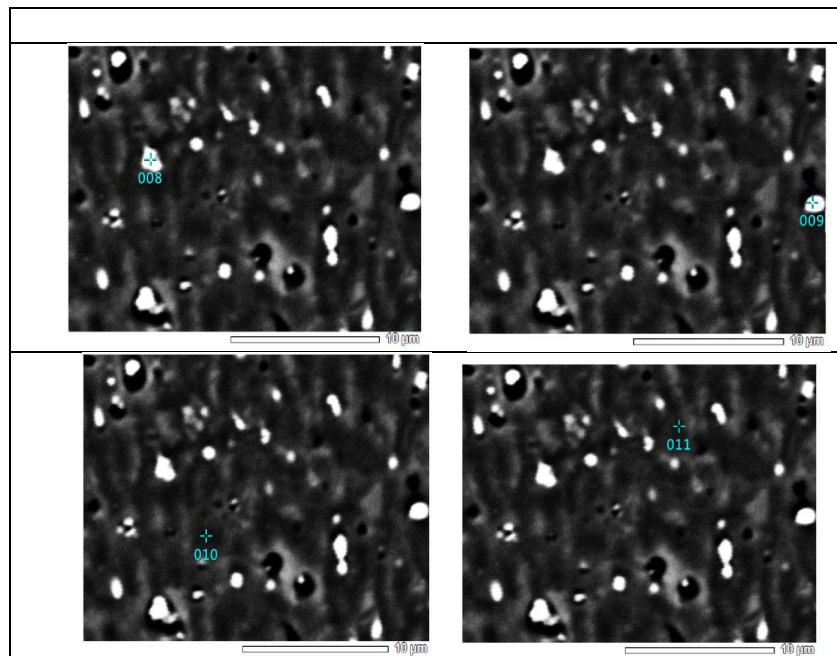
Tab. 5-19 Clad microstructure for each layer.



Also by SEM is evident a difference between the layers: in particular in the third and fourth layer constituents are found at grain boundaries instead in the first and second layer the particles are dispersed in the aluminium matrix.

In the first and second layers the clad has a very small granular structure, determined by the high dispersion of the precipitates which are not deposited at the grain boundary, but rather remained mostly in spherical form in the aluminium matrix.

Tab. 5-20 Punctual analysis of precipitates.



Tab. 5-21 Chemical composition of precipitates, weight percent.

	Mg [%]	Al [%]	Si [%]	Mn [%]	Fe [%]	Cu [%]
<b>008</b>	1.66	87.67	2.64	0.21	0.25	7.57
<b>009</b>	1.46	85.23	0.17	0.21	0.16	12.77
<b>010</b>	1.73	97.30	-	0.08	0.03	0.86
<b>011</b>	1.66	97.46	0.01	0.15	-	0.72

These precipitates are both of  $\theta$  ( $\text{Al}_2\text{Cu}$ ) and S ( $\text{Al}_2\text{CuMg}$ ) phases.

The precipitates have a higher concentration of copper and the silicon than the alloy, while in the aluminum matrix, the concentration of magnesium is high. In the third and fourth layers the precipitates take a dendritic shape at grain boundaries.

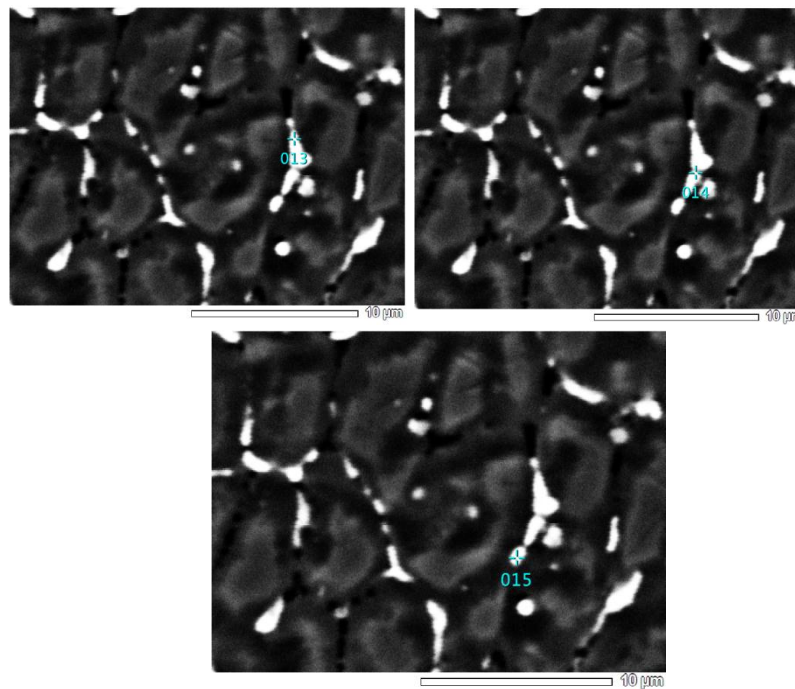


Fig.5.37: Clad precipitates in the third and fourth layer.

Tab. 5-22 Chemical composition of precipitates, weight percent.

	Mg [%]	Al [%]	Si [%]	Mn [%]	Fe [%]	Cu [%]
<b>013</b>	1.12	91.29	0.75	0.07	0.18	6.57
<b>014</b>	1.50	91.61	1.46	0.07	0.03	5.33
<b>015</b>	2.36	89.54	1.87	0.04	0.05	6.15

These precipitates are mainly of S phase,  $Al_2CuMg$ .

#### 5.2.4.4 Vickers micro-hardness

The trend of micro-hardness is discussed as a function of the distance from clad centre for each layer. Common trends and values have been found, irrespective of the processing conditions. Namely, moving from the base metal

toward the clad, micro-hardness decreases in the HAZ and a further drop is noticed in the fusion zone.

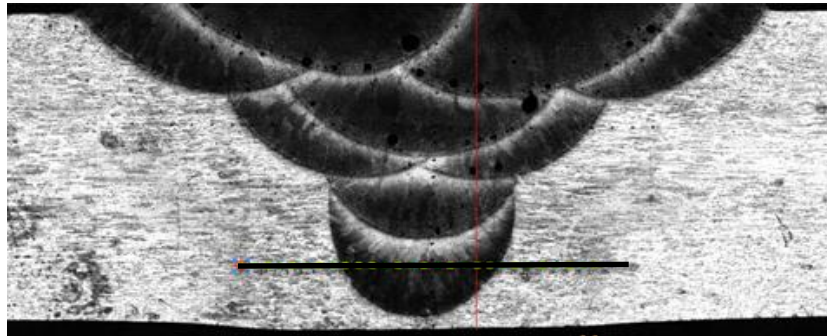


Fig.5.38: First layer microhardness path.

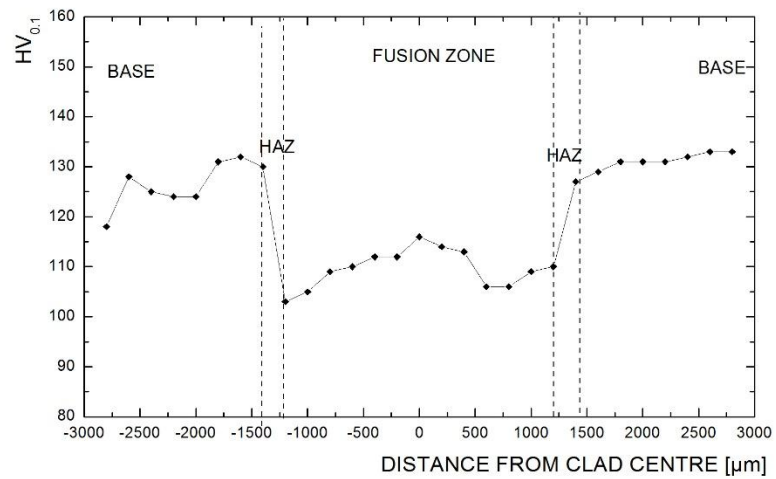


Fig.5.39: First layer microhardness trend as a function of the distance of the clad centre.

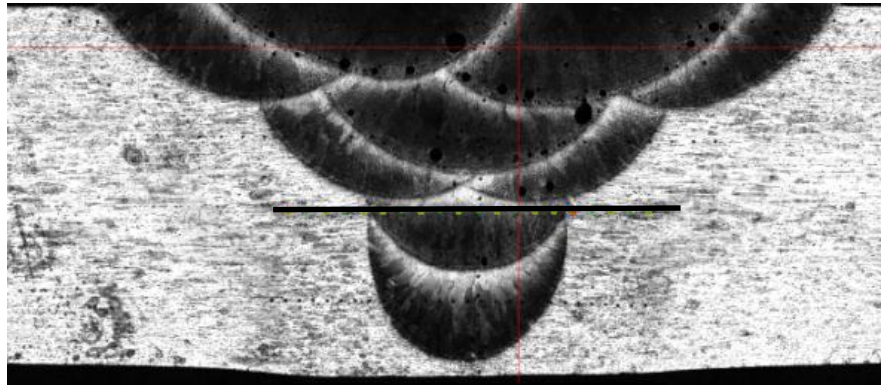


Fig. 5.40: Second layer microhardness path.

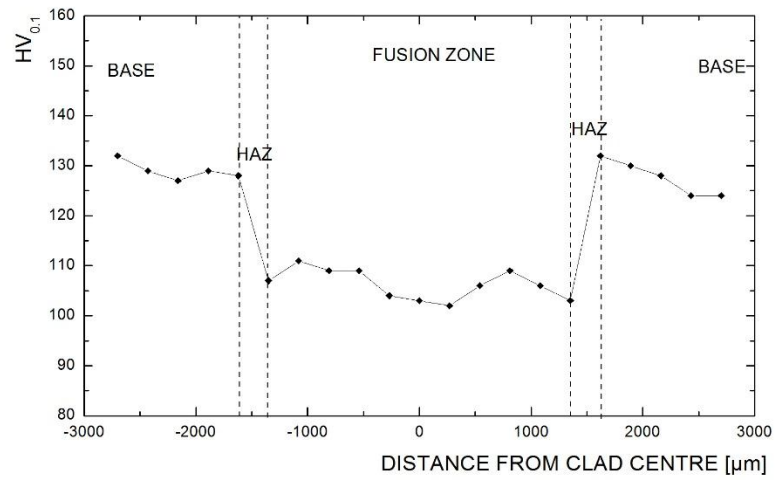


Fig.5.41: Second layer microhardness trend as a function of the distance of the clad centre.

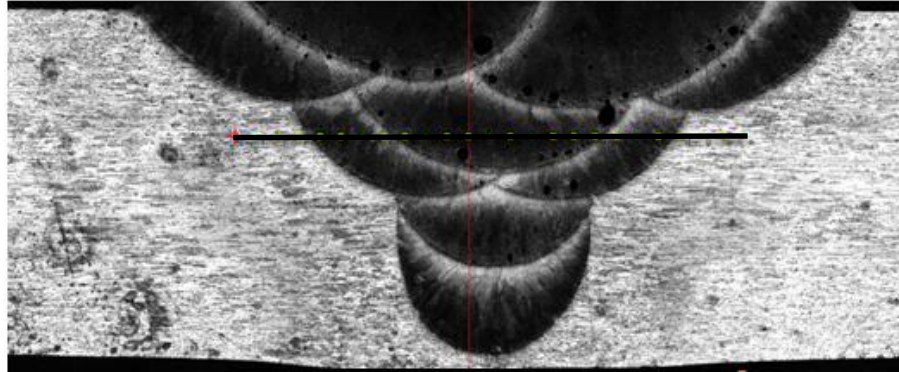


Fig.5.42:Third layer microhardness path.

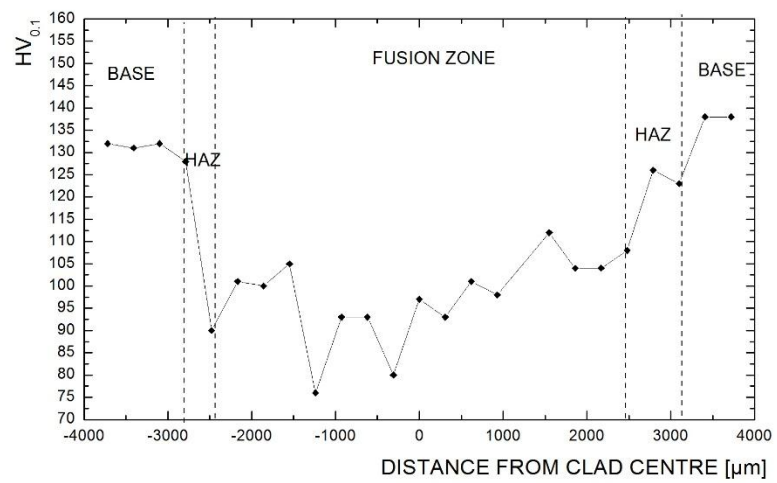


Fig. 5.43: third layer microhardness trend as a function of the distance of the clad centre.

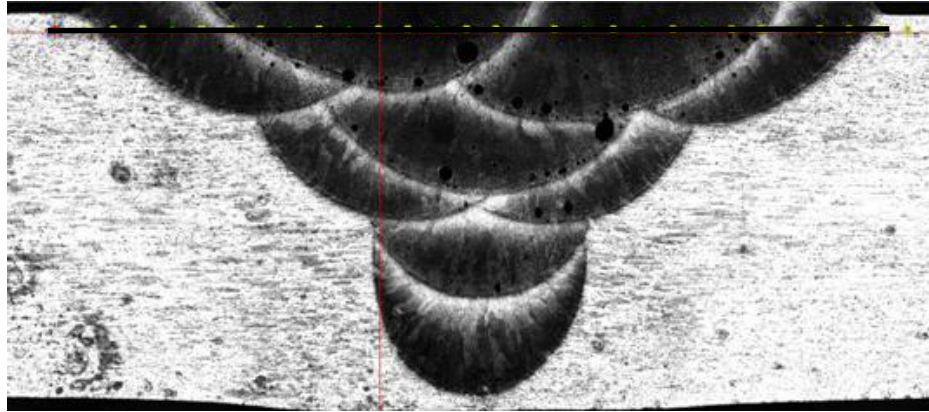


Fig.5.44: Fourth layer microhardness path.

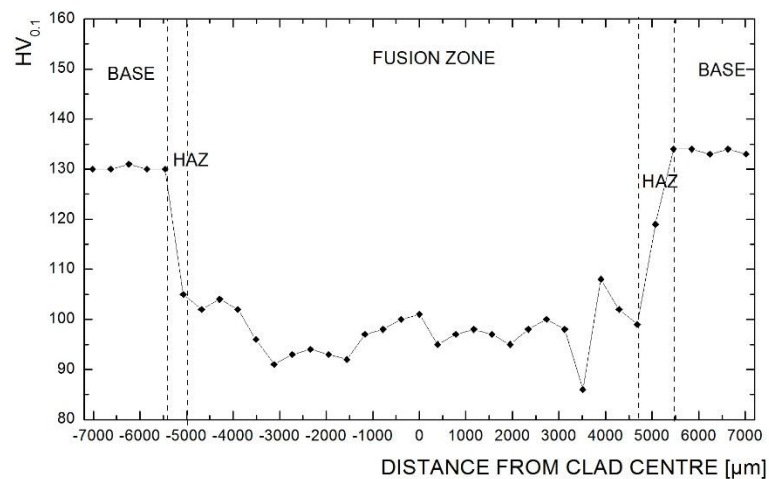


Fig.5.45: Fourth layer microhardness trend as a function of the distance of the clad centre.

From these analysis we can say that the lower layers have a microhardness greater than the upper layer. This phenomenon is associated to the the process of artificial aging. It has been observed that by subjecting the alloy AA2024 to an artificial aging was observed an increase in the microhardness of the material. In our case the clad of the first layer is subjected to a heat treatment as they are subjected to a series of successive heatings to allow the deposition and completion

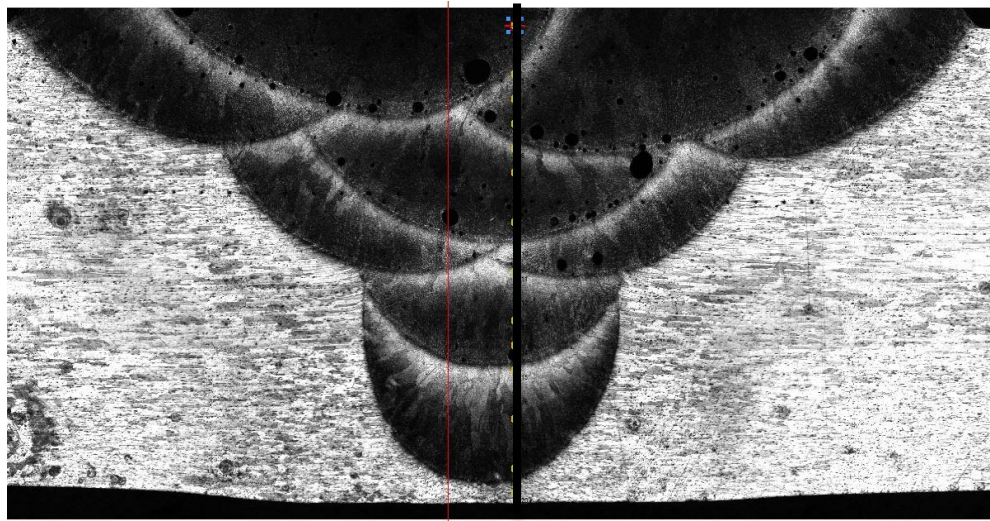
of the filling. For the same reason it was possible to observe a different structure of the grains and of the precipitates.

The fourth layer has a lower value of micro-hardness since it is not subjected to successive deposition.

*Tab. 5-23 Average microhardness for each layer.*

	<b>Average microhardness</b>
<b>1° layer</b>	112
<b>2° layer</b>	107
<b>3° layer</b>	1°clad: 99 2°clad: 106 3°clad: 86
<b>4° layer</b>	98

A suitable vertical indentation pattern starting from the top surface along the centre line of the tracks as been performed.



*Fig.5.46: Microhardness vertical path.*



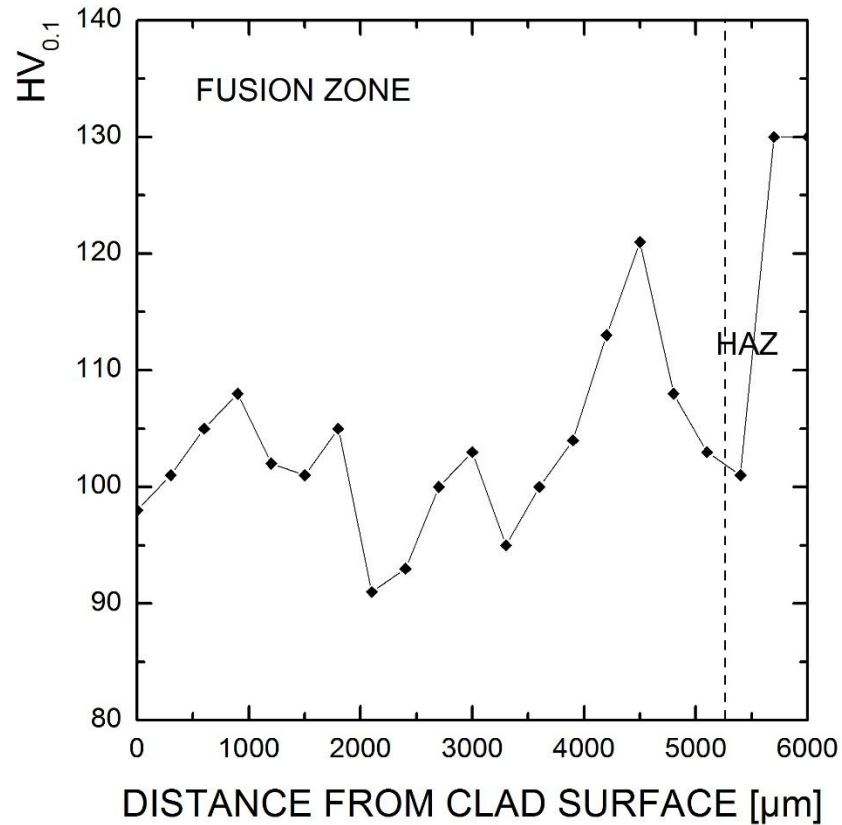


Fig.5.47: Vertical microhardness trend as a function of the distance from the clad surface.

These analysis confirmed an increase of microhardness from the fourth to the first layer.

To check the acceptability of the operating parameters, we have to verify that the difference in microhardness between clad and base metal does not exceed 100 HV. Since the base metal is characterized by a micro-hardness average of 134 HV and the minimum value of microhardness average achieved in the clad is 84 HV, these company requirement is respected.

### 5.2.4.5 Tensile tests

Mechanical properties of the cladded beads have been investigated via tensile tests.

The figure 5.48 shows shape and dimensions of tensile test specimen used.

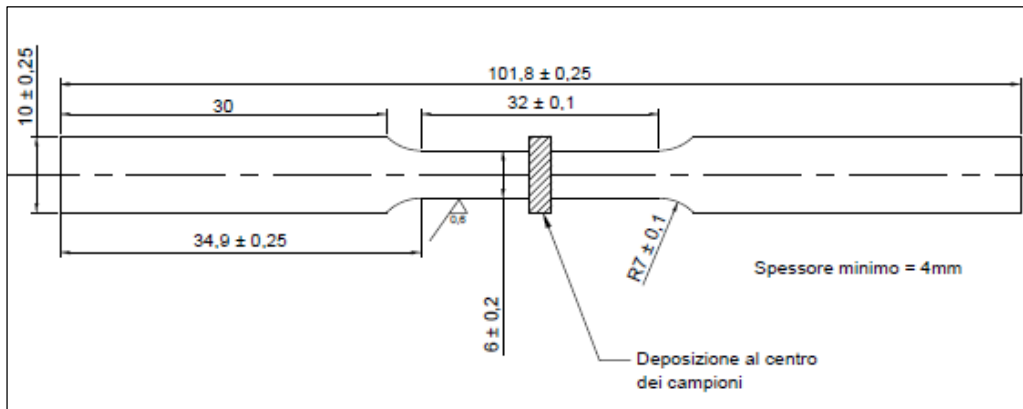


Fig.5.48: Shape and dimension of tensile test specimen.

Tensile strength tests, each one tripled to assure data reproducibility, have been performed. The ultimate tensile strength (UTS) of the original and unclad sample has been found to be  $480\text{ N/mm}^2$ . UTS values for the cladded specimens are listed in Table 5-24.

Tab. 5-24: Average ultimate tensile strength values for cladded specimens.

Test	Strain [%]	UTS [MPa]	UTS <sub>c</sub> / UTS <sub>bm</sub> [%]
1	2.29	293	61.0
2	2.25	292	60.8
3	2.17	289	60.2

First of all, porosity in clad is undesirable as they result in a reduction of the ultimate tensile strength and, as a consequence, in the rejection of the laser clad aluminum alloy parts. However, tensile tests results suggest that also the

extent of the fused zone plays an important role, as Vickers microhardness values indicate a drop in mechanical properties in the weld.

Since there is no an ISO standard to be followed, this value have been considered adequate being in according with the customer requirements.

#### 5.2.4.6 Fatigue tests

Axial fatigue tests have been performed on the specimens with the shape shown in the following figure.

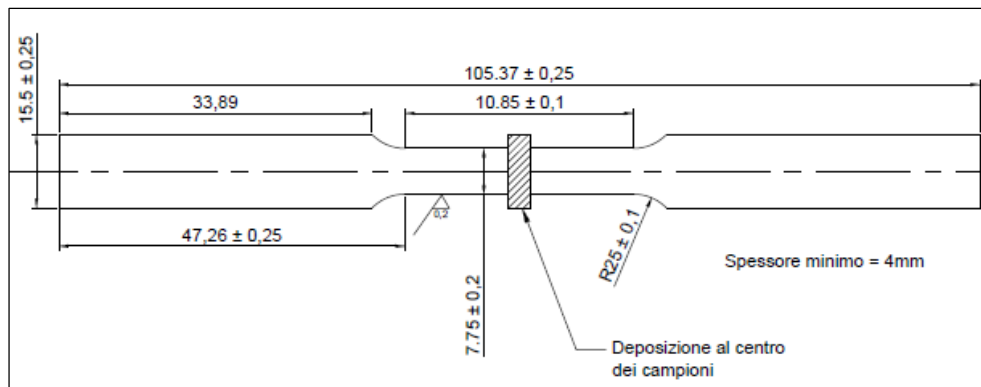


Fig.5.49: Shape and dimension of fatigue test specimen.

Constant stress amplitudes tests were used to generate endurance curves (S-N) at a stress ratio  $R=0.1$ . More tests have been performed with stress amplitudes ranging from 60 MPa to 125 Mpa.

The results of the fatigue tests are represented in figure 5.50 in the form of SN curves for both clad specimens and base material.

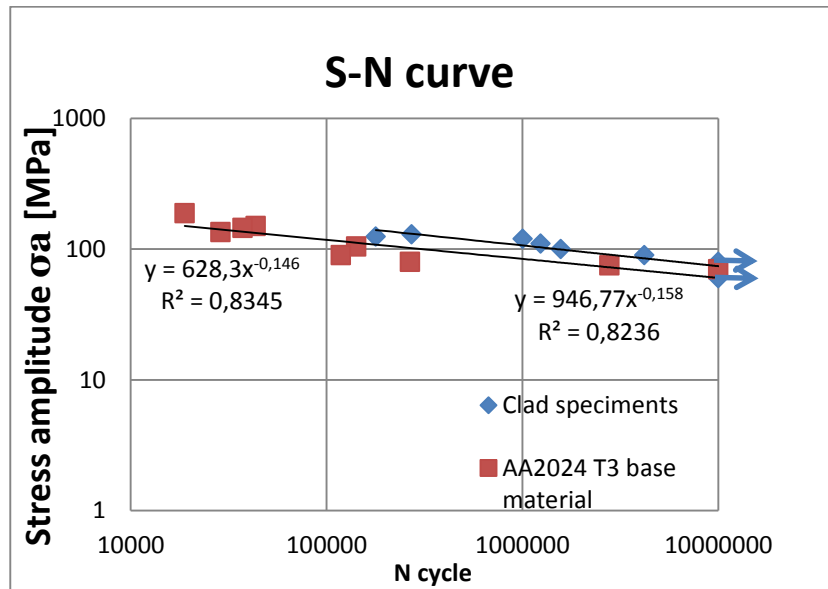


Fig.5.50: Fatigue behavior of base material and clad specimens at  $R=0.1$

The fatigue strength at  $10^7$  cycles for the base material is  $\sigma_a = 59.7$  [MPa], instead for the clad specimen is in average  $\sigma_a = 74.2$  [MPa]. It is possible to see the good quality of the clad with a fatigue behavior better than the one of the base material. Probably, the recast of the cladding process reduces the defects of the base material giving to the base material a more fine structure.

### 5.3 Laser cladding into a pre-machined V-groove of A357 aluminium alloy

In order to analyse the Laser Cladding process with another aluminum alloy, the same groove has been milled and filled on A357 aluminum alloy plates.

Since A357 aluminum alloy is a precipitation-hardenable, it has been subjected to a heat treatment. In the last paragraph, a study pre and post treatment is shown.

#### 5.3.1 Test sample and powder features

The substrate material used in this test investigation is A357 aluminum alloy.

A357 aluminum alloy is one of the high strength cast alloys that present excellent casting characteristics and are widely used to produce complex-shape aeronautical and automotive components.

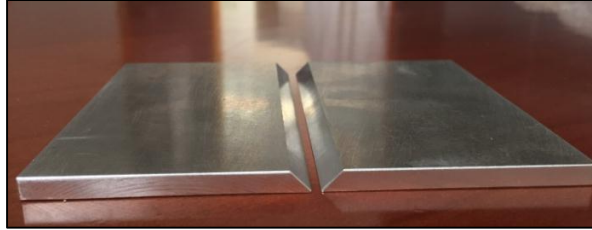
With respect to AA2024 alloy, A357 alloy has a good corrosion resistance and excellent castability thanks to Si particles presence. Moreover, this alloy exhibits a relatively high flowability, which is preferred for Additive Manufacturing processes [73].

The chemical composition is given in the following table.

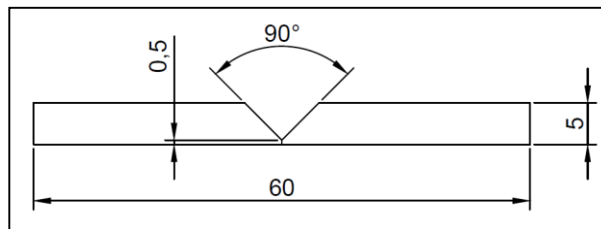
*Tab. 5-25: A357 aluminum alloy chemical composition weight percent.*

Si	Mg	Cu	Mn	Fe	Zn	Ti	Al
6.5 ÷ 7.5	0.4 ÷ 0.7	0.2	0.30 ÷ 0.90	0.2	0.1	0.04 ÷ 0.2	Bal.

The plate are shown in the following pictures. 5 mm thick A357 plates have been used as substrate material. Prior to each test, the samples were cleaned with acetone and a clean cotton cloth to remove any aluminium dust or dust particles on its surface.



*Fig.5.51: A357 V-groove.*



*Fig.5.52: A357 V-groove geometric characteristics.*

The milled groove has been filled with homologous powder.

In order to improve the powder delivery and reduce the risk of powder vaporization, a powder with mean particle size ranging from 50 to 100  $\mu\text{m}$  has been used; as a steady feed rate must be provided, the feeding powder has been preliminary dried so to flow properly in the powder conveyor.

Preliminary observations have been performed to investigate the morphology of A357 powder particles by using a SEM microscope. The objective is first of all to verify whether the conditions of the raw powders are suitable for Laser cladding process, in particular from a morphological point of view. In fact, the more is the spherical morphology of the particles, the more is the good flowability and homogeneous layer distribution in the process. As you can see in the following picture, the powder particles have spherical and regular shape. The smallest particles tend to agglomerate on the surface of the bigger ones to reduce their surface free energy, creating some clusters.

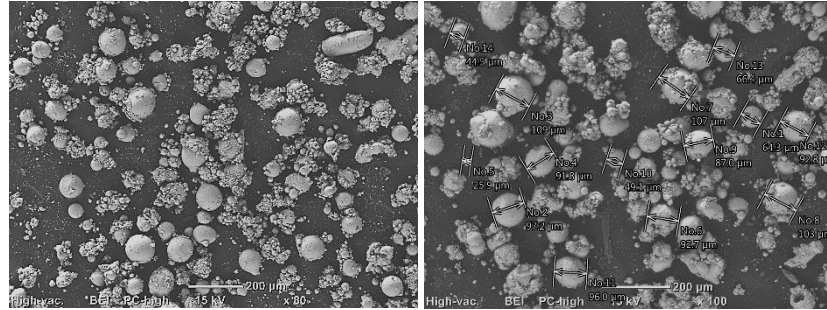


Fig.5.53: A357 particle powder morphology and size.

A micrograph of the particles taken using a scanning electron microscope (SEM) is shown in figure. The microstructure of the powder particles varied but generally consisted either of a coarse Al-Si eutectic structure or an Al-Si eutectic structure with copper crystals dispersed in it as can be seen in figure.

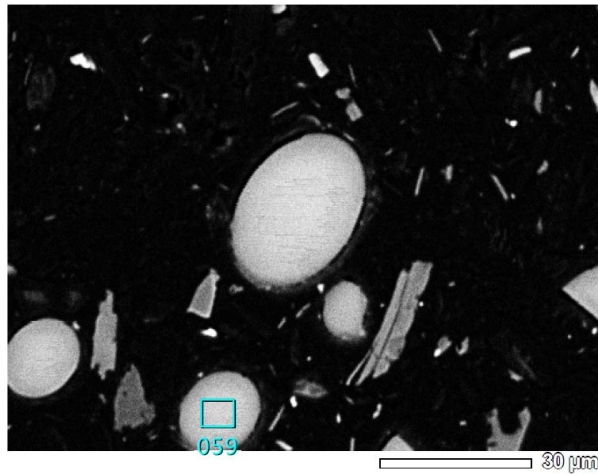


Fig.5.54: Cross section particle powder.

A punctation analysis has been conducted to evaluate the weight percentage given in the following table.

Tab. 5-26: Chemical composition of particle powder.

Mg	Si	Ti	Fe	Zn	Al
0.6	6.8	0.1	0.2	0.1	Bal.

### 5.3.2 Experimental procedure

The test on the A357 aluminum alloy have been conducted in according to the results achieved for the AA2024 aluminum alloy. In this case a layer by layer strategy analysis has not been used since the deposition strategy has already been optimized. Therefore, a continuous process has been carried out, without moving the specimen from the machine table.

First of all a relation has been found to express the mass flow as a function of input voltage inducing vibration to the conveyor by a command and control unit Reovib 168. The voltage signal changes in the range 0-10 V.

*Tab 5-27 Powder mass flow as a function of Voltage*

<b>Voltage [V]</b>	<b>Powder mass flow [g/min]</b>
3	1,5
4	3
5	5,6
6	8,6
7	11,3
8	14,5
9	18,9
10	23,5



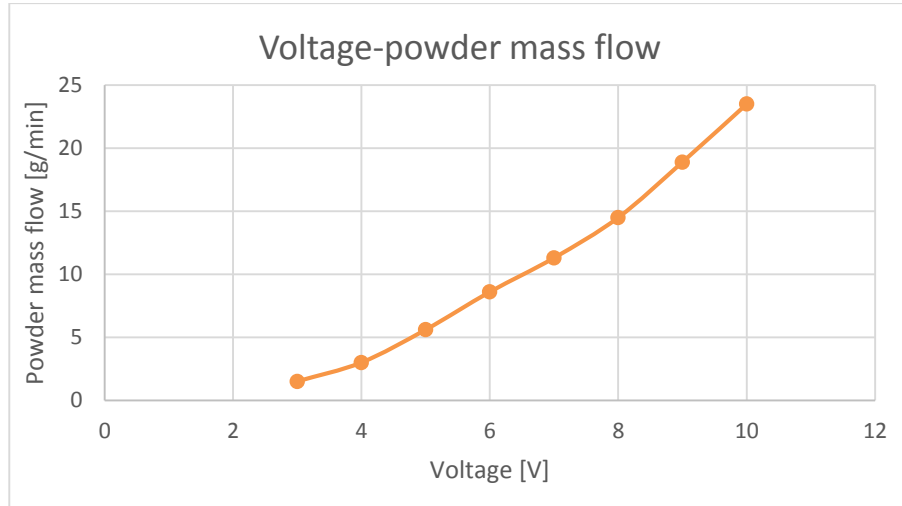


Fig. 5.55 Powder mass flow as a function of voltage.

The clads have been deposited according to the strategy shown in the picture below. The table shows the process parameters used for the deposition of each layer.

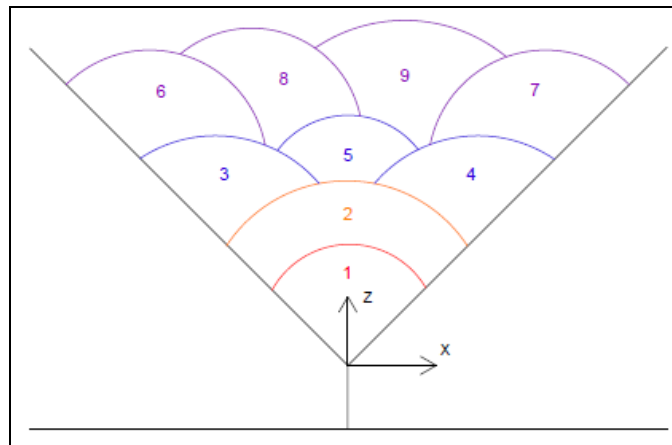


Fig.5.56: Deposition strategy.

Tab. 5-28 Process parameters for each layer.

PARAMETERS	LAYER 1	LAYER 2	LAYER 3	LAYER 4
Power [W]	3000	2300	2530	2760
Laser speed [mm/min]	1000	400	400	400
Powder feeding [g/min]	3	3	3	3
Offset [mm]	1) $\begin{cases} \Delta x = 0 \\ \Delta z = 0 \end{cases}$	2) $\begin{cases} \Delta x = 0 \\ \Delta z = 0,96 \end{cases}$	3) $\begin{cases} \Delta x = 1,3 \\ \Delta z = 1,7 \end{cases}$ 4) $\begin{cases} \Delta x = -1,3 \\ \Delta z = 1,7 \end{cases}$ 5) $\begin{cases} \Delta x = 0 \\ \Delta z = 1,4 \end{cases}$	6) $\begin{cases} \Delta x = 3,2 \\ \Delta z = 3,8 \end{cases}$ 7) $\begin{cases} \Delta x = -3,2 \\ \Delta z = 3,8 \end{cases}$ 8) $\begin{cases} \Delta x = 1,5 \\ \Delta z = 3,8 \end{cases}$ 9) $\begin{cases} \Delta x = -1,5 \\ \Delta z = 3,8 \end{cases}$

The flow rate for both helium and argon has been found based on preliminary trials and has been taken as a constant, 8 and 10 l/min, respectively. With respect to the experimental process of AA 2024 filling groove, in this case the laser power has been increased since a powder with a coarse particles powder and a higher density has been used.

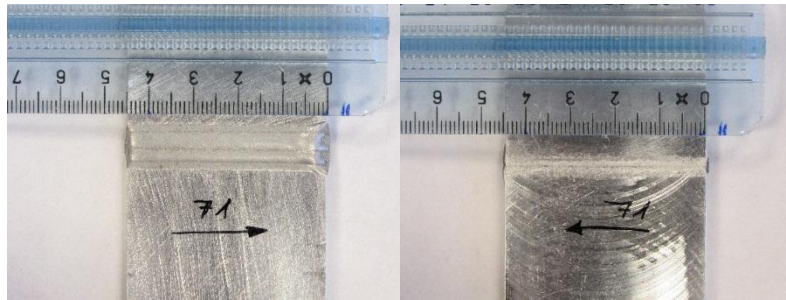
### 5.3.3 Results and discussion

The following analysis are conducted:

- Distortion and deformation analysis;
- Defects analysis: by the use of the optical microscope in order to identify and analyze the defects such as pores and cracks, inclusions or any separations between clad and material basis;
- Metallurgical analysis: by means of optical microscope and scanning electron microscope (SEM), in order to investigate the structure of the base material and the clad, distinguishing the composition of the phases by means of the analysis EDS (energy dispersive spectrometry);
- Mechanical Analysis: analysis of Vickers microhardness, to determine the hardness in various locations along the transversal section of the groove.

### 5.3.3.1 Buckling and deformation analysis

In the following pictures of the filling is given both front and back.

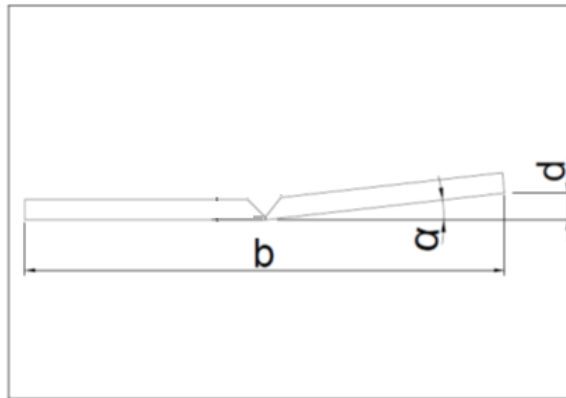


*Fig.5.57: Filled V-groove, front (left) and back (right).*

In order to evaluate the distortion and deformation of the specimens, a lot of measures are made pre and post deposition.

In particular, the following characteristics are analyzed:

- $b$ : width of the plates;
- $d$ : deformation of the plates
- $\alpha$ : distortion of the plate.



*Fig.5.58: Deformation measurements.*

In the table the mean measurements for each parameter are given.

The subscripts  $_i$  and  $_u$  indicate measurements carried out respectively in the area of entry and exit after the deposition.

Tab. 5-29 Deformation measurements.

<b>b[mm]</b>	<b>b<sub>i</sub>[mm]</b>	<b>b<sub>u</sub>[mm]</b>	<b>d<sub>i</sub>[mm]</b>	<b>d<sub>u</sub>[mm]</b>	<b>α<sub>i</sub>[°]</b>	<b>α<sub>u</sub>[°]</b>
107.08	106.63	106.17	0.52	0.52	0.56°	0.56°

Since a milling has to be made to remove the unmelted material at the bottom and the overlap material at the top, distortion must not exceed 1,50 °. The requirements are always respected.

The samples have been cutted, imblobed, polished and attached. In the following a cross section of the sample is shown.

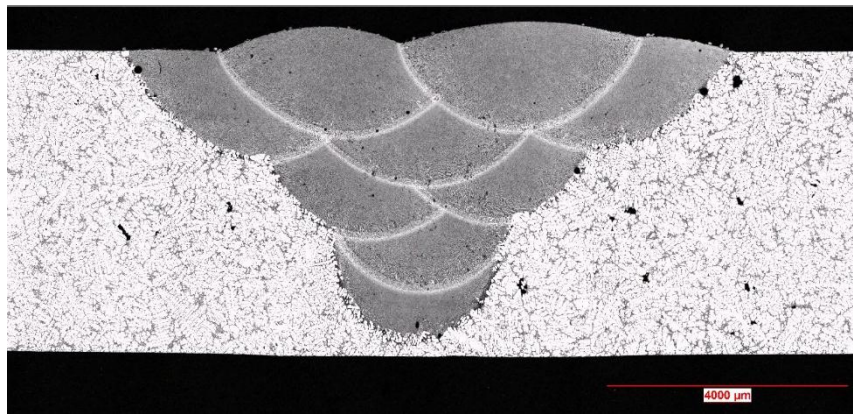


Fig.5.59: V-groove cross section.

### 5.3.3.2 Defects analysis and X-ray inspections

The specimen has been subjected to observation through an optical microscope in order to characterize the structure and identify any present defects. From the pictures of the sections analyzed it is possible to observe the presence of a good metallurgical bond between the base metal and clad (Fig 5.60 a). In addition, the sections considered do not show cracks. To better understand the very fine microstructure that form, due to the extremely rapid solidification after the laser local melting, so very high heating and subsequent cooling rates, it is necessary to go to higher magnifications, as shown in figure b-c. The grains are elongated in the heat affected zone (Fig. 5.60 b), since they follow the direction of heat dissipation, while in the clad have a rounded shape (Fig.5.60 c). The as-

built microstructure is characterized by cellular dendrites of  $\alpha$ -Al (grey zone) and the interdendritic Si-particles (black zone).

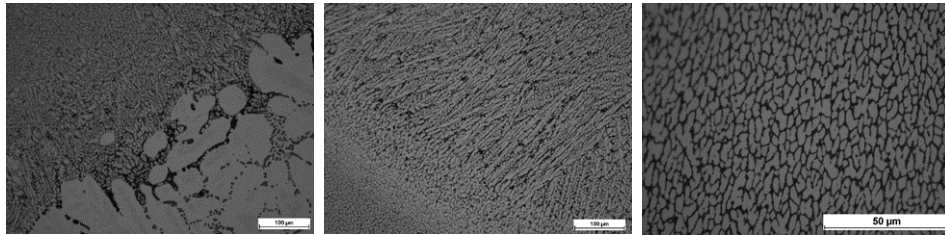
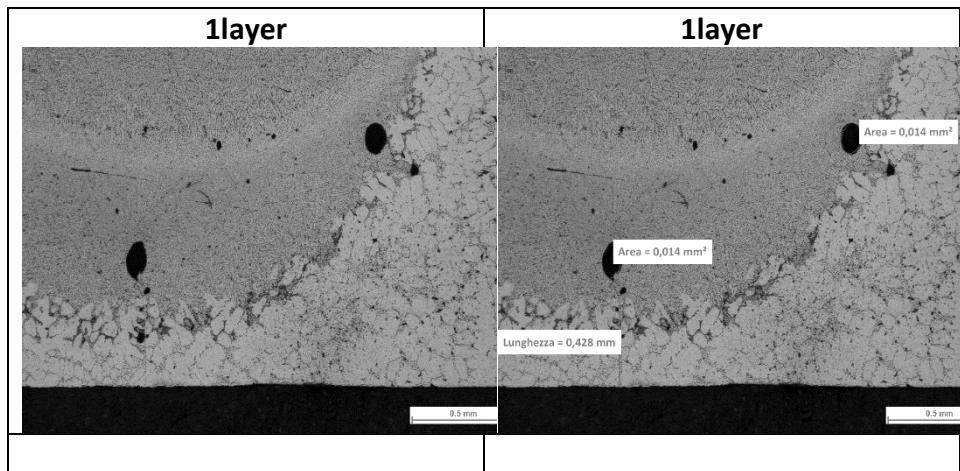
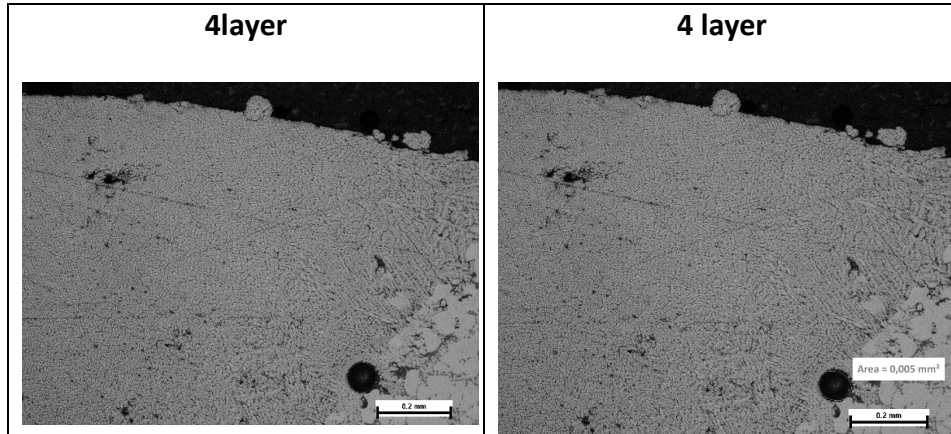


Fig.5.60. Metallurgical bond a) b: HAZ c: Clad

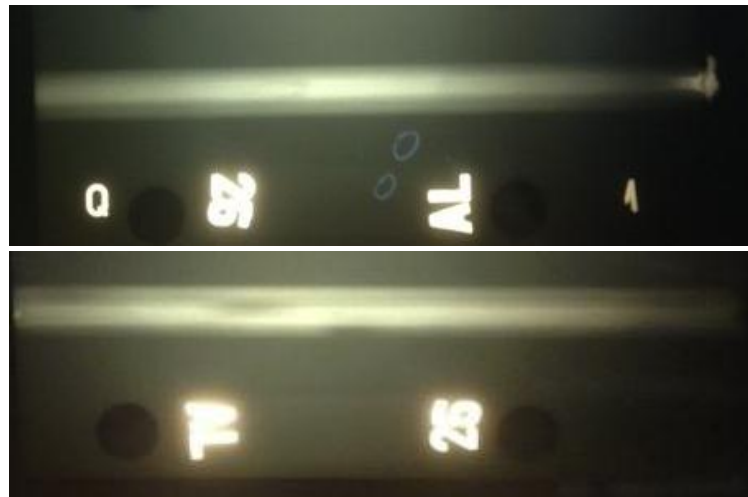
An important problem in the laser cladding of aluminum alloys is their susceptibility to porosity. The presence of micropores has been observed, but they respect the company requirements. The measurements are shown in the images below. At high magnifications it can be seen that the porosity is low. Both irregular and spherical pores can be detected. Irregular pores are located at melt pool boundaries, and their maximum dimension is around  $0,014 \text{ mm}^2$ . It could be assumed that these pores formed due to un-melted powder or insufficient overlapping between scan tracks. On the other hand, spherical pores are generally a consequence of entrapped gasses.

Tab. 5-30 Defects analysis.





X-ray inspections have been therefore conducted, because random cross section analysis do not give a complete and reliable evaluation for porosity content and position. Ten runs have been performed and subjected to this analysis in according to the the following acceptance criteria: the dimension of any discontinuity is defined by its largest dimension. Two or more discontinuities are treated as one when the spacing between them is less than the dimension of the larger discontinuity.



*Fig.5.61: Picture of X-ray inspections.*

In all the specimens there are porosity aligned to the center of the clad for the total length of the joint, having a diameter of 0.1-0.5 mm. Some samples

present a partial melting at the beginning of the clad that will be solved by a post-machined of the clad bottom. These defects comply with the company requirements since the measurements are in the range of the acceptability.

### 5.3.3.3 The effect of artificial aging: metallurgical an mechanical analysis

A357 is a precipitation-hardenable aluminum alloy and the heat treatment is the key parameter to improve the quality of the investigated material.

The effect of artificial aging is assessed on the microstructure and microhardness property.

The specimens analysed in this work have been treated for 6 h at a 160 °C.

The base material as built and after the heat treatment appear as follow:

#### As built

#### Artificial aged

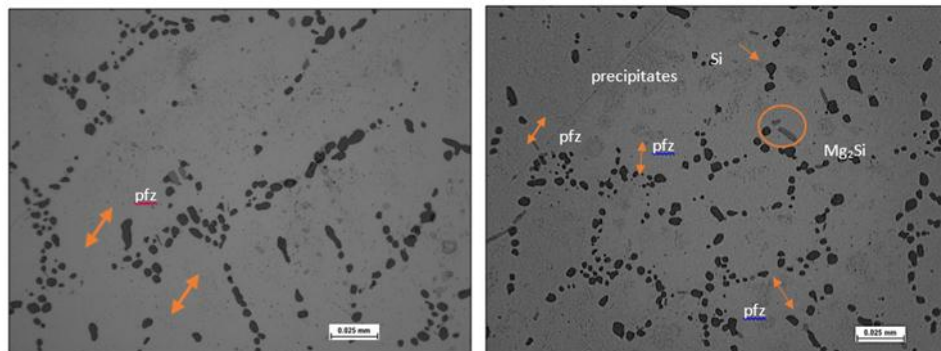


Fig. 5.62: SEM analysis of base material of as built sample (left) and artificial aged sample (right).

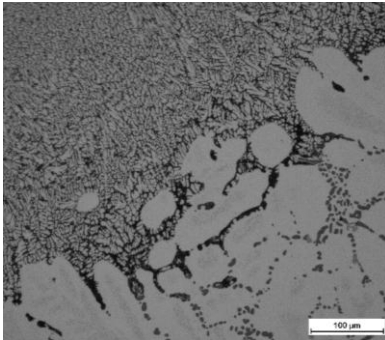
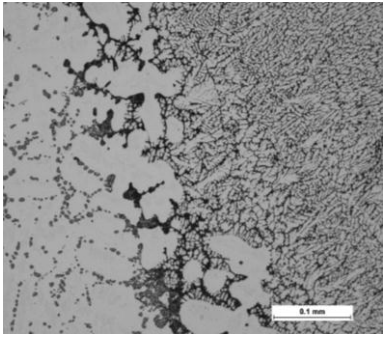
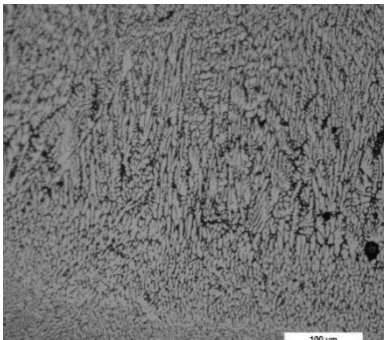
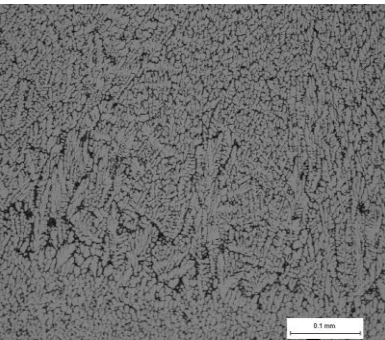
The pictures show a typical microstructure of the cast aluminum alloy A357 with precipitates formed in the Al matrix. After the artificial aging, precipitates are formed inside the aluminum grain and away from eutectic Si particles that denote the grain boundaries. This images show very clearly some regions with no precipitates particles, called precipitate free zone (pfz). The sample after the artificial aging present this zone very close to the grain boundaries. The aluminum matrix is rich of soluted atoms, in this case Mg and excess Si, as confirmed by EDS analysis.

The metallurgical analysis of the clad show that the cladding process resulted in significant break-up of Si particles and their redistribution. In

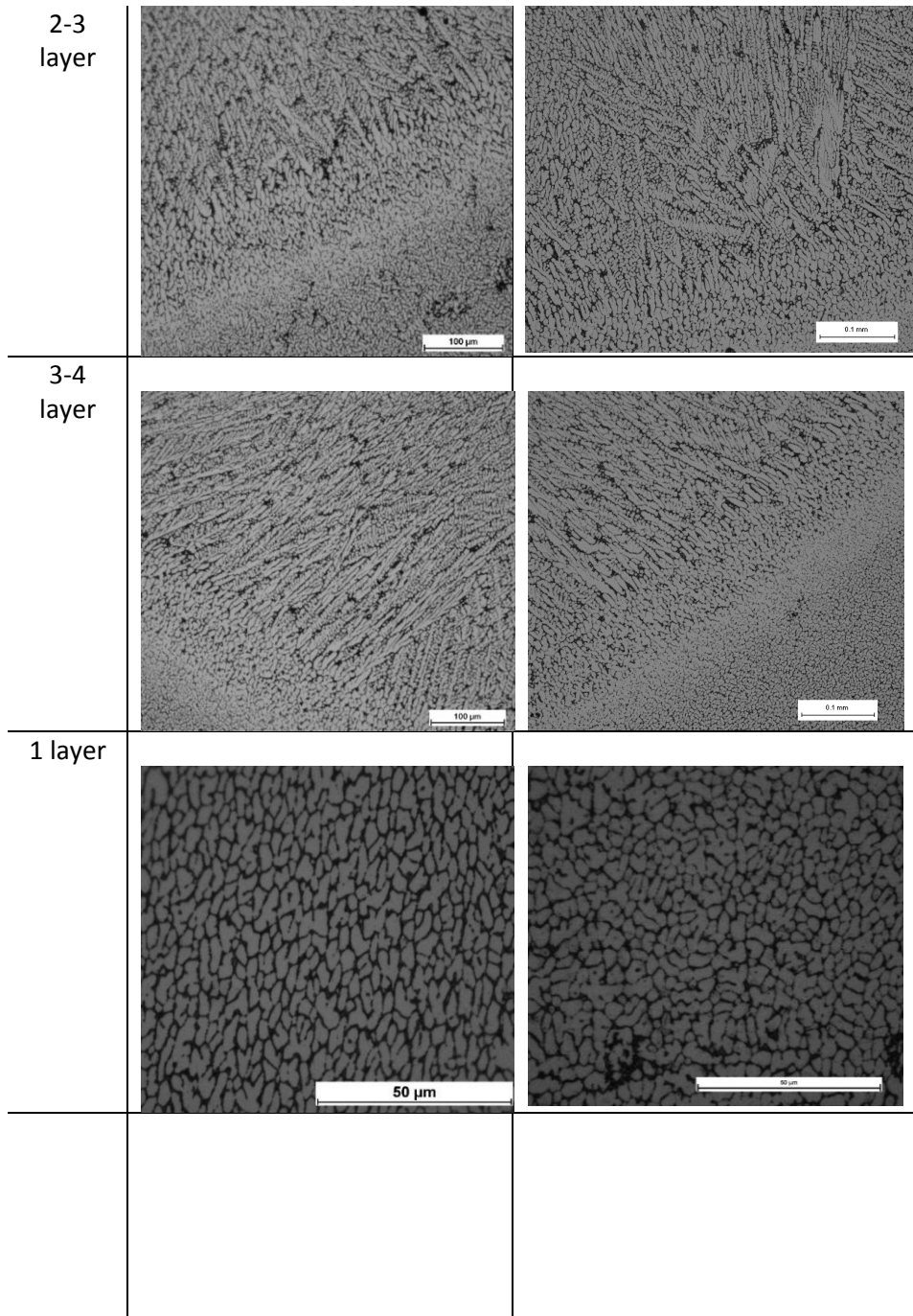
particular the Si particles are located at the grain boundaries. This structure is the same for each layer.

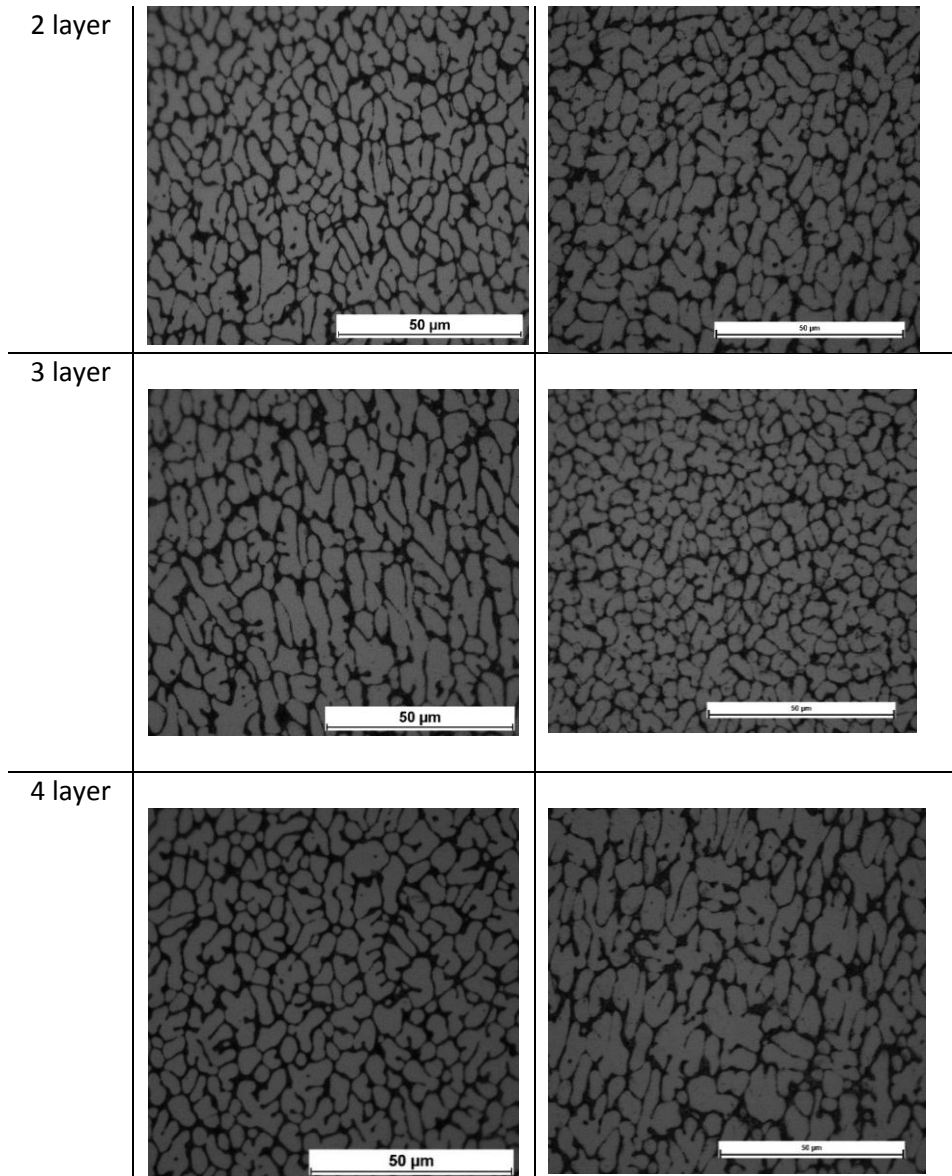
In the following table a magnification observations of the HAZ and clad is given for the clad as built and artificial aged.

*Tab. 5-31 Comparison analysis as clad and artificial aged.*

	<b>As clad</b>	<b>Artificial aged</b>
1 layer- base material		
1-2 layer		







In the HAZ, the average growth direction during solidification is approximately perpendicular to the solid/liquid interface and aligned with the heat flow direction.

Considering the cross-section in figure it can be seen how the dendrites orientated themselves in the direction of heat flow, almost perpendicular to the solid/liquid interface.

In the following the grain size in the clad for each layer, calculated as the average of the grains contained in four segments having a length of 50  $\mu\text{m}$  and directed at angles of 0 °, 45 °, 90 ° and 135° is shown.

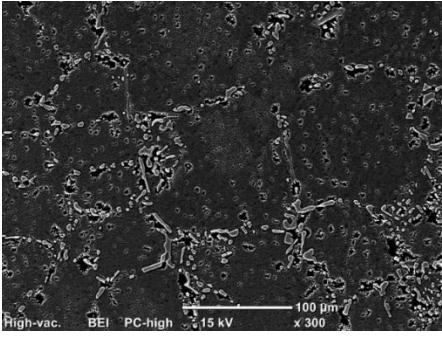
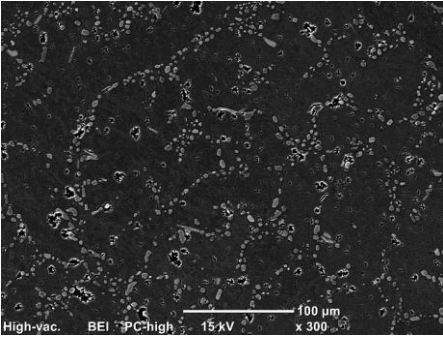
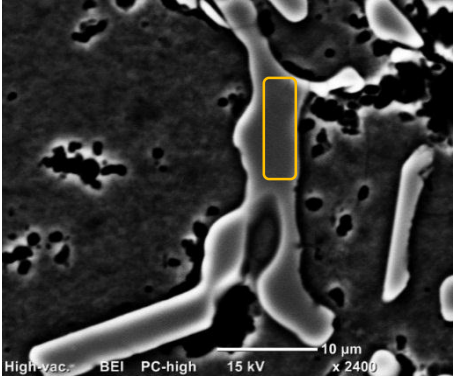

*Tab. 5-32 Main grain size for each laayer.*

<b>Layer</b>	<b>Main grain size as built [<math>\mu\text{m}</math>]</b>	<b>Main grain size after heat treatment [<math>\mu\text{m}</math>]</b>
1	4,0	3,5
2	6,9	6,7
3	7,7	7,0
4	10,0	9,0

The first layer deposited have a more fine microstructure since they are subjected to continuous heating and cooling as a consequence of the deposition of the successive clad. With respect to the clad as built, the artificial aged clad present a more fine microstructure too.

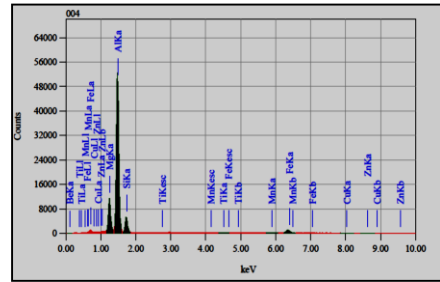
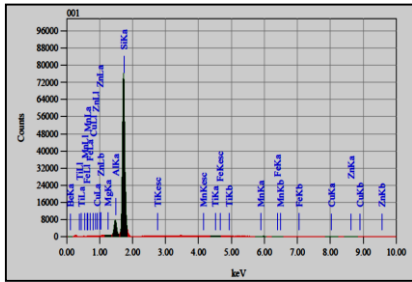
To investigate the different phases present in the A357 cladding samples pre and post heat treatment, EDS analyses were performed on cross sections of polished etched samples.

Tab. 5-33 EDS analysis as clad and artificial aged.

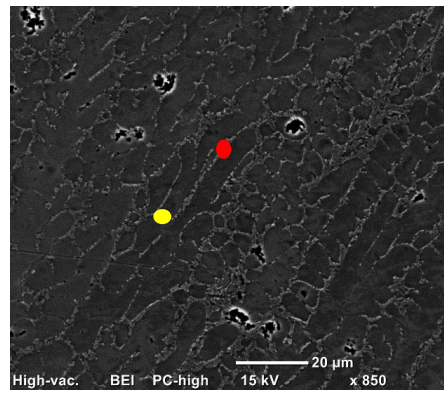
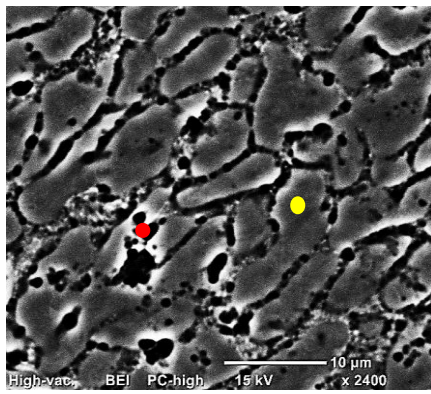
As clad	Artificial aged
<b>Base material</b>	
	
	

Element	(keV)	Mass%
Be K		
Mg K	1.253	0.07
Al K	1.486	7.98
Si K	1.739	91.82
Ti K		
Mn K	5.894	0.03
Fe K	6.398	0.01
Cu K		
Zn K	8.630	0.09
Total		100.00

Element	(keV)	Mass%
Be K		
Mg K	1.253	13.74
Al K	1.486	66.94
Si K	1.739	13.91
Ti K	4.508	0.03
Mn K		
Fe K	6.398	5.18
Cu K	8.040	0.19
Zn K		
Total		100.00



Clad up



Aluminum matrix

Element	(keV)	Mass%
Be K		
Mg K	1.253	0.81
Al K	1.486	97.82
Si K	1.739	1.19
Ti K	4.508	0.03
Mn K	5.894	0.07
Fe K		
Cu K	8.040	0.09
Zn K		
Total		100.00

Precipitates

Element	(keV)	Mass%
Be K		
Mg K	1.253	0.93
Al K	1.486	95.96
Si K	1.739	2.92
Ti K		
Mn K		
Fe K	6.398	0.08
Cu K	8.040	0.08
Zn K	8.630	0.02
Total		100.00

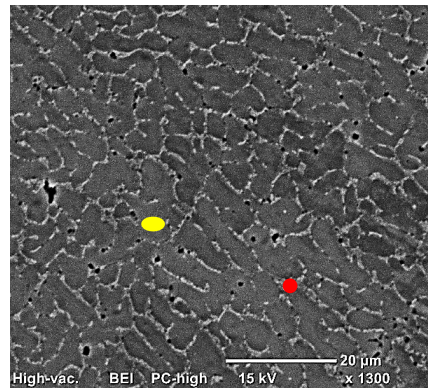
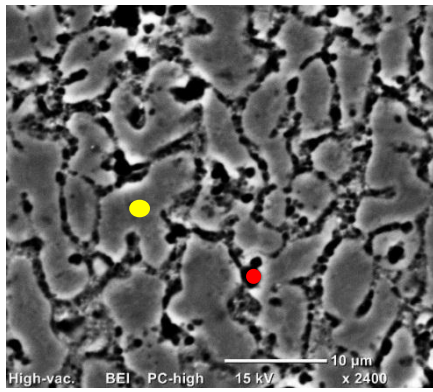
Aluminum matrix

Element	(keV)	Mass%
Be K		
Mg K	1.253	3.20
Al K	1.486	74.29
Si K	1.739	21.29
Ti K	4.508	0.01
Mn K	5.894	0.03
Fe K	6.398	0.97
Cu K	8.040	0.21
Zn K		
Total		100.00

Precipitates

Element	(keV)	Mass%
Be K		
Mg K	1.253	0.66
Al K	1.486	42.62
Si K	1.739	56.39
Ti K	4.508	0.06
Mn K		
Fe K	6.398	0.02
Cu K	8.040	0.06
Zn K	8.630	0.19
Total		100.00

Clad down



■ Aluminum matrix

Element	(keV)	Mass%
Be K		
Mg K	1.253	0.85
Al K	1.486	97.69
Si K	1.739	0.97
Ti K		
Mn K		
Fe K	6.398	0.15
Cu K	8.040	0.18
Zn K	8.630	0.17
Total		100.00

■ Aluminum matrix

Element	(keV)	Mass%
Be K		
Mg K	1.253	1.15
Al K	1.486	93.51
Si K	1.739	4.95
Ti K	4.508	0.01
Mn K		
Fe K	6.398	0.17
Cu K	8.040	0.20
Zn K	8.630	0.02
Total		100.00

● Precipitates

Element	(keV)	Mass%
Be K		
Mg K	1.253	0.78
Al K	1.486	97.16
Si K	1.739	1.62
Ti K		
Mn K		
Fe K	6.398	0.11
Cu K	8.040	0.09
Zn K	8.630	0.25
Total		100.00

● Precipitates

Element	(keV)	Mass%
Be K		
Mg K	1.253	16.15
Al K	1.486	58.05
Si K	1.739	18.95
Ti K		
Mn K		
Fe K	6.398	6.50
Cu K	8.040	0.14
Zn K	8.630	0.21
Total		100.00

The SEM image of the base material shows the matrix of aluminium (black region) with the precipitates dispersed within (grey points). It is a typical microstructure of the cast aluminum alloy A357. The acicular nature of the Si particles in the interdendritic regions became evident at higher magnification as shown in figure.

The EDS analysis shows that with the artificial aging soluted Mg and Si atoms in the aluminum matrix form precipitates. In particular, the artificial aging corresponds to the formation of second phase precipitations from Al-rich matrix rich of Mg and Si which could be responsible of a microhardness increase [74].

Finally, measurements were made of Vickers micro-hardness with a load of 100 gf in order to quantify the variation in hardness between the base material and the melted area. By microscopic observations and subsequent measures microhardness, it has been identified the heat affected zone.

A compare is carried out in terms of microhardness between the clad as built and artificial aged.

### 1 LAYER

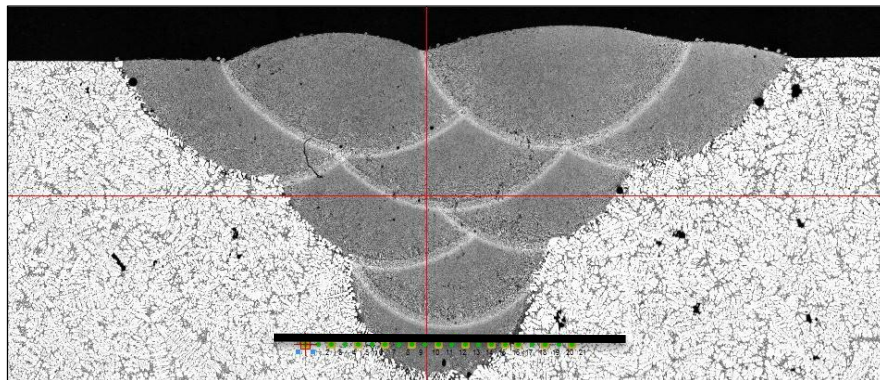


Fig.5.63: First layer microhardness path.

### As clad

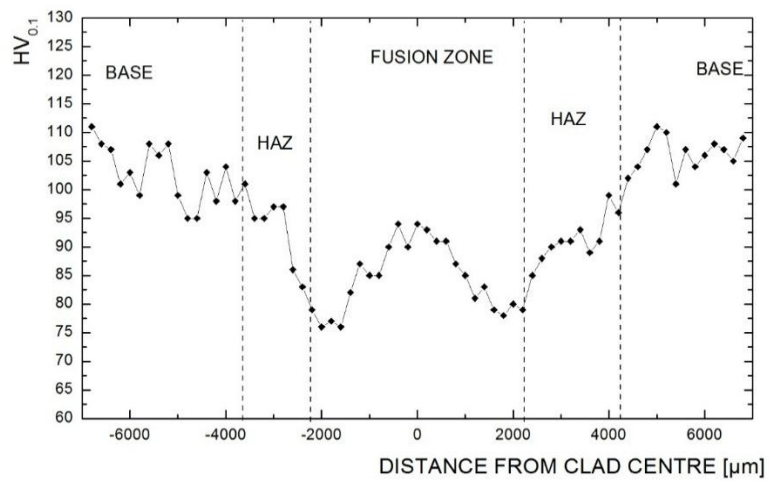


Fig. 5.64: First layer microhardness trend as clad.



Tab. 5-34 Average microhardness first layer as clad.

<b>Average micro-hardness in the clad</b>	<b>88 HV</b>
<b>Average micro-hardness in the HAZ</b>	<b>86 HV</b>

**Artificial aged**

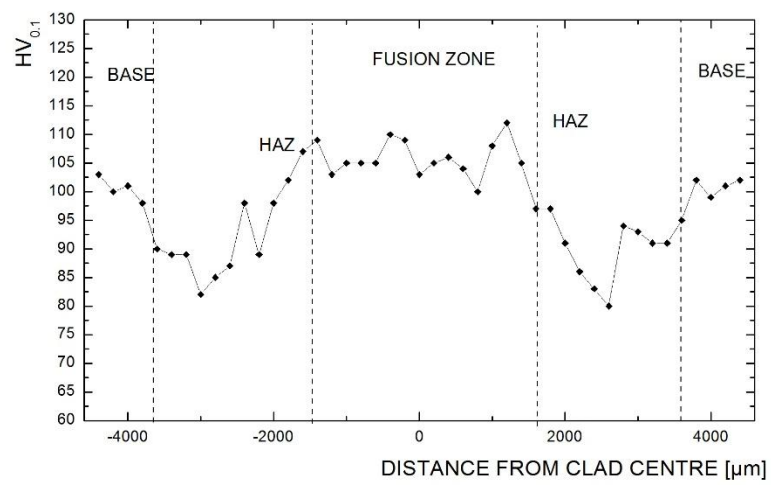


Fig.5.65: First layer microhardness trend as clad.

Tab. 5-35 Average microhardness first layer artificial aged.

<b>Average micro-hardness in the clad</b>	<b>106 HV</b>
<b>Average micro-hardness in the HAZ</b>	<b>91 HV</b>

## 2 LAYER

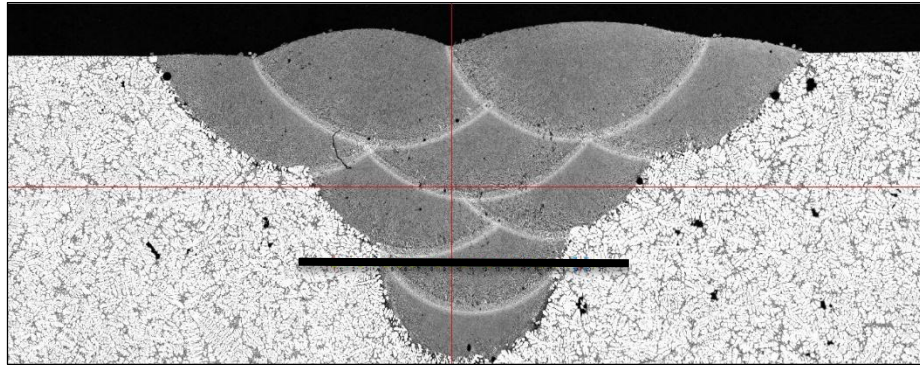


Fig.5.66: Second layer microhardness path.

## As clad

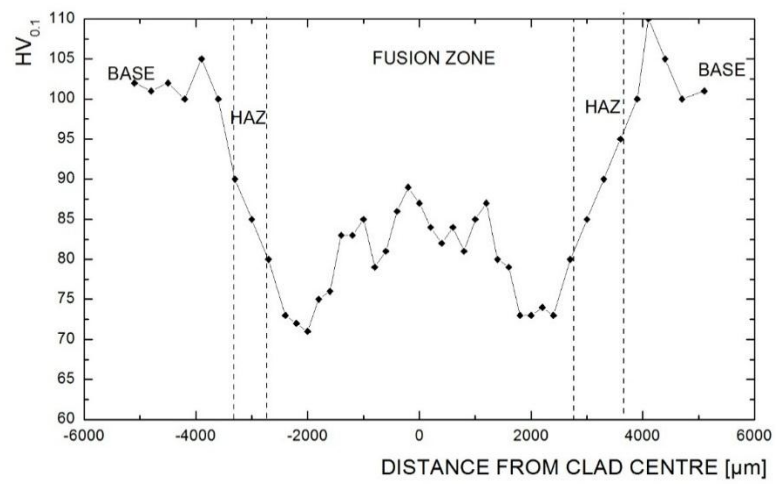


Fig. 5.67: Second layer microhardness trend as clad.

Tab. 5-36 Average microhardness second layer as clad.

<b>Average micro-hardness in the clad</b>	<b>81HV</b>
<b>Average micro-hardness in the HAZ</b>	<b>85HV</b>

**Artificial aged**

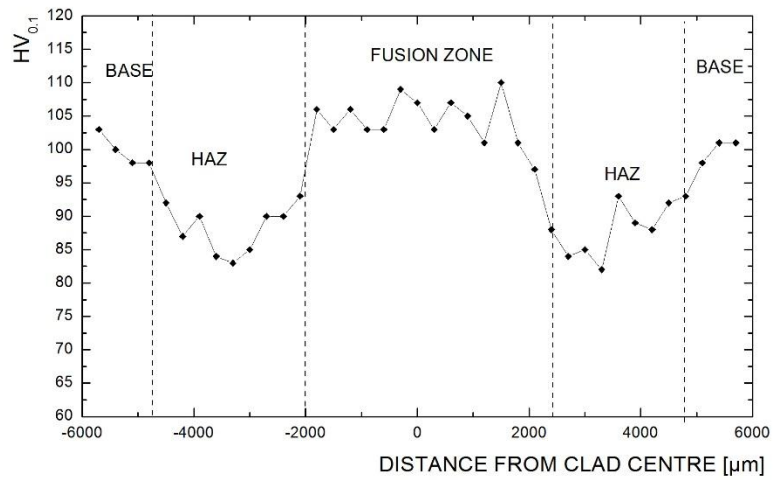


Fig. 5.68:: Second layer microhardness trend artificial aged.

Tab. 5-37 Average microhardness second layer artificial aged.

<b>Average micro-hardness in the clad</b>	<b>105 HV</b>
<b>Average micro-hardness in the HAZ</b>	<b>90 HV</b>

### 3 LAYER

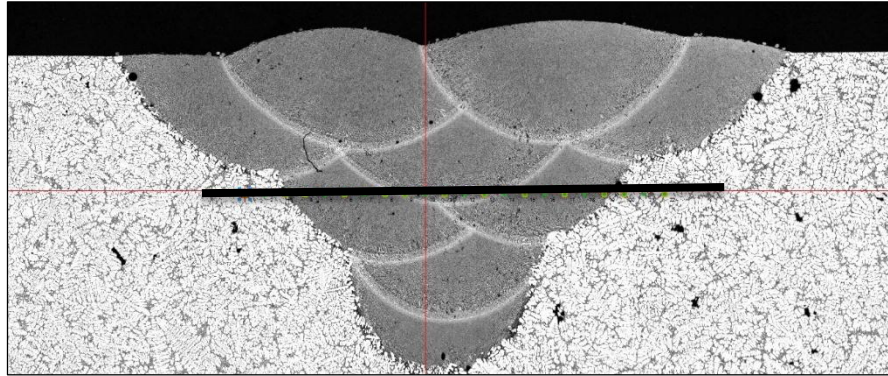


Fig.5.69: Third layer microhardness path.

### As clad

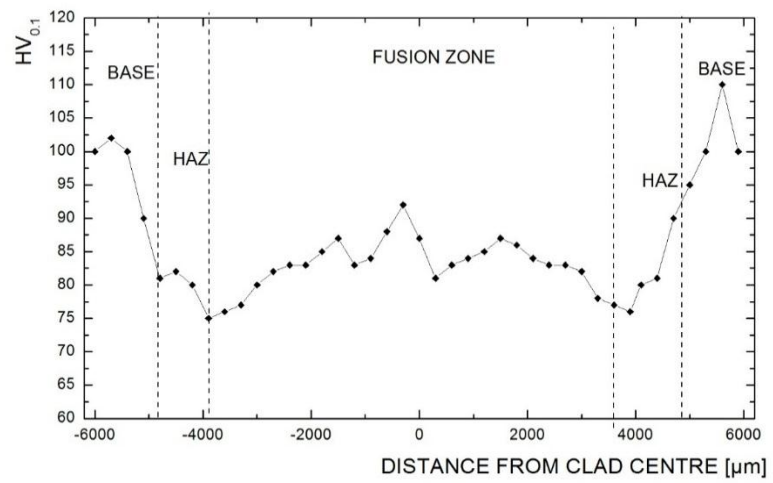


Fig. 5.70: Third layer microhardness trend as clad.

Tab. 5-38 Average microhardness third layer as clad.

<b>Average micro-hardness in the clad</b>	<b>83 HV</b>
<b>Average micro-hardness in the HAZ</b>	<b>80 HV</b>

**Artificial aged**

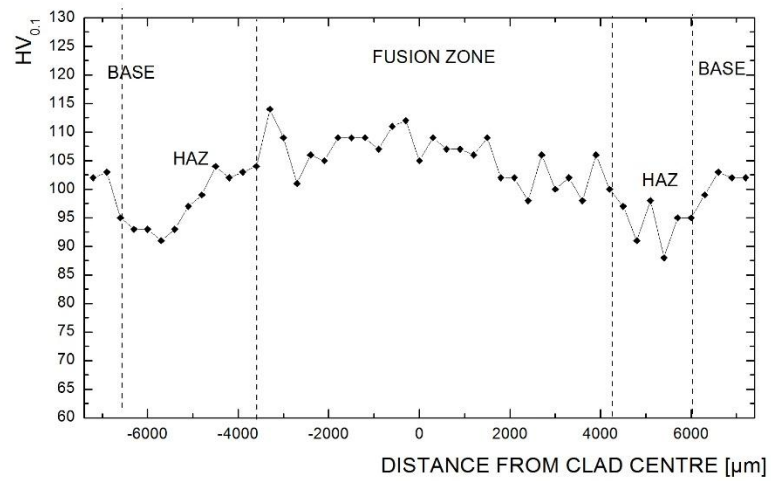


Fig. 5.71: Third layer microhardness trend artificial aged..

Tab. 5-39 Average microhardness third layer artificial aged..

<b>Average micro-hardness in the clad</b>	<b>106 HV</b>
<b>Average micro-hardness in the HAZ</b>	<b>95 HV</b>

## 4 LAYER

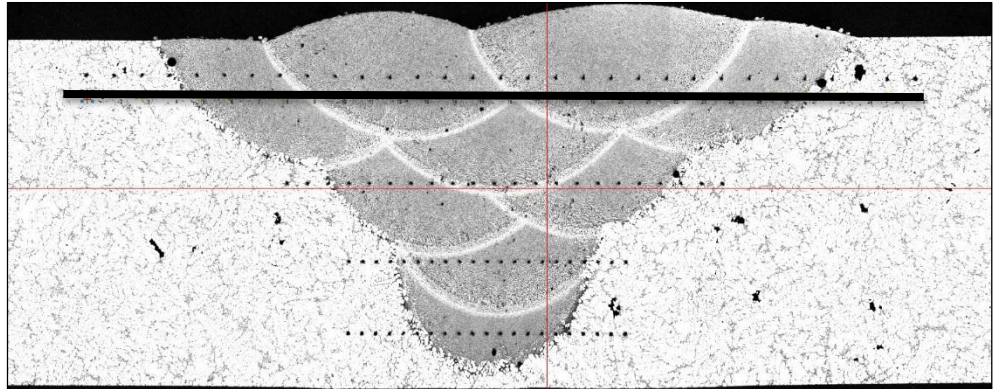


Fig. 5.72: Fourth layer microhardness path.

## As clad

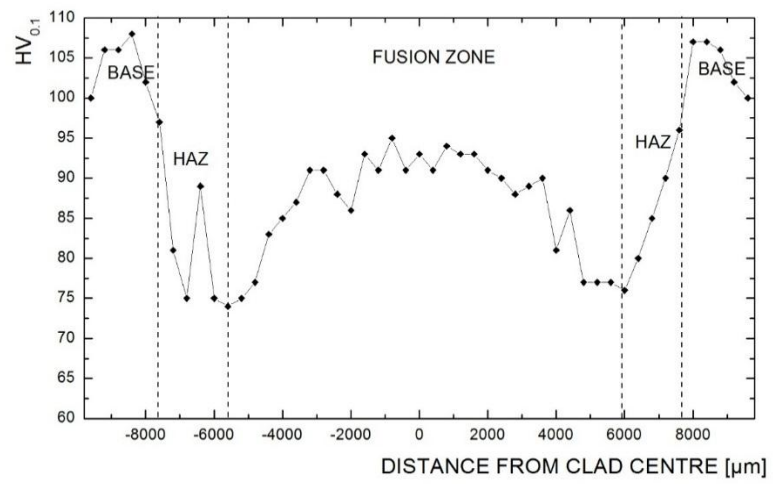


Fig. 5.73: Fourth layer microhardness trend as clad.

Tab. 5-40 Average microhardness fourth layer as clad.

<b>Average micro-hardness in the clad</b>	91 HV
<b>Average micro-hardness in the HAZ</b>	82 HV

**Artificial aged**

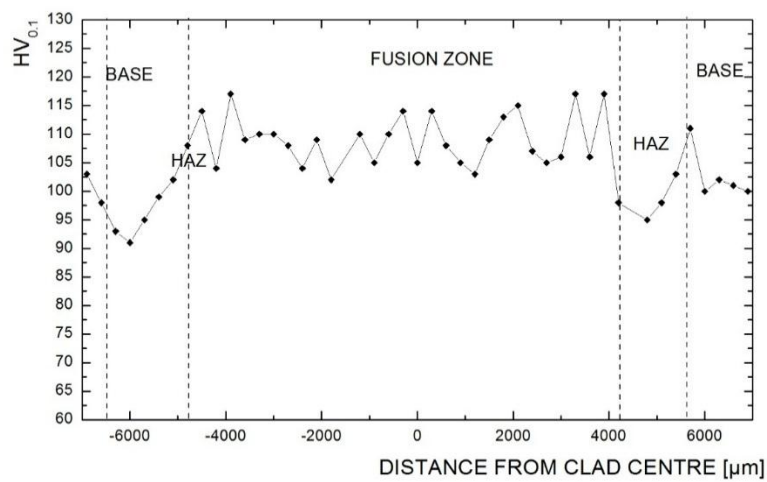


Fig. 5.74: Fourth layer microhardness trend artificial aged..

Tab. 5-41 Average microhardness fourth layer artificial aged.

<b>Average micro-hardness in the clad</b>	110 HV
<b>Average micro-hardness in the HAZ</b>	97 HV

The figures show that in the clad as built from the base material to clad the microhardness decreases in the heat affected zone and continue to decrease in the melted zone. In the clad artificial aged from the base material to clad the microhardness decreases in the heat affected zone and increases in the melted zone. These trends observed for each layer are shown in the images below.

The high hardness is reached after heat treatment by the formation of Mg and Si precipitates both in the aluminum matrix and at grain boundary. These result from the very fine microstructure and fine distribution of the Si phase in

aluminium cladding parts due the rapid cooling and solidification, and also from the presence of Mg - Si precipitates as observed by EDS analysis.

### Vertical path

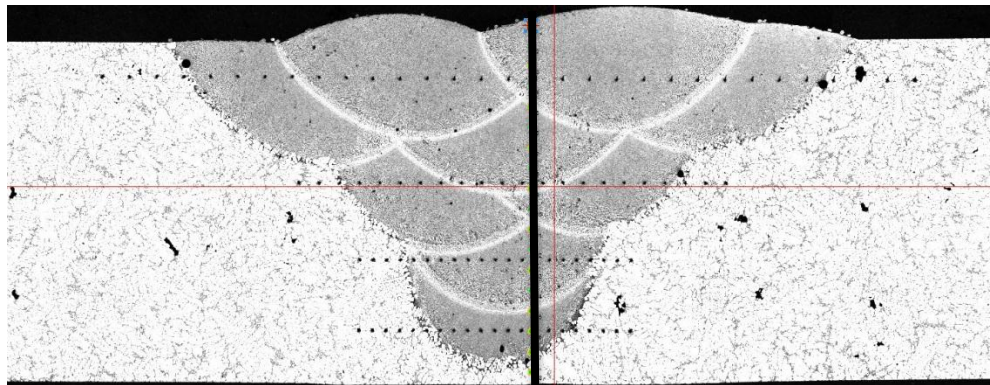


Fig.5.75: Microhardness vertical path.

As clad

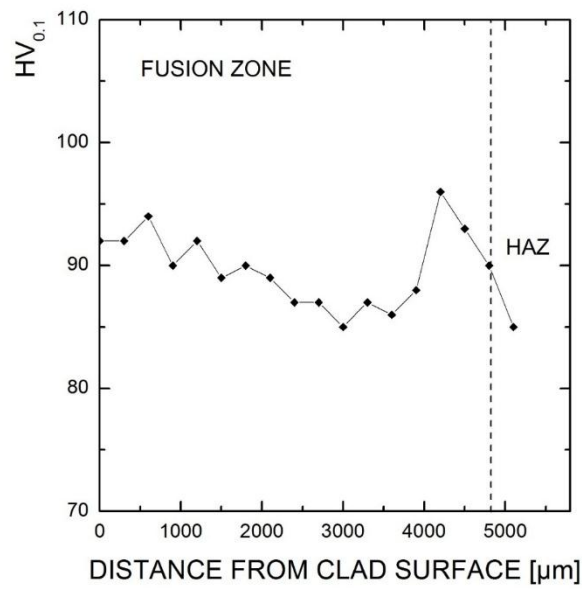
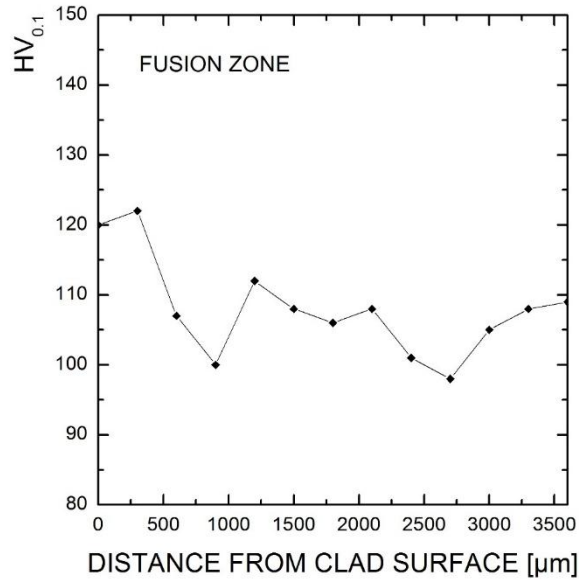


Fig. 5.76: Vertical path microhardness trend as clad.



**Artificial aged**



*Fig. 5.77: Vertical path microhardness trend artificial aged.*

Analyzing the vertical pattern, it is possible to calculate the average values of microhardness for each layer as shown in the following table pre-treatment and post heat treatment.

**Pre-treatment**

*Tab. 5-42 Average microhardness for each layer as clad.*

<b>Average micro-hardness 1 layer</b>	93 HV
<b>Average micro-hardness 2 layer</b>	87 HV
<b>Average micro-hardness 3 layer</b>	89 HV
<b>Average micro-hardness 4 layer</b>	92 HV

**Post –treatment**

*Tab. 5-43 Average microhardness for each layer artificial aged.*

<b>Average micro-hardness 1 layer</b>	107 HV
<b>Average micro-hardness 2 layer</b>	103 HV
<b>Average micro-hardness 3 layer</b>	104HV
<b>Average micro-hardness 4 layer</b>	118 HV

All the value are consistent with the averages calculated for the horizontal scans.

### 5.3.3.4 Tensile tests

Mechanical properties of the artificial aged clad specimens have been investigated via tensile tests.

The figure 5.78 shows shape and dimensions of tensile test specimen used that are the same of the AA2024 specimens.

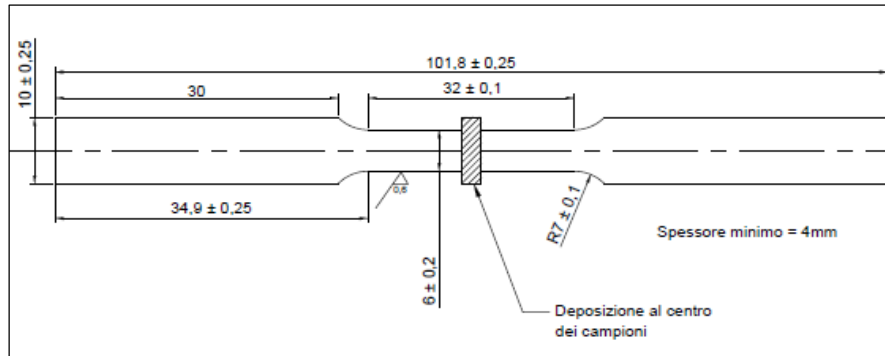


Fig.5.78: Shape and dimension of tensile test specimen.

Tensile strength tests, each one tripled to assure data reproducibility, have been performed. The ultimate tensile strength (UTS) of the original and uncladded sample has been found to be  $317 \text{ N/mm}^2$ . UTS values for the cladded specimens are listed in Table 5-24.

Tab. 5-44: Average ultimate tensile strength values for cladded specimens.

Test	Stress [%]	UTS [MPa]	UTS <sub>c</sub> / UTS <sub>bm</sub> [%]
1	6.5	283	90
2	3.6	277	87
3	5.8	271	85

The value is very similar to that of the base material and have been considered adequate being in according with the customer requirements.

## 5.4 The cost of Laser Cladding process

The cost model used in this thesis draws on energy and material cost which are combined with the labour and machine costs. The cost  $C_{clad\_build}$  can be expressed as:

$$C_{clad\_build} [\text{€}] = \text{Energy Cost} + \text{Material Cost} + \text{Labour cost} + \text{Machine cost} \\ = (\text{Energy Consumption} * \text{Energy price}) + [(\text{Powder mass} * \text{Powder price}) + (\text{Gas flow} * \text{Gas price})] + (\text{Labour Cost} + \text{Machine cost} + \text{Maintenance cost}) * \text{Total time}$$

Taking into account the filling of a V-groove discussed in the last paragraph, the following data are important in order to define the cost:

Tab. 5-45 Some process data of the V-groove filling.

	Data
Scanning speed [mm/min]	400
Average power [W]	2400
Number of clad	9
Clad Length [mm]	100
Powder feeding rate[g/min]	3
Helium flow rate [l/min]	8
Argon flow rate [l/min]	10
Volume Vgroove [cm <sup>3</sup> ]	2
Time of setup [min]	30
Time of cleaning [min]	18

By means of this data, the following variables can be calculated:

Tab. 5-46: Process variables.

Parameters	Calculation	Value
Time of build [min]	Clad length/scanning speed*number of clad	2,25
Powder mass [g]	Powder feeding rate * time of build	6,75
Energy consumption [kWh]	Power machine * time of build	0,71
Helium flow [l]	Helium flow rate * time of build	18
Argon flow [l]	Argon flow rate * time of build	22,5
Total time[min]	Time of build+Time of setup+Time of cleaning	50,25

The energy consumption has been calculated taking into account the average power set in the process parameters (2400 W) and the laser efficiency which is of 22%. The power of the other components of the laser cladding station has also been considered (8000 W). The energy and material cost have been calculated as following:

Tab. 5-47 Energy and material cost.

Energy cost		Material cost	
		Powder mass [g]	6,75
Energy consumption [kWh]	0,71	Powder price [€/g]	0,08
Energy price [€/kWh]	0,17	Helium flow [l]	18
		Argon flow [l]	22,5
		Helium price [€/l]	0,01
		Argon price [€/l]	0,0042

**Energy cost**= Energy consumption \* Energy price = 0,12 €

**Material cost**= Powder mass \* Powder price+Helium flow \* Helium price+Argon flow \* Argon price = 0,78 €

The table below shows the Machine prices:

Tab. 5-48 Equipment costs.

	Prices
Display unit [€]	450
Flow watch [€]	735
Powder feeder [€]	9.500
Laser upgrade [€]	170.000
Laser machine (Robot, source, head) [€]	320.000
Nozzle[€]	15.000
<b>Total Machine purchase [€]</b>	<b>515.685,00</b>

The labour, machine and maintenance cost are defined as following.

Tab. 5-24 Labour, machine and maintenance cost.

<b>Labour cost [€/h]</b> = (Technician annual salary/ annual technician operating hours)		*utilization rate= <b>12,27</b>
Technician annual salary [€/years]	27.000	
Annual technician operating hours [h/years]	1760	
Utilization rate [%]	0,8	
<b>Machine cost[€/h]</b> =(Machine purchase/ years amortization/annual machine operating hours)		*utilization rate= <b>39,07</b>
Machine purchase [€]	515685	
Years amortization	6	
Annual machine operating hours	1760	
Utilization rate	0,8	
<b>Maintenance cost[€/h]</b> =(Annual maintenance cost/annual machine operating hours)		*utilization rate= 20000/1760*0,8= <b>9,09</b>

As a summary metric for the manufacturing cost, the total cost per cm<sup>3</sup> of material deposited is useful. This specific cost metric can be calculated by attributing total cost, C<sub>build</sub>, to the total volume of manufactured parts:

$$C_{\text{clad\_build}} [\text{€}] = \text{Energy Cost} + \text{Material Cost} + (\text{Labour Cost} + \text{Machine costs} + \text{Maintenance cost}) \times \text{Total time} = 0,12+0,78+(12,27+39,07+9,09) *0,84= 52$$

$$\text{Unit cost} [\text{€/cm}^3] = C_{\text{clad\_build}} / \text{Volume\_build} = 26$$

Taking into account a pre-machining to make the V-groove, a post-machining to remove the unmelted material at the bottom and the overlap material at the top and an heat treatment to improve the mechanical characteristics, the following costs must be considered:

*Tab. 5-25 Pre-post processing cost.*

<b>Pre-post processing cost</b>	
<b>Pre-machining cost [€/h]</b>	45
<b>Post-machining cost [€/h]</b>	45
<b>Heat treatment [€/h]</b>	80
<b>Time of pre-machining [h]</b>	0,5
<b>Time of post-machining [h]</b>	0,5
<b>Heat treatment time [h]</b>	6
<b>Total [€]</b>	525

A total cost can be expressed as following:

$$C_{\text{total\_build}} [\text{€}] = C_{\text{clad\_build}} + \text{Pre-post processing cost} = 577$$

## Conclusions

The purposes of this work was to discuss the application of continuous coaxial laser cladding by powder injection to repair a V-groove geometry on a substrate of aluminum alloy.

Firstly, a prototype laser cladding station has been tuned.

The laser deposition line with all the components as been arranged, integrating a welding station with some components. In particular, one of the most important and at the same time critical aspect of laser cladding process is about the steadiness and regularity of the powder flow. Therefore, it was needed to complete the station with a flow monitoring system to ensure a constant flow rate during testing. This system, developed in UNISA laboratory, is well described in this thesis.

Secondly the laser cladding process tuning has been carried out. A relation has been found between the powder mass flow and the drive unit voltage for both AA2024 powder and A357 powder. The head position has been defined in order to focuses the powder onto the workpiece. Finally, a relation has been found between the laser spot diameter and the collimator lens position setting by a voltage signal.

A literature research had to be performed to get an idea of the process state-of-the-art.

After a first experimental study by means a statistical model has been developed to analyze the effect of the parametric process on the laser cladding responses for AA2024 aluminum alloy, a V-grooves on AA 2024 and A357 aluminum plates has been repaired by the laser cladding process with AA 2024 and A357 aluminum powders alloy respectively.

All the tests have been discussed in order to comply with customer requirements. A set of parameters have been defined and experienced.

Finally an economic analysis has been carried out to quantify the cost of laser cladding process.

As a summary metric for the manufacturing cost, the total cost per cm<sup>3</sup> of material deposited has been calculated.

It is very important to underline that the convenience of the process depends primarily on the value of the component to be repaired. In any case the feasibility of the process is to be assessed for each application.



## References

- [1] A. Gunasekaran, «Agile-Manufacturing: a framework for Research and Development» *International Journal Production of Economics*, vol. 62, pp. 87-105, 1999.
- [2] J. Timothy, A. Julian, V. Sundar e M. Randall, «Time compression-rapid steel tooling for an ever-changing world» *Material and Design*, vol. 21, pp. 409-415, 2000.
- [3] D. Hu, H. Mei, G. Tao e R. Kovacevic, «Closed loop control of 3D laser cladding based on infrared sensing» *Advanced Manufacturing*, pp. 129-137.
- [4] E. Toyserkani, A. Khajepour e S. Corbin, *Laser Cladding*, CRC Press LLC, 2005.
- [5] E. Foroozmehr, *Laser Powder Deposition*, VDM Verlag Dr. Muller, 2010.
- [6] W. Steen, «Laser Material Processing» *Springer*, 2003.
- [7] J. Lambarri, J. Leunda, V. Navas, C. Soriano e C. Sanz, «Microstructural and tessile characterization of Inconel 718 laser coatings for aeronautic components» *Optics and Lasers in Engineering*, vol. 51, pp. 813-821, 2013.
- [8] P. Vuoristo, J. Tuominen e J. Nurminen, «Laser coating and thermal spraying-process basics and coating properties».
- [9] D. Verdi, M. Garrido, C. Munez e P. Poza, «Mechanical properties of Inconel 625 laser cladde coatings: Depth sensing indentation analysis» *Materials Science & Engineering*, vol. A, n. 598, pp. 15-21, 2014.
- [10] T. Abioye, D. McCartney e A. Clare, «Laser cladding of Inconel 625 wire for corrosion protection» *Journal of Materials Processing Technology*, vol. 217, pp. 232-240, 2015.

- [11] B. Carcel, A. Serrano, J. Zambrano, V. Amigo e A. Carcel, «Laser cladding of TiAl intermetallic alloy on Ti6Al4V. process optimization and properties.» *ScienceDirect*, vol. 56, pp. 284-293, 2014.
- [12] Y. Tian e R. Ge, «Laser fabrication of nickel aluminide coatings on Al2024 alloy».
- [13] S. Pantelakis, A. Chamos e T. Kermanidis, «a critical consideration for the use of Al-cladding for protecting aircraft aluminum alloy 2024 against corrosion» *theoretical and Applied Fracture Mechanics*, vol. 57, pp. 36-42, 2012.
- [14] I. Taberero, A. Lamikiz, S. Martinez, E. Ukar e J. Figueras, «Evaluation of the mechanical properties of Inconel 718 components built by laser cladding» *International Journal of Machine Tools & Manufacture*, vol. 51, pp. 465-470, 2011.
- [15] B. Graf, S. Ammer, A. Gumenyuk e M. Rethmeier, «Design of experiments for laser metal deposition in maintenance, repair and overhaul applications» *Elsevier*, vol. 11, pp. 245-248, 2013.
- [16] G. Bi e A. Gasser, «Restoration of Nickel-Base Turbine Blade Knife-Edges with Controlled Laser Aided Additive Manufacturing» *Physics Procedia*, vol. 12, pp. 402-409, 2011.
- [17] D. Gnanamuthu, «Laser surface treatment,» *Opt. Eng.*, vol. 19, pp. 783-792, 1980.
- [18] V. Weerasinghe e W. Steen, «Laser cladding by powder injection» in *ASME*, New York, 1983.
- [19] L. Li, W. Steen e R. Hibbero, «In process clad quality monitoring using optical method,» in *Laser assisted processing II*, Netherlands, 1990.
- [20] J. Lin e W. Steen, «An in-process method for the inverse estimation of the powder catchment efficiency during laser cladding» *Opt. Laser Technol.*, vol. 30, pp. 77-84, 1998.
- [21] V. Weerasinghe e W. Steen, «Computer simulation model for laser cladding» *Am. Soc. Mech. Engre*, vol. 10, pp. 15-23, 1983.

- [22] C. Sexton, W. Steen, K. Watkins, R. Vilar e M. Ferreira, «Triple hopper powder feeder system for variable composition laser cladding» in *Application of lasers and electro-optics (ICALEO '93)*, Orlando, 1992.
- [23] M. Ellis, D. Xiao, C. Lee, W. Steen, K. Watkins e W. Brown, «Processing aspects of laser cladding an aluminum alloy onto steel» *J. Mater. Process. Technol.*, vol. 52, pp. 55-67, 1995.
- [24] J. Jeng, B. Quayle, P. Modern, W. Steen e b. Bastow, «Laser surface treatments to improve the intergranular corrosion resistance of 18/13 Nb and 304L in nitric acid.» *Corros. Sci.*, vol. 35, pp. 1289-1293, 1993.
- [25] L. Li e J. Mazumder, «Study of the mechanism of laser cladding processes. Laser processing of materials.» in *AIME Annual Meeting*, Los Angeles, CA, USA, 1985.
- [26] L. Li e J. Mazumder, «One-dimensional finite-medium diffusion model for extended solid solution in laser cladding of Hf on nickel» *Acta Metall.*, vol. 36, pp. 701-712, 1988.
- [27] J. Mazumder e J. Singh, «Laser surface alloying and cladding for corrosion and wear.» *NATO ASI E, Appl. Sci.*, vol. 7, pp. 297-307, 1986.
- [28] G. Dinda, A. Dasgupta e J. Mazumder, «Laser aided direct metal deposition of Inconel 625 superalloy: microstructural evolution and thermal stability» *Mater. Sci. Eng. A*, vol. 509, pp. 397-414, 2009.
- [29] J. Mazumder, D. Dutta, N. Kikuchi e A. Ghosh, «Closed loop direct metal deposition: art to part» *Opt. Lasers Eng.*, vol. 34, pp. 397-414, 2000.
- [30] Y. Kathria, «Some aspects of laser surface cladding in the turbine industry» *Surface and coating technology*, vol. 132, pp. 262-269, 2000.
- [31] V. Fallah, S. Corbin e A. Khajepour, «Solidification behaviour and phase formation during pre-placed laser cladding of Ti45Nb on mild steel» *Surface & Coatings Technology*, vol. 204, pp. 2400-2409, 2010.

- [32] P. Balu, P. Leggett e R. Kovacevic, «Parametric study on a coaxial multi-material powder flow in laser-based powder» *Journal of Materials Processing Technology*, vol. 212, p. 1598– 1610, 2012.
- [33] Chryssolouris, C. Lalas, K. Tsirbas e K. Salonitis, «An analytical model of the laser clad geometry» *Int J Adv Manuf. Technol.*, vol. 32, pp. 34-41, 2007.
- [34] J. Choi e Y. Chang, «Characteristics of laser aided direct metal/material deposition process for tool steel» *Elsevier*, vol. 45, pp. 597-607, 2005.
- [35] Z. Xiong, G. Chena e X. Zeng, «Effects of process variables on interfacial quality of laser cladding on aeroengine blade material GH4133» *Journal of materials processing technology*, vol. 209, pp. 930-936, 2009.
- [36] B. Graf, S. Ammer, A. Gumenyuk e M. Rethmeier, «Design of experiments for laser metal deposition in maintenance, repair and overhaul applications» *Elsevier*, vol. 11, pp. 245-248, 2013.
- [37] V. Ocelik, O. Nenadl, A. Palavra e M. De Hosson, «On the geometry of coating layers formed by overlap» *Surface & Coatings Technology*, vol. 242, pp. 54-61, 2014.
- [38] M. Dhanda, B. Haldar e P. Saha, «Development and Characterization of Hard and Wear Resistant MMC Coating on Ti-6Al-4V Substrate by Laser Cladding» *Procedia Materials Science*, vol. 6, pp. 1226-1232, 2014.
- [39] Z. Xiang, J. Liu, J. Ren, J. Luo e S. Shi, «Investigation of laser cladding high temperature anti-wear composite coatings on Ti6Al4V alloy with the addition of self-lubricant CaF<sub>2</sub>» *Applied Surface Science*, vol. 313, pp. 243-250, 2014.
- [40] Z. Hui, Z. Yong, Z. Zengda e S. Chuanwei, «Effects of CeO<sub>2</sub> on microstructure and corrosion resistance of TiC-VC» *Elsevier*, vol. 32, n. 11, 2014.
- [41] X. Wang, M. Zhang e S. Qu, «Development and characterization of (Ti, Mo)C carbides reinforced Fe-based Development and characterization of (Ti, Mo)C carbides reinforced Fe-based» *Optics and Lasers in Engineering*, vol. 48, pp. 893-898, 2010.

- [42] Q. Wu, W. Li, N. Zhong, W. Gang e W. Haishan, «Microstructure and wear behavior of laser cladding VC–Cr7C3 ceramic coating on steel substrate» *Materials and Design*, vol. 49, pp. 10-18, 2013.
- [43] S. Shang, D. Welburn, Y. Sun, S. Wang, J. Cheng, J. Liang e C. Liu, «Laser beam profile modulation for microstructure control in laser cladding of an NiCrBSi alloy» *Surface & Coatings Technology*, vol. 248, pp. 46-53, 2014.
- [44] R. Liu, T. Lei e L. Guo, «Recent development in laser cladding on titanium surfaces» *Material Science and Technology*, vol. 12, pp. 524-528, 2004.
- [45] Schneider e Marcel, Laser cladding with powder, Haarlem: Print Partners Ipskamp Enschede, 1968.
- [46] C. Qu, J. Li, L. Bai, J. Shao, R. Song e J. Chen, «Effects of the thickness of the pre-placed layer on microstructural evolution and mechanical properties of the laser-clad coatings» *Journal of Alloys and Compounds*, vol. 644, pp. 450-463, 2015.
- [47] E. Amara, F. Hamadi, L. Achab e O. Boumia, «Numerical modelling of the laser cladding process using a dynamic mesh approach» *Journal of achievements in Materials and Manufacturing Engineering*, vol. 15, n. 1-2, pp. 100-106, 2006.
- [48] H. Qi, J. Mazumder e H. Ki, «Numerical simulation of heat transfer and fluid flow in coaxial laser cladding process for direct metal deposition» *JOURNAL OF APPLIED PHYSICS*, vol. 2, pp. 100-111, 2006.
- [49] S. Lee, M. Nordin, S. Babu e D. Farson, «Influence of Fluid Convection on Weld Pool» *WELDING JOURNAL*, vol. 2, pp. 292-300, 2014.
- [50] M. Thompsona, L. Bianc, N. Shamsaeia e A. Yadollahia, «An overview of Direct Laser Deposition for additive manufacturing; Part I: Transport phenomena, modeling and diagnostics» *Additive Manufacturing*, vol. 8, pp. 36-62, 2015.
- [51] P. Peyre, P. Aubry, R. Fabbro, R. Neveu e A. Longuet, «Analytical and numerical modelling of the direct metal deposition laser process» *JOURNAL OF PHYSICS*, vol. 41, pp. 1-10, 2007.

- [52] M. Griffith, D. Keicher, C. Atwood, J. Romero e J. Smugeresky, «Free form fabrication of metallic components using laser engineered net shaping» in *7th Solid Free Fabr. Symp*, Austin, USA, 1996.
- [53] C. Kong, P. Carroll, P. Brown e R. Scudamore, «The effect of average powder particle size on deposition efficiency, deposit height and surface roughness in the direct metal laser deposition process» in *Joining of Materials*, 2006.
- [54] D. Boisselier e S. Sankarè, «Influence of powder characteristics in laser direct metal deposition of SS316L for Metallic Parts Manufacturing» *Physics Procedia*, vol. 39, p. 455 – 463, 2012.
- [55] K. Shah, J. Pinkerton, A. Salman e L. Li, «Effects of Melt Pool Variables and Process Parameters in Laser Direct Metal Deposition of Aerospace Alloys» *Materials and Manufacturing Processes*, vol. 25, p. 1372–1380, 2010.
- [56] Y. Li, H. Yang, X. Lin, W. Huang e J. Li, «The influences of processing parameters on forming characterizations during laser rapid forming» *Materials Science and Engineering*, vol. A, n. 360, pp. 18-25, 2003.
- [57] U. De Oliveira, V. Ocelik e J. De Hosson, «Analysis of coaxial laser cladding processing conditions» *Surface & Coatings Technology*, vol. 197, p. 127– 136, 2005.
- [58] V. Apollonov, «High power disk lasers: advantages and prospects» *American Journal of Modern Physics*, vol. 1, n. 1, pp. 1-6, 2012.
- [59] S. Ruppik, «High power disk and fiber lasers – A performance comparison» in *Proceedings of SPIE 8235, Solid State Lasers XXI: Technology and Devices*, San Francisco, 2012.
- [60] G. Weisheit, «Powder Injection: The Key to Reconditioning and Generating Components using Laser Cladding».
- [61] F. Caiazzo, V. Alfieri, I. Fierro e V. Sergi, «Investigation on the effects of the processing parameters in powder laser cladding on 2024 aluminum alloy» in *A.I. Te.M*, Palermo, 2015.

- [62] V. Alfieri, F. Caiazzo e V. Sergi, «Autogenous laser welding of AA2024 aluminium alloy: process issues and bead features» in *Proceedings of 9th Conference on Intelligent Computation in Manufacturing Engineering, CIRP ICME*, Capri, 2014.
- [63] A. Riveiro, A. Meijas, F. Lusquinos, J. Del Val, R. Comesana, J. Pardo e J. Pou, «Laser cladding of aluminium on AISi 304 stainless steel with high-power diode lasers» *Surface & Coatings Technology*, vol. 253, pp. 214-220, 2014.
- [64] A. Riveiro, A. Meijas, F. Lusquinos, J. Del Val, R. Comesana, J. Pardo e J. Pou, «Optimization of laser cladding for Al coating production» *Physics Procedia*, vol. 41, pp. 327-334, 2013.
- [65] Q. Zhang, M. Anyakin, Y. Pan, V. Kovalenko e J. Yao, «Application of Regression Designs for Simulation of Laser Cladding» vol. 39, pp. 921-927, 2012.
- [66] A. D17.1, «Specification for Fusion Welding for Aerospace Applications» American Welding Society, Miami, FL, 2010.
- [67] M. Pastor, H. Zhao Martukanitz e T. Debroy, «Porosity, underfill and magnesium loss during continuous wave Nd:YAG laser welding of thin plates of aluminum alloys 5182 and 5754» *Welding Journal*, vol. 78, pp. 207-2016, 1999.
- [68] J. Davis, Aluminum and aluminum alloys, OH: ASM International, Materials Park, 1993.
- [69] D. Stefanescu e R. Ruxanda, «Solidification Structures of Aluminum Alloys» *Metallography and Microstructures, ASM Handbook*, vol. 9, pp. 107-115, 2004.
- [70] M. Hakem, S. Lebaili, J. Miroud, A. Bentaleb e S. Toukali, «Welding and characterization of 5083 aluminum alloy» in *Metal 2012*, Brno, Czech republic, EU, 2012.
- [71] S. Missori e A. Sili, «Mechanical behaviour of 6082-T6 aluminium alloy welds» *Metallurgical Science and Technology*, vol. 18, n. 1, pp. 12-18, 2000.

- [72] A. Gumenyuk, «Potential for repair welding technology based on laser metal deposition for petrochemicals industry» in *Fitness for service in chemical industries*, Aswan, Egypt, 2012.
- [73] D. Alexopoulos, A. Stylianos e J. Campbell, «Dynamic fracture toughness of Al-7Si-Mg (A357) aluminum alloy» *Mechanics of Materials*, vol. 58, pp. 55-68, 2013.
- [74] A. Stylianos e D. Alexopoulos, «Impact mechanical behaviour of Al-7Si-Mg (A357) cast aluminum alloy» *Materials Science and Engineering A*, vol. 528, pp. 6303-6312, 2011.